Evaluation of streambank stabilization structures on upstream and downstream bank erosion

by

Corben Christopher Monzon

B.S., Kansas State University, 2024

A THESIS

submitted in partial fulfillment of the requirements for the degree

MASTER OF SCIENCE

Department of Biological and Agricultural Engineering
Carl R. Ice College of Engineering

KANSAS STATE UNIVERSITY
Manhattan, Kansas

2024

Approved by:

Major Professor
Dr. Trisha Moore

Copyright

Abstract

For many decades streambank stabilization techniques have been used to help reduce channel erosion and restore fluvial systems to a more natural state. The overarching goal of this research is to better understand how river systems respond to streambank stabilization (SBS). In this case study, the aim is to broaden the understanding of the effects of SBS projects from a localized scale to a reach, in hopes of answering the research question: Do SBS projects reduce the net amount of sediment that is carried by the river, or do they push the 'erosion problem' upstream or downstream? To evaluate this question, a before-after construction analysis was established to examine changes in channel geometry along two reaches of the Cottonwood River, located in east-central Kansas, USA. Each reach consists of three meanders, with the middle meander containing a SBS project of rock vanes, toe rock, and bank shaping. The remaining two meanders, located upstream and downstream of the SBS project, remained unmodified. Over the past six years, these study reaches have been surveyed five to six times, with the majority of the topographic surveys occurring prior to construction. To further the understanding of the measured changes in channel geometry, a collection of channel topographic data, along with USGS stream gage data, was used to simulate flows using HEC-RAS modeling. The results from these analyses indicate (1) streambank lateral retreat rates and stream power were reduced at the stabilized sites, (2) streambank erosion and stream power increased upstream and downstream of the stabilized sites, and (3) the reaches had a net streambed deposition following construction. Overall, more monitoring is necessary to determine the long-term impacts of SBS and whether the aforementioned results are attributed to a "break in" period or a new trend.

Table of Contents

List of Figures

List of Tables

List of Equations

Acknowledgements

I want to thank my family, friends, and committee members who supported me throughout this journey.

Chapter 1 - Streambank Stabilization

Mankind has been modifying fluvial systems to cater to our economic and social needs for hundreds of years. For example, rivers were often straightened and channelized to increase farmable acres, make rivers easier to navigate, and quickly transport stormwater runoff downstream (Nunnally & Keller, 1979). Furthermore, anthropogenic changes in land use, such as urbanization and agriculture, have decreased stormwater infiltration rates. This has resulted in larger, more erosive peak flows (Wu et al., 2018). Both channelization and high peak flows promote channel instability and increased rates of bed and bank erosion (Simon & Hupp, 1986). Even though erosion and deposition are natural geomorphic processes that are required to maintain a healthy fluvial ecosystem (Florsheim et al., 2008), high erosion rates threaten valuable land and infrastructure (Fox et al., 2016). Furthermore, rivers and other closely related freshwater systems (e.g., wetlands and lakes) are the world's most damaged ecosystems, such that freshwater biodiversity is declining far faster than terrestrial and marine ecosystems (Arthington, 2012; Dudgeon et al., 2006). The source of this damage is undeniably due to the many years of human interference and modifications of these fluvial systems and the surrounding environments (Vörösmarty et al., 2010).

Channel evolution models (CEM), such as Simon and Hupp's (1986), were created after repeated observations of a series of predictable morphological adjustments following instream anthropogenic disturbances. The CEM developed by Simon and Hupp (1986) involves a linear six stage channel evolution process starting with pre-modified (stage 1) then constructed (stage 2), degradation (stage 3), degradation and widening (stage 4), aggradation and widening (stage 5), and finally, quasi-equilibrium (stage 6) (Figure 1.1). This CEM and other models (i.e., Cluer & Thorne, 2014; Schumm et al., 1984) illustrate the general trend of a stream system, which can help practitioners and researchers evaluate the stream's current stage of channel evolution (Doll et al., 2003). Accurately identifying the correct stage is a crucial step to adequately understand and correctly design restoration efforts (Doll et al., 2003).

Figure 1.1 Simon and Hupp's (1986) Channel Evolution Model.

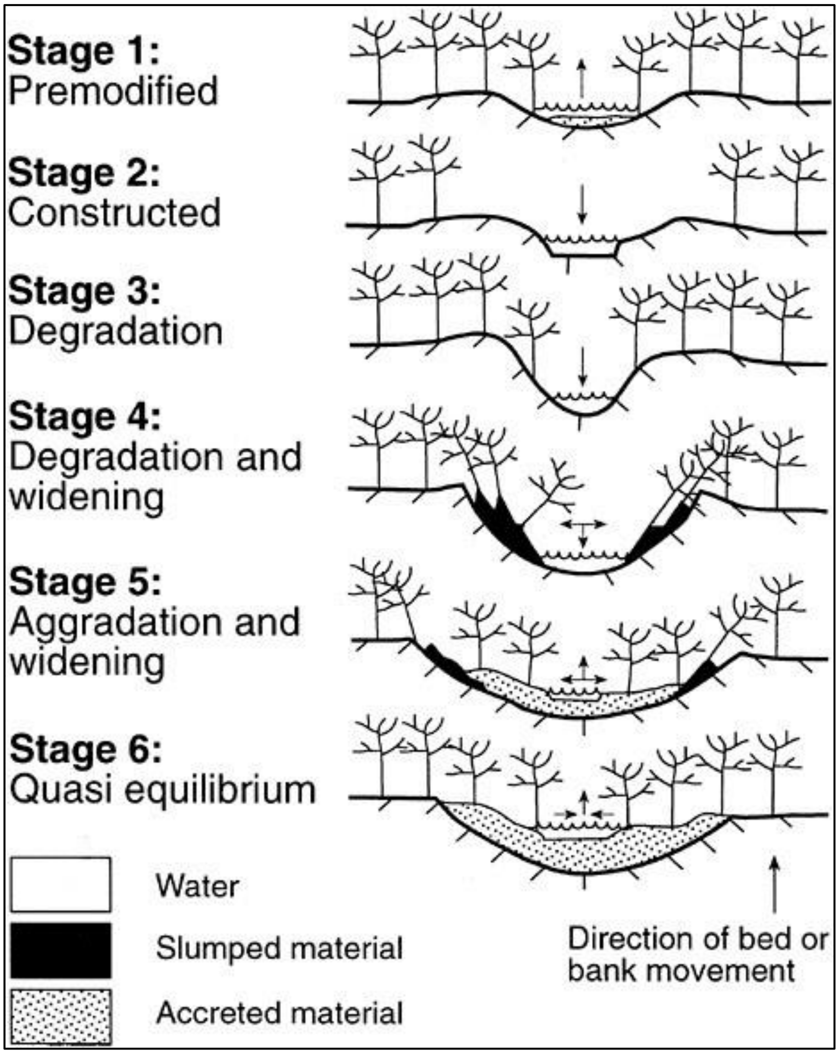

River scale restoration aims to combat hundreds of years of human disturbance by expediting the evolution of the river system to quasi-equilibrium. River scale restoration can reconnect a river to the floodplain allowing for (1) the dissipation of hydraulic energy as the water spreads out, and (2) the improvement of biodiversity in the inundation zones. Furthermore, river restoration produces fluvial systems capable of carrying the 1-year to 2-year return interval bankfull discharge and its produced sediment load (Rosgen, 1996; Shields et al., 2003). Despite its potential to yield a stable river system, the implementation of river scale restoration can be cumbersome (Bigham, 2020). Challenges arise due to the substantial cost of the projects (Moerke & Lamberti, 2004), and the possible need for collaboration among multiple landowners.

To overcome these obstacles, practitioners sometimes use streambank stabilization exclusively on the most severely degraded sections of the river. Streambank stabilization (SBS) is defined by Bigham (2020) as "a single technique or system of techniques that maximize localized streambank shear strength and/or minimize the forces acting on a streambank with intent of halting or minimizing lateral retreat (pg. 352)." Additionally, while the main intent of SBS is to minimize lateral streambank retreat, these techniques can sometimes improve the stream system's habitat (e.g., Cavaillé et al., 2013; Nassar, 2019). SBS is typically focused on a specific site, and therefore these projects tend to cost less and have fewer property owners compared to river scale stream restoration efforts.

SBS is organized into two main categories: (1) instream structures and (2) streambank management techniques (Bigham, 2020). A few examples of instream structures include impermeable and permeable spurs, bendway weirs, rock vanes, submerged vanes, and woody revetments. The main function of instream structures is to deflect flow towards the middle of the channel and/or capture sediment (Bigham, 2020; Naisargi & Mittelstet, 2017; Nassar, 2019). Additionally, instream structures can help diversify localized aquatic habitat by producing variations in habitat within the stream, such as areas of deep pools with slow moving water (Bigham, 2020; Schiff et al., 2011).

The other category of SBS is streambank management techniques, which can be subcategorized into "hard" and "soft" techniques. Hard streambank management techniques create a rigid bank boundary that increases the bank's shear strength and resistance to mass wasting via gravitational forces. In this review, hard streambank techniques include only fully hardened streambanks (i.e., from toe to top of bank) such as riprapped channels, concrete retaining walls, and gabion basket walls. These techniques are perhaps the most intuitive approach to eliminating lateral erosion but are extremely costly and often considered less beneficial to the fluvial ecosystem (Cavaillé et al., 2015).

Soft streambank management techniques can include bank shaping, bankfull benches, toe rock, vegetation, and bioengineering (e.g., live stakes, crib walls, wattles, etc.). Toe rock, or riprap placed at the toe of the streambank, is included in this subcategory because it is commonly used in combination with bank shaping or bankfull benches and does not "fully harden" the streambank. Depending on the type of soft technique, the intended function ranges from additional shear strength to the reduction of gravitational and/or hydraulic forces. For example, streambank vegetation adds surface roughness and increases the shear strength of the bank soil from the tensile strength of the root network (Bigham, 2020; Wynn et al., 2004), while bankfull benches minimize the effects of gravitational and hydraulic forces by reconnecting the floodplain (Bigham, 2020).

While streambank stabilization efforts using a combination of instream structures and soft streambank management techniques are often effective in stabilizing a specific reach, the long-term effectiveness of reach scale SBS projects has not been definitively determined, and thus more research is needed to adequately understand SBS and how it affects the entire fluvial system (Layzell, Peterson, et al., 2022; Moerke & Lamberti, 2004; Naisargi & Mittelstet, 2017; Nassar, 2019; Russell et al., 2021a; Russell et al., 2021b).

1.1 Streambank Stabilization in the State of Kansas

Streambank stabilization projects often integrate a combination of stabilization techniques within a unified design. The selection of SBS techniques varies based on the project's designers and its geographical context (Miller, 2022). For instance, professionals in one region might opt for specific approaches due to their efficacy in that environment. In Kansas, where this study focuses, streambank stabilization is of particular importance as many of the state's reservoirs are filling with sediment eroded from streambanks (Fox et al., 2016; Juracek & Ziegler, 2007). Rock vanes, toe rock, bank shaping, and vegetation are often employed in combination to establish a comprehensive streambank stabilization approach within the state of Kansas. The following sections provide an overview of findings and monitoring outcomes related to the common SBS techniques used in Kansas, which are the structures of interest in this thesis.

1.1.1 Instream Flow Deflectors: Rock Vanes

Rock vanes, also known as stream barbs, cross vanes, and j-hook vanes, are single protrusion, partially submerged rock piles positioned at an upstream angle on the outer bank of a meander to deflect stream flow away from the toe (NRCS, 2013; Figure 1.2). Rock vanes are sloped from the streambed to as high as bankfull elevation, ensuring that the vane's tip (i.e., sometimes referred to as the vane nose) remains submerged even during low flow conditions (Johnson et al., 2001). The presence of a submerged vane tip can lead to the misidentification of rock vanes as J-hook vanes. Unlike rock vanes, J-hook vanes have a distinctive hook shaped rock tip (Khosronejad et al., 2013, 2015). For the purpose of this literature review, the term "vanes" or "rock vanes" will refer to stream barb structures without the hook shaped tip. In general, the cross-sectional shape of a vane is either triangular or trapezoidal, depending on the crest width.

Furthermore, rock vane projects can be designed with variations in spacing, orientation (i.e., angle tangentially from the bank), vane geometry, and the total number of vanes depending on the site's unique hydrology and geomorphic condition (Johnson et al., 2001). For instance, some design standards found in technical references and handbooks include the vane orientation being 20 to 30° from the bank tangent line at an upstream angle (Doll et al., 2003), and the length of a single vane structure spanning 0.3 to 0.5 of the base flow channel width (Doll et al., 2003; NRCS, 2013). These design parameters can have a substantial impact on the overall effectiveness of the structure (Patel et al., 2023).

Figure 1.2 Downstream view of rock vanes on the Cottonwood River, Kansas.

Several papers have directly assessed the effectiveness of rock vanes in reducing bank erosion. One such monitoring study, conducted by Naisargi & Mittelstet (2017), evaluated the effectiveness of SBS practices on portions of the Cedar River in Nebraska. They assessed aerial imagery from the National Agricultural Imagery Program (NAIP) in ArcGIS over four periods of time: pre-stabilization, post-stabilization, flood of 2010, and post-flood to quantify erosion and deposition from 1993 to 2016. The case study evaluated two rock vanes that were constructed in 2000. Their report indicated an average reduction in streambank erosion for these two rock vane structures of 47.2% for the post-stabilization to pre-flood (i.e., 2003 to 2009) period and 66.1% for the overall period from 2003 to 2016 (Naisargi & Mittelstet, 2017). Several other case studies also reported that rock vanes, and similar flow deflecting structures, decreased erosion rates on rivers in the Midwestern US (Bressan et al., 2014; Elhakeem et al., 2017; Layzell, Peterson, et al., 2022). However, while Naisargi & Mittelstet (2017) reported results that showed the effectiveness of rock vanes, both structures failed after a breach of an upstream reservoir that caused the flood of 2010. Similarly, Miller & Kochel (2010, 2013) observed that rock vanes and other instream structures were prone to failure within a decade, especially after flood events. In addition, Radspinner et al. (2010) demonstrated that the installation of more than one rock vane may have a positive influence on the long-term success of a rock vane project. Even though the two rock vanes studied by Naisargi & Mittelstet (2017) decreased streambank erosion, due to the small sample size and complete structural failure, the overall effectiveness of rock vanes depicted by this particular case study is inconclusive.

Russell et al. (2021b) conducted a study on NAIP aerial imagery of 24 stabilization structures in ArcGIS to evaluate their impact over a pre-stabilization and post-stabilization period. In contrast to previous studies, their research encompassed a larger reach scale of 1.5 meander wavelengths upstream and downstream of SBS structures. This wider scope enabled the researchers to investigate streambanks beyond the stabilized portion, assessing their susceptibility to the effects of SBS, such as degradation and/or aggradation in unstabilized adjacent reaches due to SBS. The study's findings suggest that SBS structures, including rock vanes, were successful in reducing streambank erosion at the installation location. Furthermore, aerial imagery analysis of upstream and downstream meanders indicated that SBS had no significant impact on the adjacent unstabilized reaches. However, Russell et al. (2021b), recommended more advanced monitoring practices are necessary to accurately understand how SBS projects affect the entire fluvial system.

Layzell, Peterson et al. (2022) conducted a study in which they examined the potential of unmanned aircraft systems (UAS) to improve SBS monitoring and showcase the utility of UAS as a restoration monitoring tool. The SBS projects that were evaluated consisted of a combination of rock vanes, toe rock, bank shaping, and native vegetation. Layzell, Peterson et al. (2022) used a UAS with pre-programmed flight plans to capture nadir imagery from approximately 100 meters above the ground level, which could be georeferenced and combined using photogrammetry to produce a sub-meter accurate digital elevation model (DEM). By comparing the volumetric change in the DEM surfaces between multiple UAS flight surveys from pre-stabilization and post-stabilization periods (i.e., adjusted for the respective discharge in between each period), Layzell, Peterson, et al. (2022) found that streambank erosion continued at every SBS site after construction. Fluvial erosion was most noticeable in the lower bank directly above the toe rock in between rock vanes. The researchers attributed this to "accelerated flow over the rock vanes resulting in increased hydraulic shear stresses and thus increased fluvial erosion (pg. 10, Layzell, Peterson et al. (2022)." In some instances, the erosion was significant enough to cause rotational failures. However, Layzell, Peterson, et al. (2022) concluded that local scale erosion rates following stabilization were consistently lower than the pre-stabilization rates. The researchers also acknowledged that some of the post-construction fluvial erosion in the lower bank may be attributed to a "break-in" period while the sites settle and adjust, as noted by several other studies (e.g., Buchanan et al., 2014; Elhakeem et al., 2017; Kondolf & Micheli, 1995). This study highlights how UAS technology can enhance streambank monitoring practices and should be considered in the future when trying to assess reach scale SBS impacts.

In other studies, the effectiveness of rock vanes in mitigating bank erosion was indirectly evaluated through their ability to divert flow away from eroding streambanks and promote sediment deposition in the near bank regions. Likewise, physical models were used as tools to study the sediment transport patterns of fluvial systems that contain rock vanes, which helps predict an instream structure's efficacy in reducing bank erosion. Two such studies, both conducted by Bhuiyan et al. (2009, 2010), used a large scale mobile bed channel to evaluate vanes on meander bends. The experiments were conducted on a model channel with graded sediment and flow conditions that were similar to those found in natural meandering rivers (Bhuiyan et al., 2009, 2010). Using this configuration, the tests demonstrated that an array of vanes sloped from bed to bankfull elevation at an upstream angle effectively relocated the scour hole away from the outer bank of the meander and redirected the thalweg to the middle of the channel. Their experiments showed that vanes "induce a stronger counter-rotating secondary flow cell near the outer bank which opposes the major spiral flow pattern responsible for bank erosion in the bend (pg. 593, Bhuiyan et al., 2010)."

These results were also corroborated by Hemmati et al. (2016) and Hemmati & Daraby (2019), who found rock vanes to be more effective than bendway weirs at maximizing deposition and reducing scouring in the near bank region. Moreover, 2D numerical models by Papanicolaou et al. (2011) demonstrated that rock vanes, in combination with other stabilization techniques, were successful in decreasing near bank velocities and lateral retreat rates, which was also supported by research from Niezgoda and Johnson (2006). Additionally, Karki et al. (2018) showed that vanes effectively decreased erosion rates in meandering channels with varying sinuosity. However, stream restoration projects that incorporate several stabilization techniques, as noted by Buchanan et al. (2014), Elhakeem et al. (2017) and Layzell, Peterson et al. (2022), may require a “break-in” period, where the SBS features undergo subtle adjustments and settlements before achieving stabilization and being effective at decreasing bank erosion.

Another important focus of rock vane research is the structure’s scouring potential. Rock vanes typically develop a scour hole directly downstream of the vane tip due to the complex 3D flow that occurs around the submerged rocks (NRCS, 2013; Patel et al., 2023; Uijttewaal, 2005). It can be beneficial to have deep scour holes for habitat diversity, but excess scouring may compromise the stability of the instream structure (Buchanan et al., 2014; Khosronejad et al., 2013; Patel et al., 2023). In comparison to other instream structures, rock vanes that are designed properly have the least impact on localized scour and deposition compared to impermeable spurs and bendway weirs, as they typically do not generate a recirculation zone in the near bank area (Bhuiyan et al., 2009, 2010). An emphasis should be placed on properly designing rock vanes, as the dimensions and angle of the vanes, as well as the overall site conditions, can significantly affect scour (Patel et al., 2023). Several studies have found that scour depth increases with an increase in rock vane height, width, and length (Jamieson et al., 2013a, 2013b; Pagliara et al., 2013; Pagliara & Mahmoudi Kurdistani, 2015). Furthermore, Hemmati et al. (2016, 2019) found that scour depth increases with a decrease in crest slope.

The following four studies, which differed in bed sediment, flow conditions, planform, spacing, and length, examined how scour is affected by the rock vane height. Bhuyian et al. (2010) and Johnson et al. (2001, 2002) found that a bankfull vane height was the most effective way to reduce scour, while Matsuura & Townsend (2004) reported that vane heights between 33% and 50% of bankfull elevation were optimal. These same four studies also evaluated the effects of vane orientation on scour, and all four supported using multiple vanes angled at 30° to reduce scour near the structure (Bhuiyan et al., 2010; Johnson et al., 2001, 2002; Matsuura & Townsend, 2004). Thus, it is necessary to carefully consider the dimensions and angle of rock vanes as they affect the structure's scouring potential.

Site conditions and channel geometry also have a significant effect on a rock vane's scouring potential. For instance, Bhuiyan et al. (2009) found through laboratory models that multiple vanes are more advantageous than a single rock vane, because the multiple structures "provide more control on the flow and sediment transport pattern," while single structures produce "abrupt changes in the flow pattern and sediment transport (pg. 346)" that cause localized bed scour (Bhuiyan et al., 2009). Likewise, Ding et al. (2023) found through numerical modeling that vanes arranged in ascending order with respect to their length along a mildly meandering reach, help reduce scour near the vane field and promote sediment deposition. In addition to this, Hemmati & Daraby (2019) found through a physical model that maximum scour depth typically occurs at the tip of the furthest upstream and downstream vane, and Pagliara & Kurdistani (2015) observed an increase in scour depth with an increase in meander bend radius in laboratory experiments. Therefore, the arrangement of vanes, the presence of multiple structures, the alignment with meandering reach, and the specific meander bend radius should all be considered before implementing rock vanes to help optimize bank stabilization, while minimizing bed scour.

In summary, several studies have evaluated the effectiveness of rock vanes in reducing streambank erosion, with varying results. While some case studies have reported a decrease in erosion rates (e.g., Hemmati et al., 2016; Hemmati & Daraby, 2019; Karki et al., 2018; Russell et al., 2021b), others have shown that rock vanes can be prone to failure within a decade (e.g., Naisargi & Mittelstet, 2017), particularly after large magnitude flood events. Nevertheless, laboratory models and numerical simulations have shown that rock vanes can effectively relocate scour holes away from the outer bank of meander bends and redirect the thalweg to the middle of the channel, leading to increased sediment deposition and decreased scouring in the near bank region. Research has also shown that attention to the dimensions, angles, orientation, and quantities of rock vanes can effectively keep scouring potential to a minimum. Additionally, the use of rock vanes in combination with other stabilization techniques, such as toe rock, can decrease near bank velocities and lateral retreat rates. Overall, while rock vanes have shown promising results, more research is needed to fully understand their long-term effectiveness and impact on fluvial systems at a larger reach scale (Anstead et al., 2012; Bhuiyan et al., 2009; Bigham, 2020; Enlow et al., 2018; Khosronejad et al., 2013; Russell et al., 2021b).

1.1.2 Streambank Management Techniques: Toe Rock, Bank Shaping, and Vegetation

This section provides an overview of the streambank management techniques commonly employed in the state of Kansas, which include bank shaping, toe rock, and vegetation. Often SBS projects throughout the US use a combination of the same techniques used in Kansas. As a result, many research papers assess the combined effectiveness of these techniques in reducing bank erosion (e.g., Enlow et al., 2018; Frothingham, 2008; Layzell, Peterson, et al., 2022; Simon & Steinemann, 2000). Therefore, this review will examine the combination of streambank management techniques for a more comprehensive analysis.

Bank shaping involves reducing the slope of the streambank. According to the Illinois Department of Natural Resources (IDNR), the ideal slope for a streambank is 3H:1V or flatter. Although, in situations that are restricted by space or have limited funding, a maximum slope of 2H:1V is acceptable (IDNR, 2018). By flattening the slope of the bank, the critical bank height is increased. Critical bank height represents the maximum height that the bank can reach without being vulnerable to erosion caused by mass wasting (Simon & Rinaldi, 2000). Despite the fact that bank saturation can reduce bank stability, streambank shaping can minimize the risk of failure caused by mass wasting due to the reduced impact of gravitational and hydraulic forces (Simon & Rinaldi, 2000). Additionally, bank shaping can sometimes incorporate flat, low lying benches, often referred to as bankfull benches, that connect high frequency flow events to a mock floodplain. These benches are designed to carry specific return interval flows and enable the water to spread out further, reducing fluvial erosion (Rosgen, 1996).

Once the streambank has been shaped, it is important to protect it against fluvial erosion at the toe, which is where the streambank meets the streambed. One method is to place rock riprap along the streambank toe. Longitudinal toe dikes, often called toe rock, protect against fluvial erosion and help prevent the loss of basal support material (Lagasse et al., 2009; Shields et al., 1998b). By preventing loss of basal support, toe rock helps maintain the overall bank stability. Also, the rock's weight at the bottom of the streambank can help counteract the pore pressure and gravitational force acting on the streambank, which may lead to rotational failure (Bigham, 2020). Therefore, toe rock is a useful streambank management technique that complements bank shaping and helps ensure the long-term stability of the streambank.

Riparian vegetation is another streambank management technique that can help prevent lateral erosion along the channel by mitigating the forces acting on a streambank. Geotechnical failures are typically caused by excessive pore pressure, gravitational force, or a combination of the two (Fischenich, 1989). For instance, high moisture content within the bank leads to excess pore pressure, which can overcome the soil's effective stress that holds the particles together (Coduto et al., 2011). Additionally, gravitational forces acting on an undercut streambank can cause a geotechnical failure. The presence of vegetation on a streambank helps counteract the geotechnical forces produced from excess pore pressure and gravitational instability by reducing soil moisture levels and providing mechanical reinforcement through the root system (Bigham, 2020; Gray & Sotir, 1996; Simon & Collison, 2002; Wynn et al., 2004). In addition, streambank vegetation can reduce the hydraulic forces acting on a streambank by dissipating stream flow energy due to increased surface roughness (Bigham, 2020; Cavaillé et al., 2013, 2015; Gray & Sotir, 1996; NRCS, 2013).

Riparian vegetation can grow naturally over time, but to speed up the process and ensure effective stabilization, many SBS practitioners introduce a variety of native plants through different seeding or planting techniques. The primary objective of incorporating riparian vegetation is to jump start the growing process in an effort to allow sufficient time for the vegetation to become established before major storm events occur. This is necessary to prevent vegetation loss and bank failure due to inadequate bank protection (Logar & Scianna, 2005). Moreover, using native species is preferred because they are well adapted to the streambank conditions and are typically more resilient to local environmental stresses, such as flooding, drought cycles, and disease (Correll, 2005).

Live staking is a commonly used bioengineering technique that helps establish vegetation on recently shaped streambanks. The technique uses dormant cuttings from the trunks of woody riparian species such as willow (Bigham, 2020; Gray & Sotir, 1996). The stakes are planted upright into the bank in either rows or sporadically (Bigham, 2020). To prevent the live stakes from drying out, they are planted deep enough to reach the phreatic zone (Anstead et al., 2012; Watson et al., 1997). As the stakes take root, they create soil stability within the bank by preventing mass movement of surface sediment on the streambank and promoting soil drying through transpiration (Gray & Sotir, 1996; Niedzinski, 2021). Furthermore, live stakes are larger in size compared to seeds, which reduces the risk of them being swept away by a runoff event during the establishment period. As a result, they are capable of offering passive support to the bank immediately after planting (Niedzinski, 2021).

Research into the effectiveness of soft streambank management techniques can be split into field studies, numerical models, and physical models with field studies being the most common type of research (Bigham, 2020). As mentioned in Section 1.1.1 on rock vanes, the field study by Layzell, Peterson et al. (2022) monitored and assessed the effectiveness of multiple SBS projects along the Cottonwood River in Kansas that included a combination of bank shaping, toe rock, rock vanes, and native vegetation. Design parameters for the soft streambank management techniques included (1) a layer of toe rock 1.2 to 1.8 meters high comprised of individual rocks with an average diameter of 60 cm placed along the streambank toe, (2) bank shaping at a ratio of 2-3H:1V, and (3) vegetation comprised of cottonwood and sycamore trees spaced every 3 to 5 meters and annual ryegrass for immediate coverage (Layzell, Peterson, et al., 2022). This study noted the possibility of a “break-in” period that may take place before the management techniques settle and vegetation takes hold. Overall, the researchers found that the local scale erosion rates following stabilization were consistently lower than the pre-stabilization rates (Layzell, Peterson, et al., 2022).

Simon and Steinemann (2000) evaluated the effectiveness of soft streambank management techniques on three streams near Atlanta, Georgia. Stabilization techniques included toe rock, log toe, bank shaping, live stakes, live fascines, and brush mattresses. While several challenges in effectively monitoring these sites were identified, such as insufficient baseline data, and short-term vulnerabilities due to flooding and vegetation failure, Simon and Steinemann (2000) concluded that all three case studies showed a decrease in erosion and an increase in bed stability at the stabilized site.

Researchers have also used numerical models as tools to evaluate the effectiveness of soft streambank management techniques. For example, Enlow et al. (2018) developed a framework that used sediment and hydraulic transport models CONCEPTS, HEC-RAS, and Bank Stability and Toe Erosion Model (BSTEM), with several additional parameters, such as construction costs and effectiveness, to model and assess stabilization practices. This framework allowed for the testing of different techniques based on their sediment reduction and cost effectiveness. According to Enlow et al. (2018), bank shaping with a 2H:1V slope and vegetation was the most cost effective combination for bank stabilization in an Oklahoma stream using this tool.

Similarly, Simon et al. (2009) simulated the geotechnical and hydraulic processes responsible for mass wasting using the BSTEM. Through their numerical model, Simon et al. (2009) demonstrated that the use of toe rock reduced streambank erosion anywhere from 69% to 100% on the Upper Truckee River in California. Moreover, they found that vegetation on the banks further reduced bank erosion rates (Simon et al., 2009), which was also supported by Nassar (2019). Additionally, Frothingham (2008) used a stability threshold analysis of shear stress and velocity to analyze the ability of potential SBS techniques in reducing erosion.

Frothingham (2008) concluded that for Cazenovia Creek in New York, toe rock and vegetation would result in the most effective SBS design.

Alternatively, researchers have also used physical models to assess the effectiveness of soft techniques at reducing bank erosion. For example, Recking et al. (2019) conducted multiple flume experiments that differed in SBS design, discharge, bed mobility, and meander curvature. The study found that SBS techniques such as live fascines would often fail due to scouring caused by water recirculation behind the protective structure (Recking et al., 2019). In addition, toe rock and vegetation proved to be more effective on meanders with large radii of 22.5 to 30 meters (Recking et al., 2019). Overall, Recking et al. (2019) gave a glimpse of how physical models could be used to test the effectiveness of soft streambank management techniques under various conditions before they are implemented in the field.

In terms of field studies, Shields et al. (2000) noted that reaches that were only equipped with toe rock experienced a rise in flow velocities, which may lead to increased scouring in the near bank region, although there are no studies that actually quantify this effect (Bigham, 2020). Nevertheless, several researchers suggest using some type of instream flow deflector in addition to toe rock to promote the long-term success of projects (Anstead & Boar, 2010; Frothingham, 2008; Recking et al., 2019; Shields et al., 2000).

Soft streambank management techniques offer a promising approach to managing erosion along streams and rivers. While challenges still exist, such as the need for more comprehensive analyses of their reach scale and river scale effects (Buchanan et al., 2014; Cavaillé et al., 2018; Enlow et al., 2018; Khosronejad et al., 2013), the evidence suggests that soft streambank management techniques are a valuable tool for sustainable river management at the localized scale.

1.2 Research Gaps

Based on this literature review, several knowledge gaps that hindered the assessment of instream structures and streambank management techniques were identified and summarized here. The main research gaps with respect to SBS effectiveness include a need for longer timeframe monitoring that encompasses both pre- and post-stabilization and a broader spatial monitoring scale, such as reach scale (Anstead et al., 2012; Bhuiyan et al., 2009; Bigham, 2020; Buchanan et al., 2014; Cavaillé et al., 2018; Enlow et al., 2018; Florsheim et al., 2008; Khosronejad et al., 2013). Furthermore, Buchanan et al. (2014), Elhakeem et al. (2017), and Layzell, Peterson et al. (2022) highlighted the presence of a "break-in" period following SBS, during which SBS features undergo adjustments and settlements, a potential evolutionary stage during post-stabilization. Further monitoring is essential to accurately differentiate between a "break-in" phase and continued instability (Buchanan et al., 2014). Comprehensive collection of terrain data before and after stabilization at a broader time scale is essential to perform a thorough bank mobilization analysis and establish statistically significant results (Bigham, 2020). Understanding the spatiotemporal effectiveness of SBS hinges on addressing these gaps.

Moreover, additional localized studies of instream structures and streambank management techniques are necessary due to the inherent variability in site conditions and configurations (Bigham, 2020). While localized scale studies have garnered some attention, further research and modeling are still necessary to address these unique site specific challenges.

It is imperative to not only validate the effectiveness of SBS techniques at local and large scales but to also be able to predict where future erosion is likely to occur, in order to ensure the long-term success of these projects. While various types of stabilization techniques have been studied more closely in recent years (e.g., Layzell, Peterson, et al., 2022; Naisargi & Mittelstet, 2017; Russell et al., 2021b), this paper will evaluate the effectiveness of the SBS methods used on two specific sites along the Cottonwood River in Kansas on a reach scale, and attempt to answer the following question: “do streambank stabilization projects push the ‘erosion problem’ upstream or downstream?”

1.3 Hypothesis and Objectives

It is hypothesized that degradation will be the dominant fluvial adjustment directly upstream of the stabilized site, and aggradation will take place downstream. This prediction is based on the theory that SBS projects resemble the “area of maximum disturbance” (AMD) that was briefly described in Simon and Hupp (1986) in regard to channel evolution. Most SBS projects only focus on reducing and equalizing the sediment load on a localized scale but rarely consider the channel evolution as described by Simon & Hupp (1986). In these situations, SBS projects may produce segments of the river that act as “sediment transfer zones” or AMD (Cluer & Thorne, 2014). Based on this theory, the upstream area of the modified reach should experience channel degradation (perhaps localized aggradation following any over adjustment), and the downstream portion of the reach should experience aggradation that increases linearly with distance downstream of the SBS project.

With these hypotheses in mind, the following questions were answered in this research:

1. Does SBS decrease streambank erosion at the stabilized site?
2. Does SBS increase streambank erosion upstream or downstream of the SBS site?
3. Does SBS induce aggradation or degradation at the reach scale?
4. Does SBS affect stream power at the reach scale?

To answer these questions, a reach scale case study was conducted on two sites located upstream of the John Redmond Reservoir on the Cottonwood River in east-central Kansas. The reaches studied had length to bankfull width ratios of 40 and 20, respectively. This included an upstream unstabilized meander, a middle stabilized meander, and a downstream unstabilized meander. The following research objectives were completed:

- Evaluate lateral erosion rates pre- and post-stabilization by comparing channel cross sections from topographic surveys (Chapter 3).
- Assess reach scale bed erosion and/or deposition rates pre- and post-stabilization by comparing surface models created in Civil3D using bathymetric data (Chapter 3).
- Assess stream power at a reach scale pre- and post-stabilization by modeling SBS site configurations and reach conditions in HEC-RAS (Chapter 4).

Chapter 2 - Site Description: Cottonwood River, Kansas:

This study focuses on two specific reaches along the Cottonwood River, located in Chase and Lyon counties, in east-central Kansas, USA (Figure 2.1). The Cottonwood River, a tributary of the Neosho River, has a 4,928 km^2 watershed that is located within the Flint Hills ecoregion. This ecoregion is characterized by alternating layers of erodible shales and highly resistant cherty and flinty limestones (Frye & Leonard, 1959). The banks of the Cottonwood River are primarily composed of the Gunder Member of the DeForest Formation, which typically has silty clay loam to loam textures and relatively high clay content (Beeton & Mandel, 2011). The higher clay content in the soil of the Cottonwood River valley has been shown to be more resistant to erosion caused by hydraulic forces compared to other members of the DeForest Formation (Layzell & Mandel, 2014). However, high clay content streambanks tend to be more susceptible to mass wasting processes under rapid drawdown conditions (Simon et al., 2000).

Figure 2.1 Study area overview, highlighting the locations of the SBS sites within Kansas.

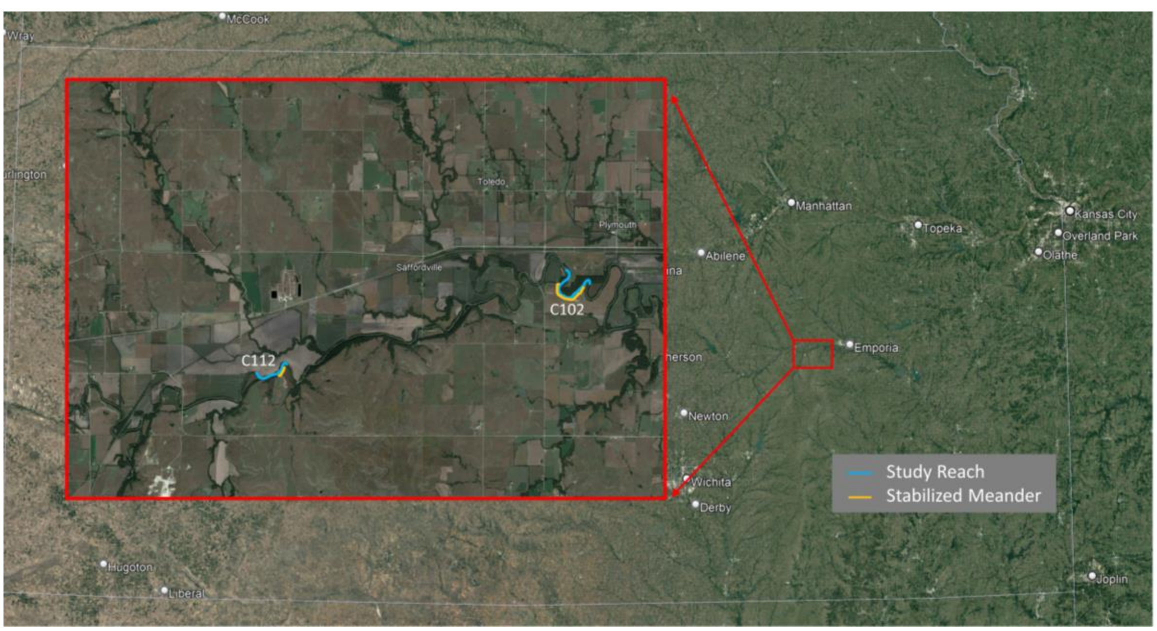

Land cover in the Cottonwood watershed is characterized as agricultural grassland (66%) and cropland (24%) (U.S. Geological Survey, 2014). The region's climate consists of warm humid summers and cold winters (Peel et al., 2007) with a mean annual precipitation that ranges from 750 mm to 900 mm (PRISM Climate Group, 2011). The Cottonwood River has a seasonally variable, storm generated flow regime with high flows normally occurring during the spring and summer months when the majority of the rainfall in this region takes place (Layzell, Peterson, et al., 2022). The stretch of Cottonwood River studied in this paper has a gravel to sand bed with a low channel gradient (0.0004 m/m to 0.0008 m/m) and an average sinuosity of 2.2 (Layzell, Peterson, et al., 2022). The typical bank heights along the Cottonwood River range from 7 to 12 m and the width-to-depth ratios range between 11 to 18 (Layzell, Peterson et al., 2022).

In the Midwestern United States, it has been shown that streambank erosion can be a leading contributor to sediment yield in a watershed (e.g., Fox et al., 2016; Juracek & Ziegler, 2007). In some cases, stream networks eventually transport this sediment into downstream reservoirs causing increased rates of sedimentation (Fox et al., 2016), and thus decreasing their storage capacity and overall effectiveness in reducing floods downstream, storing water, and providing habitat. For John Redmond Reservoir, located downstream of the Cottonwood River, this problem is especially troublesome, as this water is used for power generation, flood control, recreation, and wildlife management. The incised channel and bank failures along the Cottonwood River may suggest that the river system is undergoing channel degradation and widening (Stages III and IV; Figure 1.1; Simon & Hupp, 1986). A combination of gravitational forces acting on the channel's banks and hydraulic forces acting on the channel boundary cause bank erosion within the incised fluvial system (Layzell, Peterson et al., 2022).

Moreover, landowners along the Cottonwood River are losing valuable farm ground to bank erosion. Therefore, significant efforts are being made to stabilize the streambanks in an effort to slow bank retreat rates and extend the design life of the John Redmond Reservoir by reducing sedimentation rates. In fact, more than 350 streambank stabilization sites have been identified upstream of the John Redmond Reservoir and approximately 42 sites (12%) have already been completed by the State of Kansas Water Office in an effort to reduce downstream sedimentation rates (KWO, 2015).

As previously mentioned, this study focuses on two specific reaches of the Cottonwood River that are separated by approximately 11 river kilometers. Sites C102 and C112 (Figure 2.1) have total reach lengths of 1820 m and 1145 m, stabilized lengths of 1030 m and 400 m, drainage areas of 4478 km^2 and 4293 km^2, and average bank heights of 9.3 m and 8.9 m, respectively. These sites were identified as ideal locations for SBS projects due to historic bank retreat rates. Both sites are situated between railroad tracks to the north and higher elevation ground to the south. Approximately 350 meters of the reach immediately upstream of Site C112 is directly against the valley wall, with a nearly 10 meter high right bank and exposed limestone bedrock. Additionally, both stretches of river are surrounded by a narrow and sometimes sporadic buffer of deciduous trees before opening up to agricultural crop land. The channel slope differs slightly between the two reaches, with Site C112 having a slope of 0.00072 m/m and Site C102 having a lower slope of 0.0004 m/m.

Previous research conducted by Layzell et al., (2019, 2020, 2021, 2022) at sites C112 and C102 determined the sediment size distribution of both reaches using the modified Wolman pebble count and the wet sieve procedure. They reported the D_{50} within Site C112 to be 30 mm, corresponding to the gravel size class. In contrast, the bed material composition at Site C102 was found to be primarily fine, characterized by a D_{50} less than 0.075 mm, corresponding to the silt and clay size class (Layzell et al., 2020).

Each of the two study reaches consists of three meanders. The middle meander at each location contains a SBS project comprised of rock vanes, toe rock, bank shaping, and revegetation (Figure 2.2). The rock vanes were spaced 20 to 30 meters apart and angled upstream at 30 to 90 degrees tangential to the bank. The rock vanes were built to a height of 1.5 to 2 meters and sloped from the streambed to the bankfull elevation to ensure the vane's tip remains submerged even during low flow. Additionally, the rock vanes and toe rock were constructed using limestone rip rap with a D_{50} of 60 cm (Layzell, Peterson, et al., 2022). Toe rock was placed along the toe of the stabilized streambank of both sites at a height of 1.2 meters. The streambanks were shaped to a slope of 3H:1V, and a mix of sycamores and cottonwood trees were spaced 3 to 5 meters along the top of the bank to help establish a riparian buffer zone. The upstream and downstream meanders from the SBS project remained unmodified. Construction on sites C112 and C102 concluded in 2022.

Figure 2.2 Downstream view of the before and after construction at C112 illustrating the SBS techniques used on both C112 and C102.

This project utilized data from an USGS stream gage that is located between the two sites at the intersection of County Road A and the Cottonwood River, where Lyon and Chase County meet (Figure 2.3). USGS gaging station #07182250 has daily discharge data from March of 1963 to the present.

Figure 2.3 Map showing the location of USGS gage 07182250 and both study reaches.

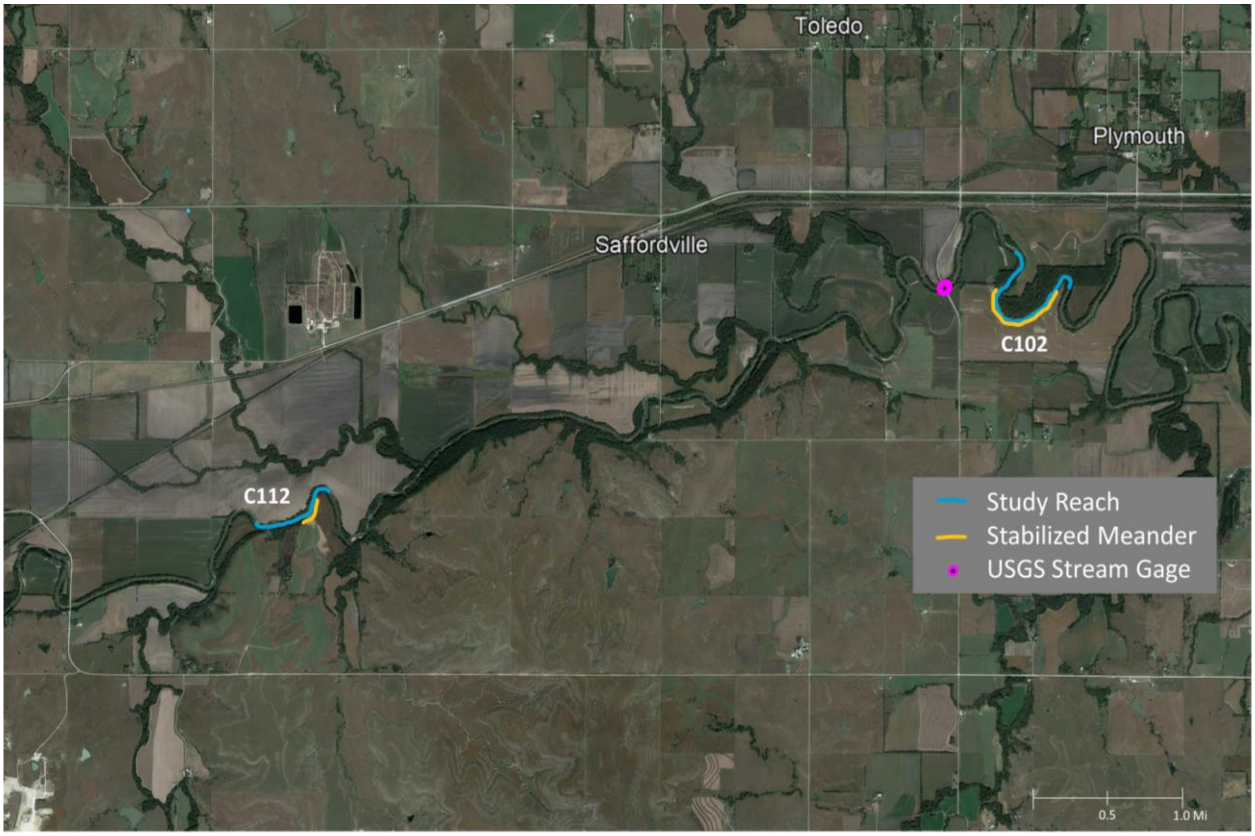

The 60 years of annual peak discharge data were used to conduct a Log-Pearson Type III Flood Frequency Analysis as shown in Figure 2.4. The bankfull discharge derived from this Flood Frequency Analysis was 299 cubic meters per second corresponding to the 1.5-year return interval flow event.

Figure 2.4 Log Pearson Type III Flood Frequency Plot for USGS Gage 07182250 near Plymouth, KS (1963 to 2023)

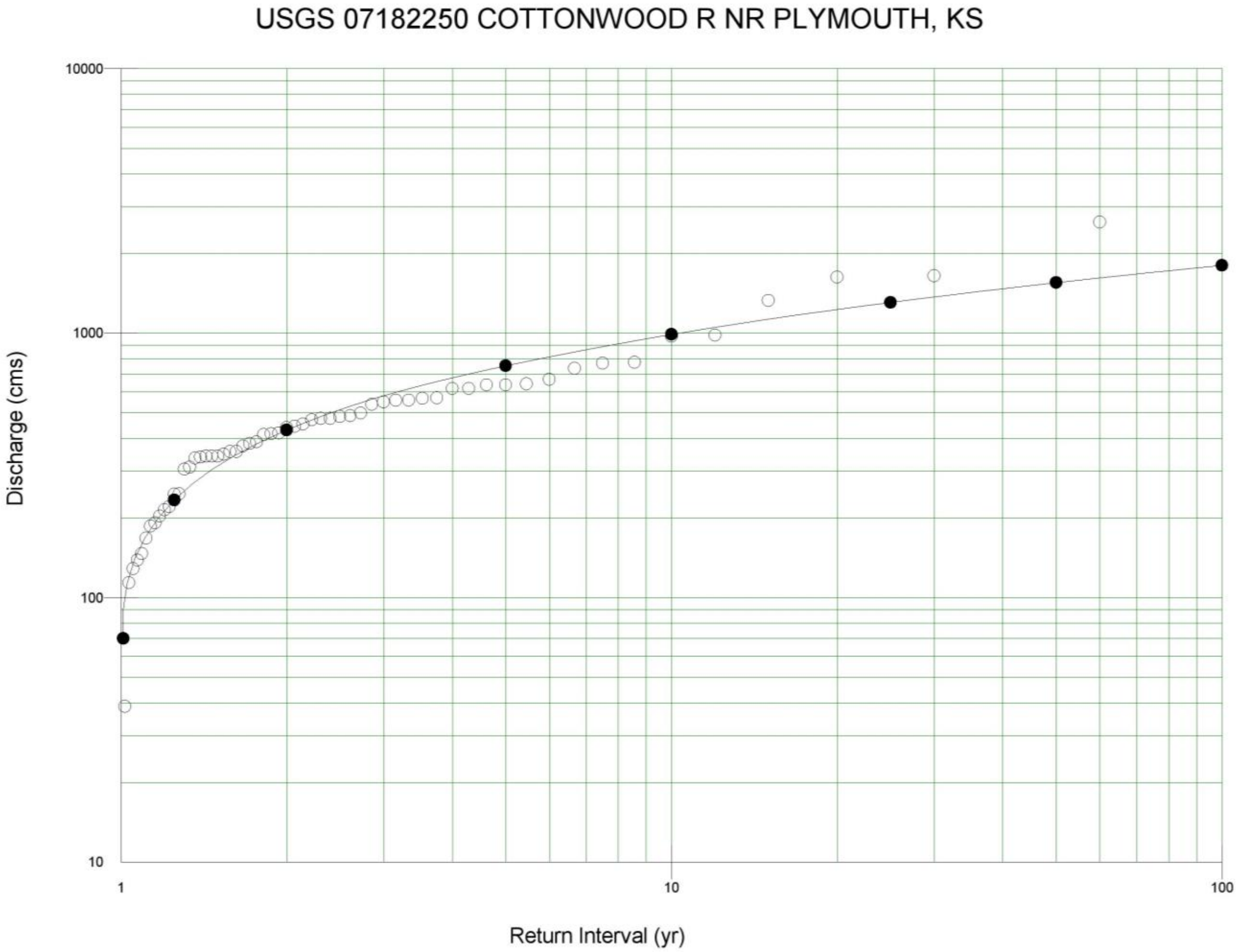

Chapter 3 - Effect of Streambank Stabilization on Reach Scale Streambank Erosion and Bed Stability

3.1 Introduction

Streambank erosion presents a significant challenge to river and stream ecosystems, often resulting in habitat loss, water quality degradation, and infrastructure damage (Arthington, 2012; Dudgeon et al., 2006; Fox et al., 2016; Nassar, 2019). To mitigate this issue, streambank stabilization (SBS) techniques have been developed and implemented, aiming to reduce erosion rates and enhance bank stability. Researchers have assessed a wide variety of SBS techniques in differing types and sizes of stream ecosystems. In particular, common methods of SBS in Kansas included rock vanes, toe rock, bank shaping, and vegetation (Layzell, Peterson, et al., 2022). While the overall effectiveness of SBS on the local scale is well documented (e.g., Hemmati et al., 2016; Hemmati & Daraby, 2019; Johnson et al., 2002; Karki et al., 2018; Layzell, Peterson, et al., 2022; Matsuura & Townsend, 2004; Naisargi & Mittelstet, 2017; Russell et al., 2021a, etc.), there is a need for longer timeframe reach scale monitoring and evaluation (Anstead et al., 2012; Bhuiyan et al., 2009; Bigham, 2020; Buchanan et al., 2014; Cavaillé et al., 2018; Enlow et al., 2018; Florsheim et al., 2008; Khosronejad et al., 2013).

The questions to be answered in this chapter include: (1) does SBS decrease streambank erosion at the stabilized site? (2) does SBS increase streambank erosion upstream or downstream of the SBS site? and (3) does SBS induce aggradation or degradation at the reach scale? This chapter will (1) evaluate lateral erosion rates pre- and post-stabilization by comparing channel cross sections from topographic surveys, and (2) assess reach scale bed erosion and/or deposition rates pre- and post-stabilization by comparing surface models created in Civil3D using bathymetric data. Streambank lateral retreat rate in units of meters of retreat per cubic kilometer of streamflow (m/km^3), net change in streambed volume in units of cubic meters (m^3), and visual overview maps showing the spatial extent of streambed elevation changes provide evidence of the impact of streambank stabilization techniques on streambank and streambed dynamics.

3.2 Methods

Beginning in 2018, sites C112 and C102 were monitored in both pre- and post-construction periods. Multiple topographic and bathymetric surveys were conducted on both reaches of the Cottonwood River from 2018 until 2024. For Site C112, three topographic surveys were completed prior to stabilization (surveyed in 2018, 2019, and 2021), and two were conducted after the project's completion (surveyed in 2022 and 2023). For Site C102, four topographic surveys were completed before SBS (surveyed in 2018, 2019, 2021, and 2022), with an additional two surveys executed after construction (surveyed in 2023 and 2024). The majority of these surveys at both sites took place before the SBS projects' implementation in order to establish a baseline for modeling and analysis. By collecting data before and after the implementation of the SBS, a before-after construction analysis could be conducted to examine changes in channel geometry along the two reaches. The topographic data were collected using a GeoMax Zoom90 Robotic Total Station. Each survey collected streambank surface data, as well as bathymetric data using the robotic total station. Data recorded at each point included northing, easting, elevation, point number, and point description.

At each site, paired rebar pins, with one on the right top of the bank and a counterpart on the left bank top perpendicular to the stream flow, were utilized as permanent benchmarks for cross sections, allowing for consistent monitoring. Sites C112 and C102 had 9 and 11 permanently marked channel cross sections, respectively. Each permanent cross section was surveyed at intervals ranging from 0.5 to 2 meters between data points, depending on surface slope changes. This detailed approach captured cross sections with heightened resolution, ensuring more accurate lateral retreat calculations.

The cross sections for Site C112 were situated in the upstream, middle, and downstream meanders as shown in Figure 3.1. Cross Section 1 is positioned at the apex of the upstream unstabilized meander, while Riffle Cross Section 1 is located midway between the upstream and middle meander. Additionally, Cross Sections 2, 3, 4, and Riffle Cross Section 2 are spaced approximately 80 meters apart in the middle stabilized meander. Finally, Cross Sections 5 through 7 are situated within the downstream unstabilized meander. The spatial distribution of the cross sections allows for a reach scale assessment of lateral retreat rates, not only in the immediate vicinity of the SBS techniques but also in the adjacent meanders.

Figure 3.1 Aerial image of Site C112 with the cross section in the upstream (bottom left), middle (center), and downstream meanders (top right). XS refers to cross section, while RXS refers to riffle cross section.

The cross sections for Site C102 were strategically positioned across the upstream, middle, and downstream meanders as shown in Figure 3.2. Riffle Cross Section 1 was located at the furthest upstream location, followed by Cross Sections 1 and 2 within the upstream unstabilized meander, and then Cross Sections 3 through 7 in the middle stabilized meander. Moving downstream, Riffle Cross Section 2 and Cross Section, 8 and 9 were situated within the downstream unstabilized meander. This spatial distribution of the cross sections allows for an evaluation of lateral retreat rates of the entire reach.

Figure 3.2 Aerial image of Site C102 with the cross sections in the upstream (top), middle (bottom), and downstream meanders (right). XS refers to cross section, while RXS refers to riffle cross section.

Supplementary channel data were gathered throughout the entire longitudinal extent of each reach to fill in the spaces between permanent cross sections and enhance the triangulated irregular network (TIN) surface models produced in AutoCAD Civil3D. Non-benchmarked cross sections were surveyed approximately every 10 meters down the length of the channel in order to gather additional terrain data at key breakline features such as the streambank toe, edge of water, scour holes, and other distinct changes in slope. When combined with the higher resolution permanent cross sections, these non-benchmarked cross sections helped create detailed channel TIN models.

3.2.1 Streambank Lateral Retreat Rate Analysis

Streambank lateral retreat rates were calculated for the pre- and post-stabilization periods by comparing sequential channel cross sections. The average lateral retreat rate (R) for a given channel cross section was calculated using the formula:

Equation 3.1 Normalized Lateral Retreat Rate

$$R = \frac{A_d}{V * H}$$

Where R represents the average lateral retreat rate (m/km^3), A_d represents the difference in area between consecutive cross sections (m^2), V represents the total streamflow volume that occurred between survey missions (km^3), and H represents the average bank height of the compared cross sections (m). This equation normalizes the lateral retreat rate with the corresponding flow volume observed between survey periods, allowing for direct comparisons across different time period lengths with various flow volumes. In this context, positive lateral retreat rates represent erosion, while negative lateral retreat rates represent deposition.

The streambank analysis began with importing station and elevation data from each permanent cross section into Microsoft Excel. The concave bank of the meander served as the focus for lateral changes (i.e., the bank of interest; Nunnally & Keller, 1979). The next step was to calculate the area of the bank of interest between the top of the streambank and the streambank toe. The midpoint estimation method was used in Excel to calculate these areas. After determining the area of each streambank, the difference in area (A_d) was obtained by subtracting the area of the cross section surveyed in the previous year from that of the more recent cross section. For example, Cross Section 2 at site C112 was surveyed in 2018 and 2019, with calculated areas of 154.65 and 165.10 square meters, respectively, resulting in a positive A_d of 10.45 square meters, as shown in Figure 3.3.

Figure 3.3 Elevation profile depicting the difference in cross-sectional area for the right bank of Cross Section 2 at Site C112 between 2018 and 2019.

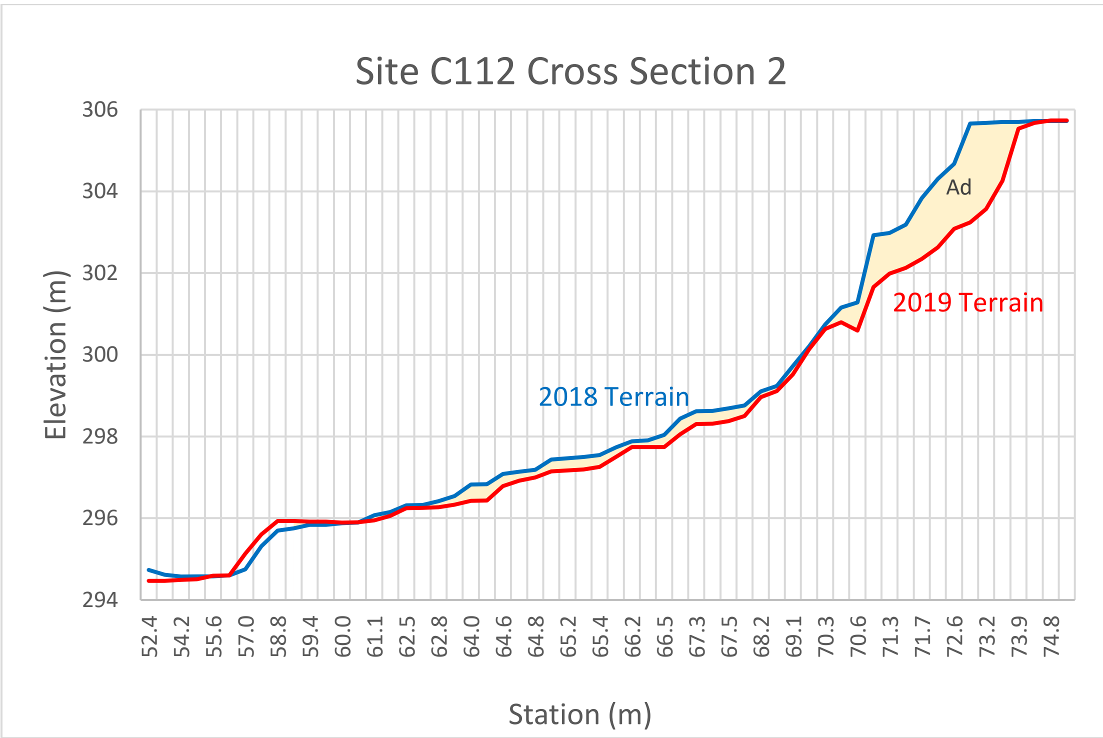

For Site C112 and C102, the differences in area for each cross section between all pre- and post-stabilization monitoring periods were calculated and summarized in Appendix A.

The next step was to determine the total volume of streamflow that passed through the cross sections between each survey. Daily streamflow data from the USGS stream gage (USGS 07182250) on the Cottonwood River near Plymouth, Kansas were downloaded and inserted into Excel. The average daily streamflow rates were assumed to closely approximate the average daily streamflow that passed through each site, due to the relatively close proximity of the USGS stream gage to both study sites, as shown in Figure 2.3. The average daily streamflow was then converted into total daily flow volumes by multiplying the flow rate by seconds in a day. Finally, the total daily flow volumes were summed together based on their corresponding timeframe. Refer to Appendix A for the flow volumes at each site.

The final parameter needed to calculate the lateral retreat rate is the average bank height. To obtain this value, the bank height for each cross section was derived from surveyed elevations at the top of bank and the streambank toe. The bank heights were then averaged between consecutive surveys. Appendix A has the complete summary of average bank heights for each site. Lastly, the variables were input into Equation 3.1 to calculate the lateral retreat rates for each of the timeframes between the survey missions.

3.2.2 Streambed Volume Surface Analysis

A streambed analysis was conducted using AutoCAD Civil3D 2019 to examine changes in the streambed elevation during both pre- and post-stabilization periods. The process began by importing topographic and bathymetric data from each survey mission into Civil3D, organizing each survey into distinct point groups, and assigning them to their own TIN surface models. Before analyzing the surfaces generated in Civil3D, adjustments were made to the TIN to ensure the surface models captured distinct features observed in the field, such as rock vanes, scour holes, and debris piles. After refining each individual streambed surface, consecutive streambed surface models were overlaid to create volume surfaces. The output provided numerical net cut (erosion) and fill (deposition) values, along with plan view maps for visually representing bed changes spatially.

3.3 Results and Discussion

3.3.1 Streambank Analysis Results

The cross section identification (XS ID), corresponding bank of interest (BOI), and lateral retreat rates for Site C112 are summarized in Table 3.1. The retreat rates for Site C112 were predominantly erosional in the years leading up to construction, especially within the soon to be stabilized portion of the reach. However, the majority of the stabilized cross sections switched from positive retreat rates to negative lateral retreat rates, suggesting that the SBS techniques caused the river to deposit sediment on the surface of the streambank at a localized scale. In contrast, the majority of the unstabilized cross sections in the upstream and downstream meanders became more erosional in the timeframe immediately after the project's completion.

Table 3.1 Summary of Normalized Lateral Retreat Rates for Site C112. Bolded XS IDs correspond to the stabilized cross sections. * denotes post-stabilization timeframe. A negative retreat rate corresponds to streambank deposition.

Site C112 Lateral Retreat Rate (m/km^3)				
XS ID - BOI	2018 to 2019	2019 to 2021	2021 to 2022	2022 to 2023*
XS 1 - Right	-0.20	-0.30	-0.39	0.29
XS 2 - Right	0.47	0.55	Construction	0.71
XS 3 - Right	0.99	0.71	Construction	-2.45
XS 4 - Right	1.26	0.13	Construction	-1.92
RXS 2 -Right	1.74	0.11	Construction	-0.90
XS 5 - Left	-0.46	1.39	-0.14	2.87
XS 6 - Left	0.43	0.72	0.92	0.02
XS 7 - Left	0.25	0.29	0.44	5.00
Negative Retreat Rate = Deposition (Green)		Positive Retreat Rate = Erosion (Red)		

Taking a closer look at the results revealed several details. Starting at the upstream end of Site C112, Cross Section 1 displayed a notable shift from deposition before and during construction, with rates ranging from -0.20 to -0.39 m/km^3, to an erosional rate post-construction as shown by the positive lateral retreat rate of 0.29 m/km^3. Despite being the only cross section in the upstream unstabilized meander, Cross Section 1 provides evidence suggesting the potential impact of downstream construction efforts on the upstream segment of Site C112; however, more years of post-construction data are required to confirm.

Moving downstream, Riffle Cross Section 1 was positioned as a "control" cross section on a nearly 350 meter long exposed bedrock riffle (see Figure 3.5). The yearly survey data and streambed analysis confirm that this section of the reach is extremely stable, and thus the lateral retreat rates for this riffle cross section were not included in Table 3.1. Furthermore, the presence of bedrock serves as grade control, preventing knickpoints from migrating upstream.

For Cross Section 2 found within the SBS, the lateral retreat rates were determined to be 0.47 and 0.55 m/km^3 in the timeframes before construction. Following construction, the lateral retreat rate slightly increased to 0.71 m/km^3, consistently maintaining an erosional trend before and after construction. Additionally, it is worth noting that Cross Section 2 is located at the beginning of the construction zone and the end of a bedrock riffle. Therefore, Cross Section 2 may be influenced by the transition from the riffle's steeper bed slope to the shallower slope of the meander bend.

The right banks of cross sections 3, 4, and Riffle Cross Section 2, all found within the SBS, exhibited erosional rates during the pre-construction periods, ranging from 0.11 to 1.74 m/km^3. Following construction, these three cross sections transitioned to negative lateral retreat rates spanning from -0.90 to -2.45 m/km^3, indicating localized deposition. The reduced lateral retreat rates within the stabilized zone are consistent with the decrease in streambank erosion reported by Naisargi & Mittelstet (2017) and Russell et al. (2021b), who both evaluated rock vane structures using aerial imagery. Additionally, the reduced erosion rates post-stabilization align with the findings of Layzell, Peterson, et al. (2022), who also observed lower local scale erosion rates following stabilization.

In terms of the streambank downstream of the SBS, the left bank of Cross Section 5 displayed lateral retreat rates ranging from -0.46 to 1.39 m/km^3 before the completion of construction. However, during the initial post-construction period, the lateral retreat rate increased to 2.87 m/km^3. In contrast, Cross Section 6 shifted from lateral retreat rates ranging from 0.43 to 0.92 m/km^3 to a nearly neutral retreat rate of 0.02 m/km^3 during the post-construction period. Meanwhile, Cross Section 7 maintained consistently low lateral retreat rates in the pre-construction periods, ranging from 0.25 to 0.44 m/km^3, but then increased to 5.00 m/km^3 during the post-construction era. This increase in the lateral retreat rate at Cross Section 7 aligns with the broader trend observed in the unstabilized segments of C112, where numerous cross sections experienced increased erosion rates immediately after construction.

The XS ID, corresponding BOI, and lateral retreat rates for Site C102 are summarized in Table 3.2. The retreat rates for Site C102 were predominantly erosional in the years leading up to construction, especially within the soon to be stabilized portion of the reach. After construction, all of the stabilized cross sections switched from positive retreat rates to negative lateral retreat rates, suggesting that the SBS techniques caused sediment to be deposited on the surface of the streambank at the localized scale. In contrast, the majority of the unstabilized cross sections in the upstream and downstream meanders became more erosional in the timeframe immediately after the completion of Site C102.

Taking a closer look at the lateral retreat rates for C102 revealed several details. Starting at the upstream end of the reach, cross sections 1 and 2 recorded their highest lateral retreat rates during the post-stabilization timeframe, with rates of 1.94 and 2.17 m/km^3, respectively. These two upstream cross sections provide evidence suggesting the potential impact of downstream construction efforts on the upstream segment of Site C102, however, more years of post-construction data are required to confirm.

Table 3.2 Summary of Lateral Retreat Rates for Site C102. Bolded XS IDs correspond to the stabilized cross sections. * denote post-stabilization timeframe. A negative retreat rate corresponds to streambank deposition.

Site C102 Lateral Retreat Rate (m/km^3)					
XS ID - BOI	2018 to 2019	2019 to 2021	2021 to 2022	2022 to 2023	2023 to 2024*
XS1 - Left	0.44	0.55	1.61	-6.39	1.94
XS2 - Left	0.06	0.57	0.32		2.17
XS3 - Right	1.00	0.67	-0.47	Construction	-4.44
XS4 - Right	0.85	0.02	2.50	Construction	-2.63
XS5 - Right	0.69	0.85	0.72	Construction	-2.72
XS6 - Right	0.56	1.29	0.23	Construction	-1.86
XS7 - Right	1.05	0.60	0.44	Construction	-5.65
XS8 - Left	NA	0.63	-0.01	0.35	8.51
XS9 - Left	NA	0.53	0.32	-1.93	-4.99
Negative Retreat Rate = Deposition (Green)			Positive Retreat Rate = Erosion (Red)		

For Cross Section 3 found within the SBS, the lateral retreat rates were determined to be 1.00, 0.67, and -0.47 m/km^3 in the timeframes before construction. Following construction, the lateral retreat rate decreased to -4.44 m/km^3, switching from mainly erosional retreat rates to a large depositional retreat rate after construction. Similar observations can be made with cross sections 4, 5, 6, and 7, all found within the SBS. The right bank of these cross sections exhibited erosional rates during the pre-construction periods, ranging from 0.02 to 2.50 m/km^3. Following construction, these four cross sections transitioned to negative lateral retreat rates spanning from -2.63 to -5.65 m/km^3, indicating localized deposition. Notably, the post-construction retreat rates for sites C102 and C112 and numerous papers that also found similar SBS techniques to be effective at reducing erosion rates locally (e.g., Bressan et al., 2014; Elhakeem et al., 2017;

Layzell, Peterson et al., 2022; Naisargi & Mittelstet, 2017; Russell et al., 2021b; Simon & Steinemann, 2000).

The left bank of Cross Section 8, in the downstream unstabilized cross section, displayed lateral retreat rates ranging from -0.01 to 0.63 m/km^3 before the completion of construction. However, during the initial post-construction period, the lateral retreat rate increased to 8.51 m/km^3. In contrast, Cross Section 9 shifted from lateral retreat rates ranging from 0.32 to 0.53 m/km^3 to retreat rates of -1.93 and -4.99 m/km^3 during construction and post-construction, respectively. This shift in the lateral retreat rate from erosional to depositional may be explained by localized deposition stemming from a tree that fell down the left bank between the 2023 and 2024 surveys. The medium sized tree is positioned along the cross section line of Cross Section 9 and is anchored by the remaining roots still attached to the top of the bank.

The streambank analysis determined the pre- and post-stabilization lateral retreat rates of 17 permanent cross sections spread between the lengths of sites C112 and C102. For Site C112, seven out of eight cross sections were consistently erosional pre-stabilization (see Table 3.1). For Site C102, all of the permanent cross sections were erosional the majority of the time prior to being stabilized (see Table 3.2). However, after implementing the SBS techniques, a pattern emerged in the lateral retreat rates of both sites. In general, the streambank in the upstream and downstream unstabilized meanders began to retreat laterally at even higher rates. This held true even for Cross Section 1 at Site C112, which exhibited deposition throughout the periods leading up to construction. Some exceptions to the pattern were observed, such as Cross Section 9 in the downstream unstabilized meander of Site C102, which switched to deposition in the post-stabilization period (Table 3.1). However, this anomaly could be explained by localized deposition caused by a fallen tree along the cross section line.

For the middle stabilized meanders at both sites, a new depositional pattern emerged. All of the stabilized cross sections switched from erosional to depositional lateral retreat rates, except for Cross Section 2 at Site C112 which is located just downstream of an exposed bedrock shelf that acts as a grade control structure. This suggests that the SBS techniques were effective at stabilizing the eroding banks at the localized scale, but may have increased streambed erosion along the outside bend of the adjacent unstabilized meanders.

It is noted that these results are limited by a lack of post-stabilization data and only encompasses one timeframe in the post-construction phase for both sites. This makes it difficult to determine whether the initial post-stabilization results are indicative of a localized or perhaps a reach scale "break-in" period, or if these patterns can be expected long-term.

While the streambank analysis was designed to be comprehensive, several factors made this difficult. For instance, the analysis lacked survey data from 2020 due to restrictions during the COVID-19 pandemic. Consequently, the timeframe from 2019 extends to 2021. Additionally, the summer of 2022 survey for Site C102 was hindered by vegetation that obstructed the line of sight between the total station and the survey rod. As a result, the timeframe for Cross Section 2 extends from 2021 to 2023. Moreover, cross sections 8 and 9 were added to Site C102 after the project received additional funding. Therefore, the assessment of these two cross sections started in 2019 (refer to Table 3.2). Lastly, bank shaping activities occurred between 2021 and 2022 for Site C112, and between 2022 and 2023 for Site C102. This resulted in artificially high lateral retreat rates during these timeframes. Ultimately, this led to neglecting the retreat rates for the stabilized cross sections during those periods, as evident by the greyed out “construction” cells in Tables 3.1 and 3.2.

3.3.2 Streambed Analysis Results

The location, monitoring timeframes, and estimates of sediment erosion and deposition within the bed for both sites are summarized in Table 3.3. Additionally, Appendix B contains plan view maps visually highlighting areas of streambed deposition and erosion within each reach. The monitoring period from 2018 to 2019 contained a notable streamflow event on May 9th, 2019, reaching a peak of 892 m^3/s and corresponding to a 10-year return interval flow as derived from the Flood Frequency Analysis (Figure 2.4). This monitoring period exhibited higher cut values for both reaches. At Site C112, a net streambed change of 2,311 cubic meters was observed, with 62% attributed to erosion and 38% to deposition. The bed bathymetry remained predominantly stable between cross sections 1 and 2, where the river is positioned against the valley wall, exposing limestone bedrock. However, substantial erosion occurred along the outer bend of the middle meander, extending from Cross Section 2 to Riffle Cross Section 2 (refer to Appendix B, Figure B.1).

Table 3.3 Summary of reach scale streambed erosion (cut) and deposition (fill) for Sites C112 and C102. Shaded cells correspond to the timeframes when construction took place. Positive net values correspond to net cut (erosion). APD refers to annual peak discharge.

Location	2018 to 2019			2019 to 2021			2021 to 2022			2022 to 2023			2022 to 2024		
	Cut (m^3)	Fill (m^3)	Net (m^3)	Cut (m^3)	Fill (m^3)	Net (m^3)	Cut (m^3)	Fill (m^3)	Net (m^3)	Cut (m^3)	Fill (m^3)	Net (m^3)	Cut (m^3)	Fill (m^3)	Net (m^3)
c112	5,967	3,656	2,311	3,453	3,691	-238	4,967	2,016	2,951	1,947	1,985	-38	N/A	N/A	N/A
c102	10,464	4,311	6,153	7,908	4,402	3,506	4,473	4,060	413	700	4,503	-3,803	2,223	7,673	-5,451
APD Return Interval	10-year			1.6-year			1.8-year			< 1-year			1-year		

Meanwhile, Site C102 experienced a net streambed change of 6,153 cubic meters, characterized by 71% erosion and 29% deposition. This resulted in a lowering of the thalweg by approximately 0.3 meters across the majority of the reach (refer to Appendix B, Figure B.5). The observed pattern during this timeframe highlights the potential impact of significant streamflow events on streambed erosion. This monitoring period recorded substantial cut quantities, with both sites displaying notable changes in streambed morphology, indicating a response to the intensified flow conditions.

During the 2019 to 2021 timeframe which had a peak flow of 374 m^3/s and a return interval of 1.6 years (Figures 2.4 and 3.4), the streambed at Site C102 continued to lower along the outer bank of meander bends, accounting for 64% of the observed changes, while deposition only amounted to 36%. This resulted in a net cut of 3,506 cubic meters. In contrast, the active streambed at Site C112 exhibited a nearly balanced net change of 238 cubic meters of fill, with 52% deposition and 48% erosion. This marked a significant switch from the previous monitoring period, where a net export of sediment was observed in 62% of the reach.

Figure 3.4 Stream discharge data from USGS Gage 07182250 on the Cottonwood River and the corresponding survey timeframes for sites C102 and C112. Blue bars denote construction period.

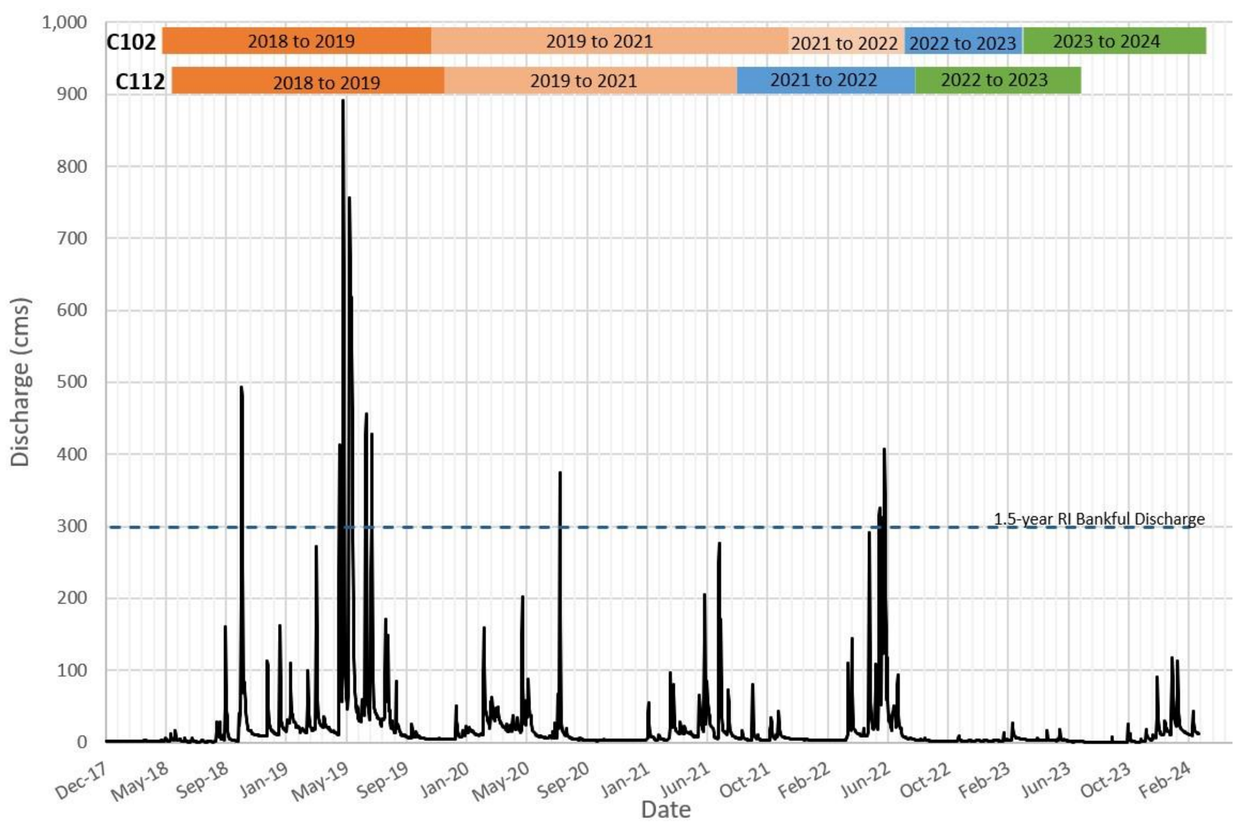

The monitoring period from 2021 to 2022 marked the implementation of SBS techniques at Site C112. During this timeframe, which had a peak flow of 408 m^3/s and a return interval of 1.8 years (Figures 2.4 and 3.4), a notable shift was observed for Site C112, as the active bed experienced 4,967 cubic meters of cut (71%). These results were similar to the 2018 to 2019 period. However, this timeframe was influenced by bank shaping activities and the fill volume of six newly constructed rock vanes (Layzell et al., 2022). As a result, the formation of scour holes off the tips of several rock vanes was observed (Figure 3.5). While these scour holes added to the overall cut volume, the majority of streambed degradation took place in the downstream meander as evident in Figure B.3 in Appendix B.

Figure 3.5 Site C112 streambed elevation map from August 2022 depicting newly formed scour holes between Cross Section 3 and Riffle Cross Section 2.

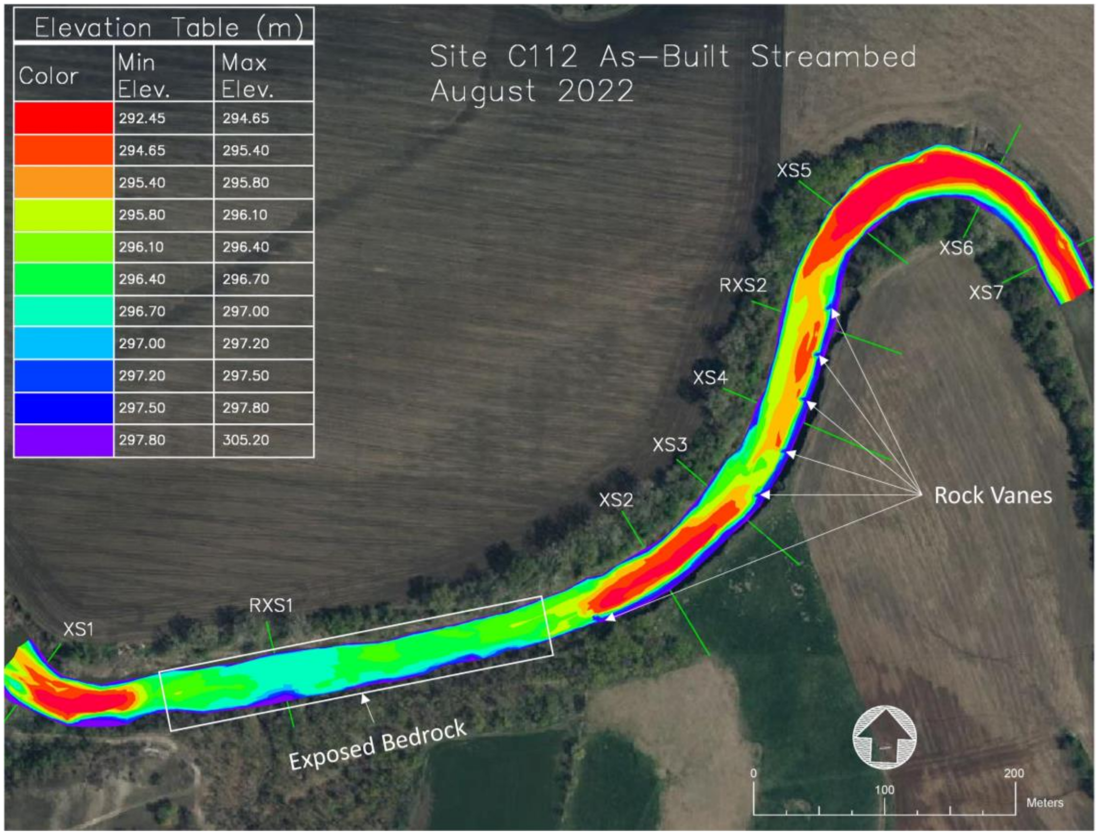

Meanwhile, Site C102 remained unmodified during the 2021 to 2022 period. The streambed analysis revealed bed erosion and deposition to be nearly equivalent with 52% and

48%, respectively. Despite a historical trend of greater cut than fill quantities in the previous periods, the cut volume during this timeframe was considerably low compared to earlier periods. The cause behind this observation remains unclear, and Layzell et al., (2022) questioned whether these results are related to upstream construction activities, such as those on Site C112, or if they represent a natural rate of bed change.

In the period from 2022 to 2023 in which the peak flow was 27 m^3/s (Figure 3.4), both sites exhibited a net deposition, shifting away from previous trends. Site C112 demonstrated the closest value to zero net change compared to all other timeframes, with 38 cubic meters of deposition, resulting from 1,947 cubic meters cut and 1,985 cubic meters fill. Notably, Site C102 experienced a dramatic shift towards streambed deposition, registering a net fill of 3,803 cubic meters, with 13% cut and 87% fill. This major shift aligns with the SBS construction and lack of large magnitude floods at Site C102 during this timeframe. Field observations also supported the streambed analysis, noting extreme sedimentation within the active streambed following the bank shaping activities. Additionally, the streambed analysis for Site C102 during this timeframe focused exclusively on the stabilized portion of the reach. Limited topographic data availability in the upstream and downstream meanders restrained a comprehensive evaluation of the entire streambed during this timeframe for Site C102 (Appendix B, Figure B.8).

To combat the lack of streambed data in the upstream and downstream meanders from the 2023 survey of Site C102, an additional timeframe was developed to span from 2022 to 2024, encompassing the 2023 survey and the SBS construction. During this period, in which the peak flow was 118 $m^3/$ corresponding to a 1 year return interval (Figures 2.4 and 3.4), Site C102 exhibited a net deposition of 5,451 cubic meters, with 22% cut and 78% fill.

The post-stabilization depositional trend is likely due to the low stream flow that both sites experienced after construction. While the net change during the timeframe was mainly depositional throughout both sites, the streambed in the upstream and downstream unstabilized meanders did experience erosion along the outside bank as evident by the majority of the erosion coming from these locations (Appendix B, Figures B.4 and B.9). Table 3.4 illustrates how each section of the reach—upstream unstabilized meander, middle stabilized meander, and downstream unstabilized meander—varied in the ratio of cut to fill. By comparing the relative percentages of cut and fill for the entire reach to those of the segmented sections, it becomes clear that the upstream and downstream meanders often had a higher percentage of erosion compared to the overall percentage of cut for the entire reach. Although the net change tended to remain depositional, the higher relative percentage of streambed erosion in the adjacent unstabilized meanders is consistent with increased lateral retreat rates in those same unstabilized areas, suggesting a connection between SBS, streambed dynamics, and streambank retreat. However, it's worth noting that the post-stabilization streambed analysis for C102 lacked streambed data from 2023 within the adjacent unstabilized meanders. Therefore, the analysis for C102 spans from 2022 (pre-construction) to 2024 (post-construction), which may contribute to the subtle differences in the cut and fill percentages between the two sites. Additional data collection from the post-stabilization timeframe is needed to better understand the effects of SBS on the streambed of both sites.

Table 3.4 Summary of post-stabilization streambed erosion (cut) and deposition (fill) for Sites C112 and C102 categorized by location within the reach as both volume and relative percent volume. Green cells correspond to the timeframes with net deposition. Red cells correspond to timeframes with net erosion (positive net values). * denotes the timeframe for C102 encompasses construction activities.

Location:	**Entire Reach**			**Upstream Unstabilized Meander**			**Middle Stabilized Meander**			**Downstream Unstabilized Meander**		
Site (Timeframe)	**Cut (m^3)**	**Fill (m^3)**	**Net (m^3)**	**Cut (m^3)**	**Fill (m^3)**	**Net (m^3)**	**Cut (m^3)**	**Fill (m^3)**	**Net (m^3)**	**Cut (m^3)**	**Fill (m^3)**	**Net (m^3)**
C112 (2022 to 2023)	1,947	1,985	-37	1,113	610	503	424	602	-179	410	771	-361
	49.5%	50.5%	N/A	64.6%	35.4%	N/A	41.3%	58.7%	N/A	34.7%	65.3%	N/A
C102 (2022 to 2024*)	2,223	7,673	-5,451	731	1,288	-556	596	4,760	-4,164	895	1,625	-730
	22.5%	77.5%	N/A	36.2%	63.8%	N/A	11.1%	88.9%	N/A	35.5%	64.5%	N/A

The elevated percentage of fine material in Site C102, in contrast to Site C112, likely contributes to the increased bed lowering observed in the streambed analysis, as the unconsolidated fine bed material (D_{50} = 0.075mm) in Site C102 can be mobilized more easily over a broader range of flow events. In comparison, the prevalence of coarser sand and gravel sediments (D_{50} = 30mm), as well as the bedrock riffle in Site C112 may explain the slightly greater streambed stability (Layzell et al., 2020).

The streambed analysis determined the pre- and post-stabilization streambed volume changes of sites C112 and C102 (see Table 3.3). The first monitoring timeframe experienced a high net loss of streambed material due to the 10-year return interval flow event that occurred during this period. In the subsequent periods leading up to the construction activities, the streambed cut values dwindled towards zero. This reduction in streambed erosion is most likely attributed to the corresponding decrease in the frequency and intensity of flow events.

For Site C112, the combination of lower flow events and larger streambed particle size compared to Site C102 resulted in a net gain of streambed material during the 2019 to 2021 timeframe leading into the construction phase. However, the similarities between the two sites diverged during their respective construction phases. Site C112 recorded its highest net cut value during this timeframe, while Site C102 recorded its lowest cut value, resulting in a high net fill (Table 3.3). Several factors may have contributed to these differences. For example, during the construction phase of Site C112, three flow events greater than the 1.5-year return interval flow were measured at the USGS stream gauge. These flow events, ranging between 300 to 400 m^3/s (see Figure 3.4), helped remove loose sediment caused by bank shaping activities. In contrast, during the construction phase of Site C102, the greatest flow event was recorded at 27 m^3/s. This, combined with the increased sediment load from nearby bank shaping activities, resulted in a high net fill value.

During the post-stabilization timeframes, the USGS stream gage recorded zero flow events that exceeded the 299 m^3/s bankfull discharge threshold (Figure 3.4). This resulted in net streambed deposition for both sites (Table 3.3). The streambed deposition observed post-stabilization for both sites may be attributed to additional sediment being mobilized from the streambank as a result of the bank shaping activities and the absence of substantial flow events necessary to transport sediment. Further analysis into the most recent streambed survey from the post-stabilization phase of Site C102, which was hindered by a lack of bathymetry data in the upstream and downstream meanders from the 2023 survey, reveals that a net deposition of sediment occurred throughout the entire reach.

The hypothesis presented in Chapter 1 proposed that degradation would dominate upstream of the stabilized site, with aggradation occurring downstream. However, the data collected during the initial post-construction period did not support this hypothesis. Instead, both upstream and downstream reaches predominantly experienced deposition. This suggests that the stabilized site did not function as expected as a "sediment transfer zone." The sediment deposition occurred in both directions from the stabilized site, contrary to the predicted patterns of erosion and deposition. This discrepancy may be attributed to fluctuations in stream flow, particularly the low magnitude flows following stabilization, which were insufficient to transport sediment effectively.

However, despite both sites favoring deposition at the reach scale during the post-stabilization timeframe, the streambed maps presented in Appendix B depict erosion along the outside bend of the upstream and downstream meanders, suggesting potential areas where the bank toe is being destabilized. Simultaneously comparing the streambank and streambed analyses reveals that the localized bed erosion along the outside of meander bends aligns with the increased lateral retreat rates recorded in the upstream and downstream permanent cross sections. This connection between the streambank and streambed analyses, which were based on field data, helps provide a deeper understanding of the river's dynamics.

3.4 Summary

This chapter evaluated reach scale lateral retreat rates and bed erosion and/or deposition rates pre- and post-stabilization by comparing channel cross sections and TIN surface models, respectively. The streambank analysis of sites C112 and C102 offered insights into the morphological changes along the Cottonwood River. For example, the streambank analysis of both sites showed a decrease in lateral retreat rates within the stabilized meander, whereas the upstream and downstream unstabilized meanders displayed an increase in retreat rates.

The streambed analysis conducted on both Site C112 and Site C102 offered insights into the bed dynamics of the Cottonwood River. Notably, considerable variations in net streambed volume change were observed across different timeframes for both sites, likely influenced by fluctuations in flow conditions and the implementation of SBS techniques. The analysis highlighted a connection between the magnitude of net volume change and the particle size distribution of each site, with Site C102, which was characterized by finer particles, consistently exhibiting greater cut and fill values compared to Site C112. Over the period from 2018 to 2024, the streambeds of both sites experienced a net sediment loss, totaling 4,986 m^3 for Site C112 and 4,621 m^3 for Site C102, pointing to an overall lowering of the streambed during this survey timeframe. However, it's important to note that most of the streambed surveys were conducted before the implementation of SBS, possibly skewing the data towards pre-stabilization conditions. Therefore, further monitoring is crucial to assess the long-term effects of SBS and accurately understand the ongoing dynamics of the Cottonwood River's streambed.

Chapter 4 - Effect of SBS on Reach Scale Stream Power

4.1 Introduction

Streambank erosion poses a major threat to the stability of river and stream ecosystems, often resulting in habitat loss, water quality degradation, and infrastructure damage (Arthington, 2012; Dudgeon et al., 2006; Fox et al., 2016; Nassar, 2019). In response, SBS techniques have been developed to reduce erosion rates and enhance bank stability. The State of Kansas, for instance, has implemented various methods such as rock vanes, toe rock, bank shaping, and vegetation (Layzell, Peterson, et al., 2022). While the local-scale effectiveness of these techniques is well-documented (e.g., Hemmati et al., 2016; Hemmati & Daraby, 2019; Johnson et al., 2002; Karki et al., 2018; Layzell, Peterson, et al., 2022; Matsuura & Townsend, 2004; Naisargi & Mittelstet, 2017; Russell et al., 2021a, etc.), there remains a crucial gap in longer-term, reach scale monitoring and evaluation (Anstead et al., 2012; Bhuiyan et al., 2009; Bigham, 2020; Buchanan et al., 2014; Cavaillé et al., 2018; Enlow et al., 2018; Florsheim et al., 2008; Khosronejad et al., 2013). This chapter aims to analyze the effects of SBS on the reach scale by using stream power as an indicator of channel morphology and erosion (Bizzi & Lerner, 2013).

The question to be answered in this chapter is: does SBS affect stream power at the reach scale? To answer this, stream power was assessed at a reach scale for both pre- and post-stabilization periods by modeling site configurations and reach conditions in HEC-RAS using 2D hydrodynamic numerical modeling. According to Miller (2022), HEC-RAS is often utilized as a hydraulic modeling tool to aid in the design of streambank stabilization practices across various locations and organizational affiliations in the U.S. This chapter describes the development of two HEC-RAS 2D models for the study sites along the Cottonwood River, where SBS projects have previously been executed. The HEC-RAS models help provide insight into the effects of

SBS on stream power along the Cottonwood River. Results from the RAS model can be used to better understand observed bank erosion and bed dynamics, as discussed in Chapter 3.

4.2 Methods

4.2.1 HEC-RAS 2D Modeling

HEC-RAS is capable of computing a wide range of hydraulic calculations. The numerical methods for hydrodynamic modeling are briefly described in this section. Foundational equations in the 2-dimensional HEC-RAS models are described below. The mass conservation equation (Equation 4.1) ensures both the conservation of mass and the continuity of water volume within the models, assuming that water is incompressible.

Equation 4.1 Mass Conservation Equation (USACE, 2024b)

$$\frac{\partial h}{\partial t} + \nabla \cdot (hV) = \mathrm{q}$$

Here, h is water depth, t is time, ∇ is the gradient operator, V is the velocity vector, and q is a source/sink flux term.

The Shallow Water Equations (SWE) and the Diffusion Wave Equations (DWE) are the two equation sets capable of routing 2-dimensional unsteady flow through the models (Equations 4.2 and 4.3). While DWE is faster and more stable, it approximates the more mathematically robust SWE. The SWE accounts for the acceleration term, making it suitable for natural channels and more precise computations around structures characterized by mixed flow regimes. The SWE also has options for modeling Coriolis effects and turbulence (USACE, 2024b). The primary advantages of the simplified momentum equation in the DWE are its stability and computational efficiency, while also being reasonable accurate in steady and consistent stream flow scenarios (USACE, 2024b).

Equation 4.2 SWE Conservation of Momentum (USACE, 2024b)

$$\frac{\partial V}{\partial t} + (V \cdot \nabla)\mathrm{V} + f_c k \times V = -g\nabla z_s + \frac{1}{h}\nabla \cdot (\nu_t \mathrm{h}\nabla \mathrm{V}) - \frac{\tau_b}{\rho R} + \frac{\tau_s}{\rho h} - \frac{1}{\rho}\nabla p_a$$

Here, V is the velocity vector, t is time, ∇ is the gradient operator, f_c is the Coriolis parameter, k is the unit vector in the vertical direction, g is the gravitational acceleration, z_s is the water surface elevation, h is the water depth, ν_t is the horizontal eddy viscosity coefficient, τ_b is the bottom shear stresses, ρ is the density of water, R is the hydraulic radius, τ_s is the surface wind stresses, and p_a is the atmospheric pressure.

Equation 4.3 DWE Conservation of Momentum (USACE, 2024b)

$$V = -\frac{R^{2/3}}{n} \frac{\nabla z_s + \frac{1}{\rho g}\nabla \mathrm{pa} - \frac{\tau_s}{\rho g h}}{|\nabla z_s + \frac{1}{\rho g}\nabla \mathrm{pa} - \frac{\tau_s}{\rho g h}|^{1/2}}$$

Here, V is the velocity vector, R is the hydraulic radius, n is Manning's roughness coefficient, ∇ is the gradient operator, z_s is the water surface elevation, ρ is the density of water, g is the gravitational acceleration, p_a is the atmospheric pressure, τ_s is the surface wind stresses, and h is the water depth.

The Manning's equation (Equation 4.4) is used to calculate flow velocity in open channels. The shear stress equation calculates the magnitude of shear stress exerted on a surface by water (Equation 4.5). The stream power equation is closely linked to shear stress and can be used as in indicator of fluvial dynamics (Equation 4.6; Bizzi & Lerner, 2013).

Equation 4.4 Manning's Equation (USACE, 2024b)

$$V = \frac{1.486}{n} * R^{2/3} * S^{1/2}$$

Here, V is flow velocity (m/s), n is Manning's Roughness Coefficient, R represents the hydraulic radius (m), and S is the friction slope (m/m).

Equation 4.5 Shear Stress Equation (USACE, 2024b)

$$\tau = \gamma * R * S_f$$

Here, τ symbolizes shear stress (Pa), ɣ represents the specific weight of water (kg/m^3), R represents the hydraulic radius (m), and S represents the friction slope (m/m).

Equation 4.6 Stream Power Equation (USACE, 2024a)

$$\omega = v * \tau$$

In this equation, ω symbolizes stream power (kg*m^2/s^3), v represents flow velocity (m/s), and τ represents shear stress (Pa). For a more in-depth explanation of the calculations performed by HEC-RAS refer to the United States Army Corps of Engineers HEC-RAS Hydraulic Reference Manual (USACE, 2024b).

4.2.2 HEC-RAS Model Development

Figure 4.1 illustrates the step-by-step process of developing the HEC-RAS models of sites C112 and C102, encompassing data collection through result analysis. The process of developing 2D hydrodynamic models for the two sites began using HEC-RAS 6.3 (USACE, 2024b). A geometry file was generated within the RAS project, and the spatial reference system was set to "North American Datum of 1983 Kansas South State Plane FIPS 1502" and units to meters. A terrain layer was generated, and the TIN surface derived from topographic data was converted into a digital elevation model (DEM) and imported into the HEC-RAS software. In addition to bed and bank topographic data collected using a robotic total station (see Chapter 3), annual UAS surveys were conducted to complement the yearly topographic surveys. These UAS surveys focused on acquiring detailed DEMs of the post-stabilization streambank surface, providing a high resolution depiction of the streambank following bank shaping activities. The UAS data bridged the gap between the topographic survey of the channel and the LiDAR data of the surrounding floodplains. For further details on the UAS survey methods, refer to Layzell, Peterson et al. (2022). The 2018 LiDAR data captured the elevation of the surrounding terrain and floodplain. The assumption was that the surrounding terrain remained constant from the pre- to post-stabilization timeframe.

Figure 4.1 Flowchart of 2D HEC-RAS modeling process.

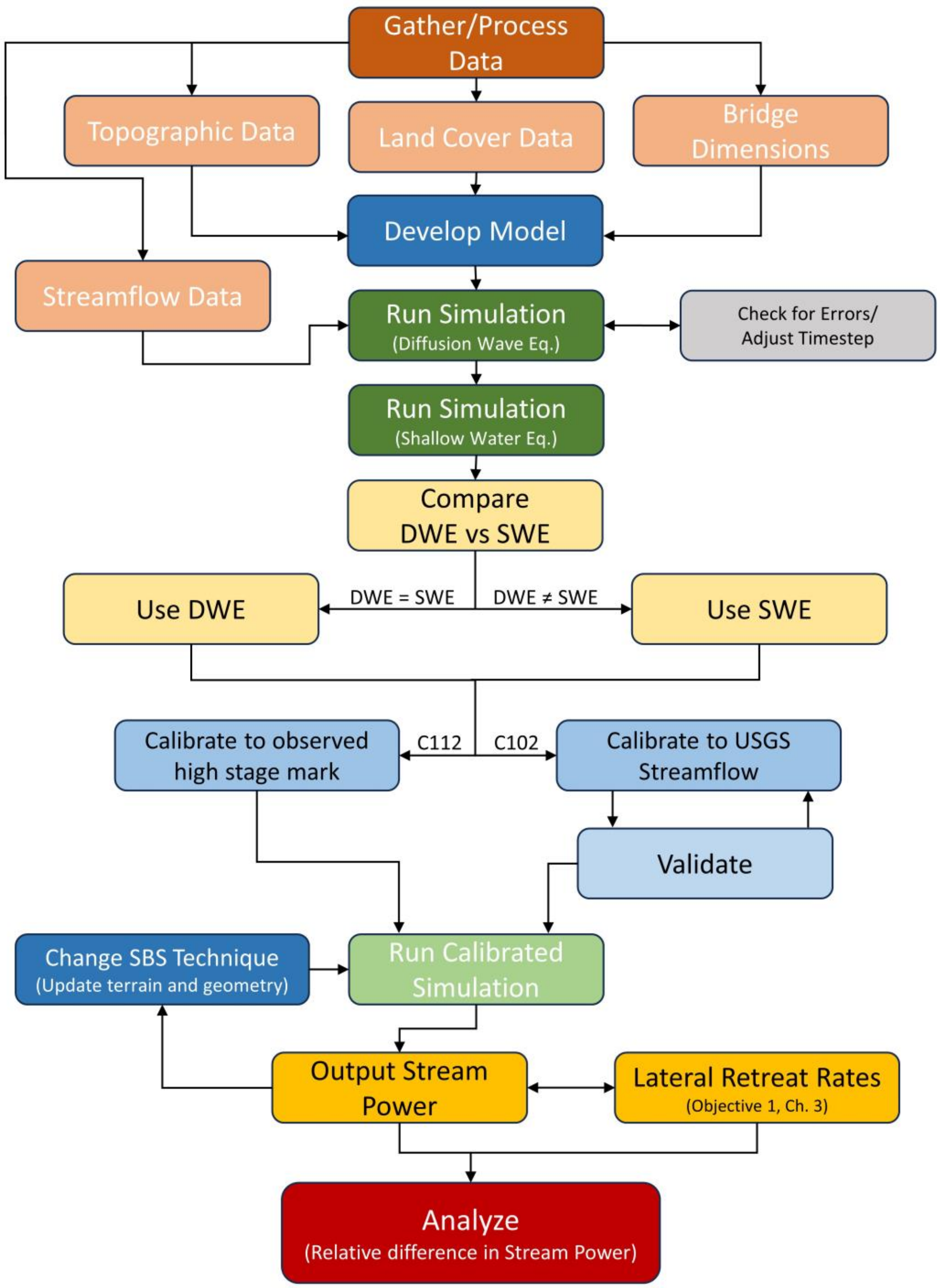

The total station, UAS, and LiDAR data were all processed into DEMs in the tiff file format to import into HEC-RAS. The total station data were positioned above the UAS data and the UAS data was positioned above the LiDAR data, ensuring field-collected data took priority over the other data sources. This resulted in a complete DEM with each raster pixel assigned an elevation value. Once the appropriate terrain layer was generated, it was associated with the geometry file, thereby connecting the terrain with the geometry for future computation.

Land use and cover data were sourced from the National Land Cover Database (NLCD) and used as a baseline for Manning’s n values (Equation 4.4) and spatial extent of various land cover types. The NLCD data, which is a raster with 30 by 30 meter resolution, was imported into a newly established land cover layer. This created an approximation of the land cover in general locations. However, this resolution did not accurately represent the actual land cover in specific areas. To address this limitation, a sub layer was generated, and classification polygons were created over the latest aerial imagery to precisely delineate the boundaries between land cover types. Next, each distinct land cover was assigned an initial Manning’s n value based on the values reported by Chow (1959). In addition, the classification polygons were modified for the post-construction simulations to align with the anticipated land cover. The land cover layers were associated with the corresponding geometry file.

Once the terrain and land cover layers were incorporated into the project file, the next steps involved creating the 2D flow area and boundary condition lines. First, a perimeter outlining the boundary of the 2D flow area was developed (Appendix C, Figure C.1). To guide the perimeter placement, a Log Pearson Type III Flood Frequency Analysis was used to determine the return intervals of streamflow events during the monitoring timeframe, with the largest flow event in May 2019 estimated to have a 10-year return interval (Figure 2.4). The boundary was then delineated based on terrain features with higher elevations, guided by the FEMA floodplain map, representing the 1% AEP flood. For example, both sites utilized the railroad tracks as the northern boundary because they were situated above the FEMA floodplain. Additionally, higher elevation features such as roads and hills were used to define the southern boundary for both sites (refer to Appendix C, Figure C.1).

The 2D flow area configurations enabled the western and eastern borders to serve as the inlet and outlet, respectively, for simulated flow events. Careful consideration was given to select these boundaries to align with straight sections of the river, ensuring one-dimensional flow along the perimeter. The boundary lines were designed to encompass the study sites, while also accommodating the potential extent of floodplains in future simulations.

During this process, the standard cell mesh size for the entire 2D flow area was established at 30 meters by 30 meters, resulting in hundreds of cells, each containing computation points that could be refined and adjusted to prevent errors. One common issue encountered was cells with more than eight sides, which were flagged in red by HEC-RAS. These cells could be fixed by either adding or removing cells to reduce the number of sides. Additionally, further refinements to the standard cell size could be made in specific areas that require more detail (i.e., main channel, roads, etc.).

The next step involved integrating breaklines into the 2D flow area. Breaklines align the cell faces to important features such as top of bank, river centerline, roads, ditches, creek channels, and swales. These features, where terrain slopes vary, affect the flow of water and require more detail to be properly computed by the model. The breaklines were configured to refine the resolution in the adjacent cells to be as detailed as 7.5 meters by 7.5 meters depending on the breaklines location. The main channel required the highest resolution, while less significant features, such as swales far from the study sites, were set to relatively larger cell sizes (Appendix C, Figure C.2).

After incorporating the breaklines into the 2D flow area, refinement regions were introduced to provide additional resolution and detail within the main river channel. The refinement regions allowed for the adjustment of mesh resolution within a designated multipoint polygon. The refinement regions were placed along the main channels of Site C112 and Site C112, with a cell size of 7.5 meters by 7.5 meters (Appendix C, Figure C.3).

Finally, boundary condition lines were established just outside the 2D flow area to mark the inlet and outlet of the models. Positioned parallel to the perimeter of the computational mesh, these lines delineated where the flow would initiate and terminate through the computational mesh. Figure 4.2 provides a visual representation of the final computational mesh and boundary lines for each site.

Figure 4.2 HEC-RAS boundary condition lines for Site C112 (top) and Site C102 (bottom). The pink line corresponds to the upstream boundary condition (west), and the blue line corresponds to the downstream boundary condition (east).

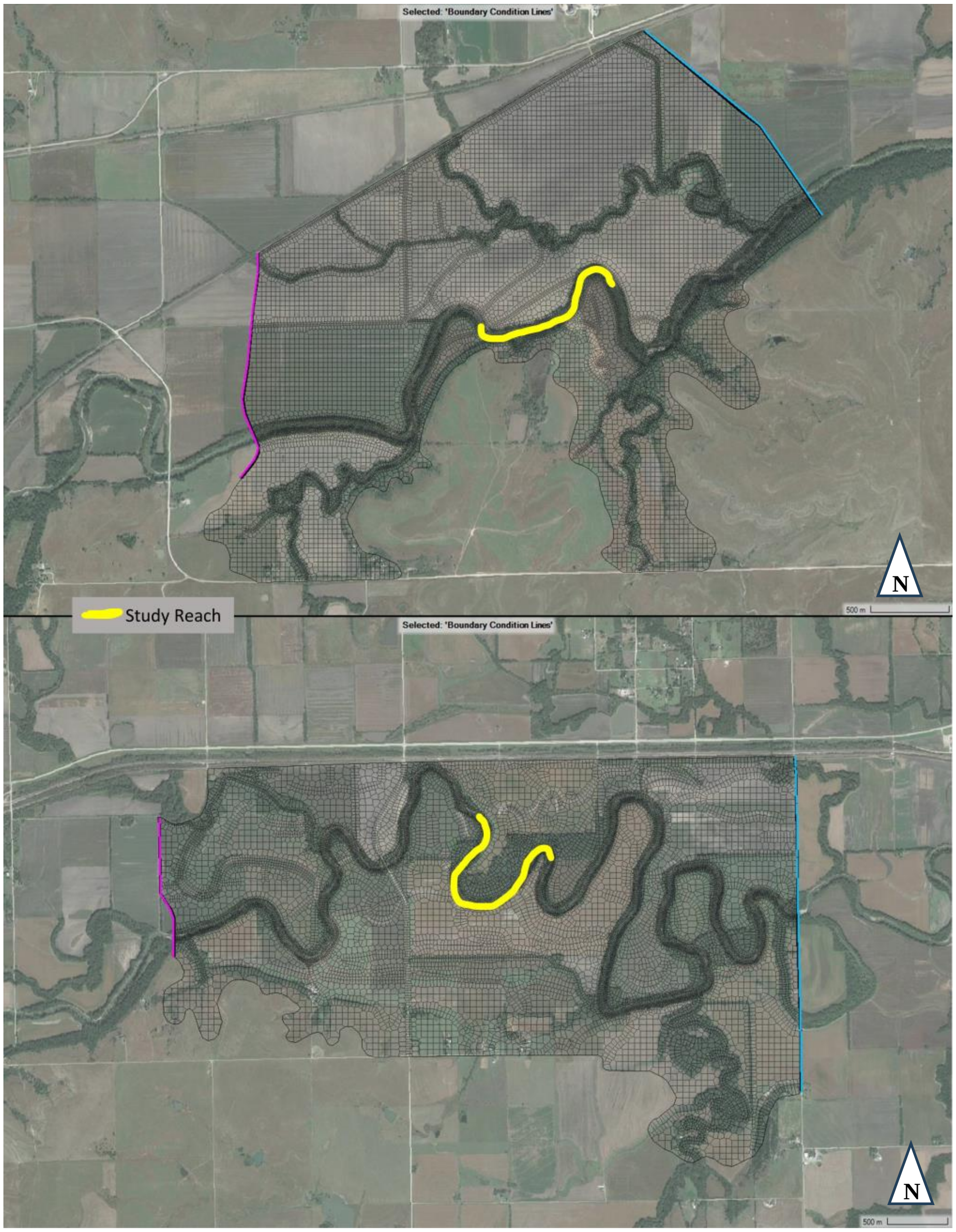

The upstream boundary condition for both sites utilized a flow hydrograph derived from observed daily flow data obtained from the USGS stream gage. Hydrologic data were collected from USGS Gage 07182250 from September 5, 2018, to December 31, 2023, and the flow hydrograph was used to calibrate, validate, and simulate various flow conditions in the 2D HEC-

RAS models. Precipitation was not factored into the models, and the sole flow into the systems occurred through the western boundary. Conversely, the downstream boundary condition was set as the normal depth, which was calculated in HEC-RAS using the quasi-equilibrium friction slope of the respective reaches. Based on the annual surveys, friction slopes were determined to be 0.00072 m/m and 0.0004 m/m for sites C112 and C102, respectively. The model for Site C102 also needed to incorporate the bridge located approximately 1.5 kilometers upstream of the monitored reach at the intersection of the Cottonwood River with County Road A (location of the USGS stream gage). The bridge deck and piers were modeled into HEC-RAS using surveyed bridge dimensions (Figure 4.3).

Figure 4.3 HEC-RAS bridge plan view map (top) and cross section view (bottom).

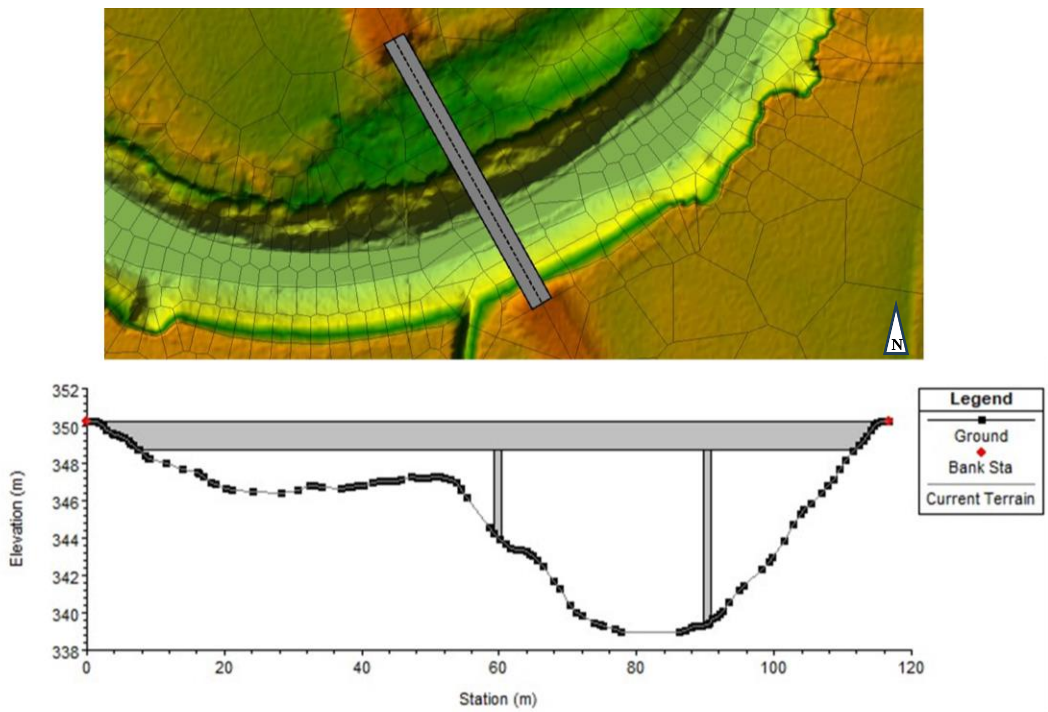

4.2.3 HEC-RAS Model Simulations

After creating the models, the next step was to run HEC-RAS simulations (refer to Figure 4.1). Unsteady flow analysis simulations were conducted in HEC-RAS utilizing the flow hydrograph data spanning from April 15th, 2019, to May 15th, 2019. This simulation timeframe included the largest flow event observed during the monitoring period, which was chosen for its significance in assessing the model's response to extreme hydraulic conditions.

The "Geometry Preprocessor" and "Unsteady Flow Simulation" options were enabled, followed by the selection of time step controls. A maximum Courant number of 1 and a minimum Courant number of 0.4 were specified, with 5 steps below the minimum before doubling. Additionally, the maximum number of doubling base time steps was set to 3 (80 seconds), and the maximum number of halving base time steps was also set to 3 (1.25 seconds). The Courant methodology was defined as velocity/length. Moreover, the "Initial Conditions Time" was configured to 48 hours to ensure the channel was filled with water before commencing the simulation.

The final step before running the unsteady flow analysis plan was to select the "Equation Set." Initially, both sites were set to the DWE due to its faster computation time and stability. The models were executed, and the results were saved within RAS Mapper. Then, both HEC-RAS models were switched to use the full SWE. The results for the SWE plan were also saved into RAS Mapper and the two different equation sets were compared using RAS Mapper. As previously depicted in Figure 4.1, if the water surface elevations and velocities produced by both equation sets are similar, then the DWE would be chosen for all future simulations due to its computation speed and comparable results (refer to Equation 4.3). However, if the two equation sets produced different results, then the SWE would be preferred for its enhanced accuracy in calculating flow velocities and water surface elevations within natural channels and around structures (refer to Equation 4.2).

After conducting simulations with both the DWE and the SWE, discrepancies were observed between the outputs of the two equation sets. Specifically, the SWE yielded flow velocities ranging from 0.61 m/s faster to 1.31 m/s slower than those calculated by the DWE, varying depending on the specific location within the channel. Similarly, there were notable variations in water surface elevations between the two equation sets. Therefore, for the remainder of this study, simulations were conducted exclusively using the SWE to ensure more mathematically sound and accurate results.

4.2.4 HEC-RAS Model Calibration

The next phase, as depicted in the flowchart in Figure 4.1, involves calibrating the 2D HEC-RAS models. The model for Site C112 is located approximately 10 river kilometers upstream of the USGS stream gage, while Site C102 encompasses the stream gage near the upstream extent of the model. Due to each site's proximity to the USGS stream gage, two different approaches were used to calibrate the models. Site C112 was calibrated to a flood event that drowned crops in a field, leaving behind a prominent high stage mark captured in an aerial image. In contrast, the calibration of Site C102 relied on stream flow data recorded by the USGS stream gage.

4.2.4.1 C112 Model Calibration

For the calibration of Site C112, aerial images captured in October 2019 were utilized, providing clear indications of a high stage mark resulting from a recent flood event. The flow hydrograph from the preceding growing season was analyzed, identifying the flow event with the highest magnitude as the probable cause of the high stage mark. Figure 4.4 highlights the high stage mark in the 2019 aerial image.

Figure 4.4 Aerial image from October 12th, 2019, highlighting the high stage mark at Site C112.

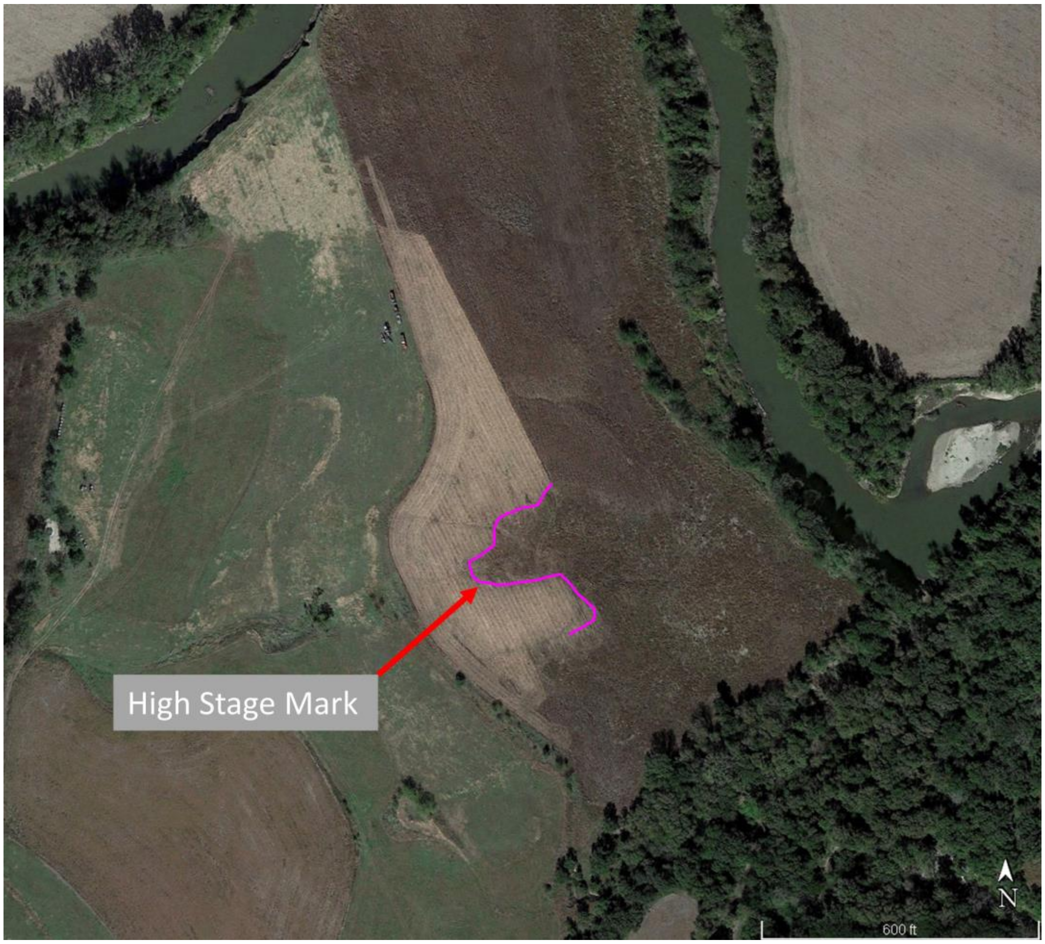

The flow event occurring from May 6th to May 12th, 2019, with a peak flow of 892 m^3/s, was the largest stream flow event, surpassing other flow events by nearly 150 m^3/s. This event was identified as the likely cause of the high stage mark captured in the aerial image. To calibrate the model to this mark, adjustments were made to the Manning's n values within the land cover layer until the water surface elevation aligned with the observed aerial image. All adjustments adhered to the recommendations outlined by Chow (1959), and the final adjusted Manning's n values are detailed in Table 4.1. Figure 4.5 shows the water surface elevation matching the high stage mark captured in the aerial image using the finalized Manning's n values from Table 4.1.

Table 4.1 Finalized Manning's n Values for Site C112 HEC-RAS model.

NLCD ID	Name	Manning's n
1	Main Channel	0.04
11	Open Water	0.04
21	Developed, Open Space	0.035
22	Developed, Low Intensity	0.08
23	Developed, Medium Intensity	0.12
24	Developed, High Intensity	0.15
31	Barren Land Rock-Sand-Clay	0.03
41	Deciduous Forest	0.08
42	Evergreen Forest	0.15
43	Mixed Forest	0.12
52	Shrub-Scrub	0.05
71	Grassland-Herbaceous	0.045
81	Pasture-Hay	0.045
82	Cultivated Crops	0.04
90	Woody Wetlands	0.07
95	Emergent Herbaceous Wetlands	0.045

Figure 4.5 Calibrated HEC-RAS model depicting water surface elevation aligning with the high stage mark at Site C112.

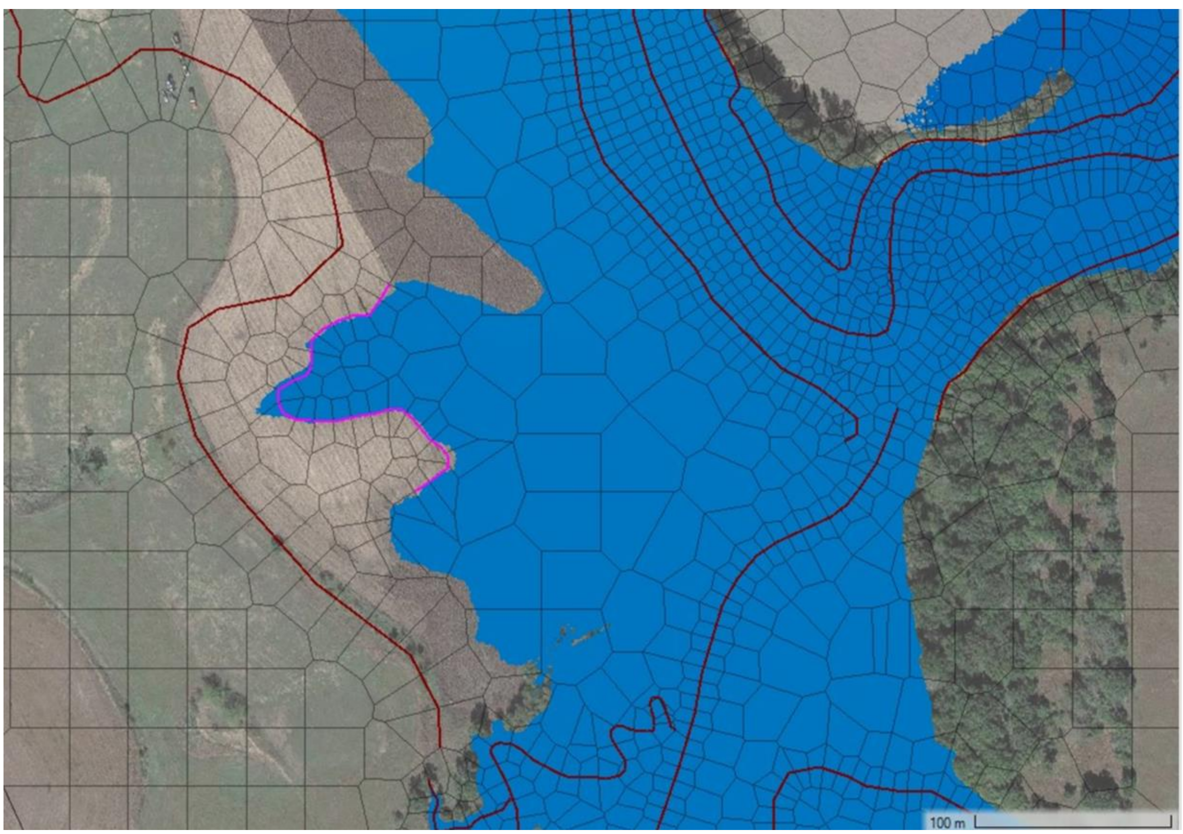

4.2.4.2 C102 Model Calibration and Validation

For Site C102, the calibration process involved comparing the simulated flow at the bridge cross section with the flow recorded by the USGS stream gage (USGS 07182250) between September 10th, 2018 to November 10th, 2018. Initially, the model utilized Manning's n values from recommendations from Chow (1959). Adjustments were made systematically to the main channel and deciduous forest Manning's n values. It was determined that the model was most sensitive to changes to these two land covers and were therefore the focus of adjustment.

A spreadsheet was developed in Excel to compare the simulated versus measured flows by calculating several goodness-of-fit statistics including Nash-Sutcliffe Efficiency (NSE), percent bias (PBIAS), and root mean square error (RMSE, Moriasi et al., 2007; Koehn, 2023). Moriasi et al., (2007) states that if the NSE approaches 1 and the PBIAS and RMSE both approach zero, then there is a good fit between measured and simulated. Table 4.2 summarizes the goodness-of-fit statistics for each calibration trial and presents the finalized Manning's n value for the main channel and deciduous forest. In addition, the calibrated model was validated using the timeframe from July 1st, 2020 to August 31st, 2020, as well as a post-stabilization timeframe from April 20th, 2023 to May 30th, 2023. The validation results, as depicted in Table 4.3, show the model's ability to estimate stream flow in timeframes outside of the calibration window. Table 4.4 summarizes the finalized Manning's n values for Site C102.

Table 4.2 Summary of goodness of fit statistics for Site C102 calibration trials.

Calibration Number	Manning's n for Main Channel	Manning's n for Deciduous Forest	NSE	PBIAS	RMSE
1	0.045	0.10	0.9904	3.856	10.22
2	0.040	0.10	0.9960	2.085	6.61
3	0.035	0.10	0.9988	0.702	3.68
4	0.035	0.11	0.9984	0.905	4.17
5	0.035	0.09	0.9990	0.493	3.32
6	0.035	0.08	0.9992	0.274	3.04

Table 4.3 Summary of goodness of fit statistics for Site C102 validation trials.

Validation Trials	Manning's n for Stream Channel	Manning's n for Deciduous Forest	NSE	PBIAS	RMSE
Summer 2020 Flow Event	0.035	0.08	0.9984	0.1881	2.6941
Post-construction Spring 2023 Flow Event	0.035	0.08	0.9975	-0.3500	0.1688

It is important to note that none of the flow events during the monitoring periods from 2018 to 2024 resulted in a scenario where the water surface matched the bridge chord elevation. However, if such a situation were to occur, the model would require recalibration to account for pressurized flow, and potentially weir flow if floodwaters reached a level where they could overtop the bridge deck.

Table 4.4 Finalized Manning's n Values for Site C112 HEC-RAS model.

NLCD ID	Name	Manning's n
1	Main Channel	0.035
11	Open Water	0.035
21	Developed, Open Space	0.035
22	Developed, Low Intensity	0.08
23	Developed, Medium Intensity	0.12
24	Developed, High Intensity	0.15
31	Barren Land Rock-Sand-Clay	0.03
41	Deciduous Forest	0.08
42	Evergreen Forest	0.15
43	Mixed Forest	0.12
52	Shrub-Scrub	0.05
71	Grassland-Herbaceous	0.045
81	Pasture-Hay	0.045
82	Cultivated Crops	0.04
90	Woody Wetlands	0.07
95	Emergent Herbaceous Wetlands	0.045

When comparing the finalized Manning's n values between Site C112 and Site C102, it's evident that the calibrated values were remarkably similar, with only one notable difference observed in the land cover values for the "main channel" or "open water". For Site C112, the

Manning’s n for open water was determined to be 0.040, whereas for Site C102, the value was slightly lower at 0.035. This discrepancy could potentially be attributed to subtle variations in the streambed sediment size distribution between the two reaches. Site C112 exhibited more gravel and sand compared to the predominantly silt and clay composition of Site C102. This difference in sediment composition may result in a slightly rougher channel surface at Site C112, thereby leading to a marginally higher Manning’s n value.

Additionally, the models underwent testing with the conservative turbulence model option activated in HEC-RAS. This feature allows the user to adjust the longitudinal mixing coefficient, transverse mixing coefficient, and the Smagorinsky coefficient. All three coefficients were left at the default values during the testing. Results indicated that when the turbulence model was activated, overall stream power values were lower compared to simulations without the turbulence model, as depicted in Figure 4.6. This discrepancy is likely due to the turbulence model's capability to consider energy losses caused by expansions and contractions within the channel, leading to turbulence and eddies in the streamflow (Equation 4.2). While simulations without the turbulence model enabled may overpredict stream power for individual scenarios, the analysis method in this paper evaluates the differences in stream power between pre- and post-stabilization simulations. This shifts the focus from the absolute values to relative changes in stream power and helps bypass errors associated with not using the turbulence model. Moreover, due to the lack of necessary data such as stream velocity profiles from an acoustic doppler current profiler (ADCP), accurately calibrating the turbulence model coefficients would be futile. Given the models' relatively low sensitivity to the turbulence model when comparing multiple scenarios and the absence of ADCP data, the turbulence model was disabled for the remainder of simulations for sites C112 and C102.

Figure 4.6 HEC-RAS stream power results for Site C112 at the 892 m^3/s flow depth. The top image displays the simulation with the turbulence model disabled, while the bottom image shows the simulation with the turbulence model enabled.

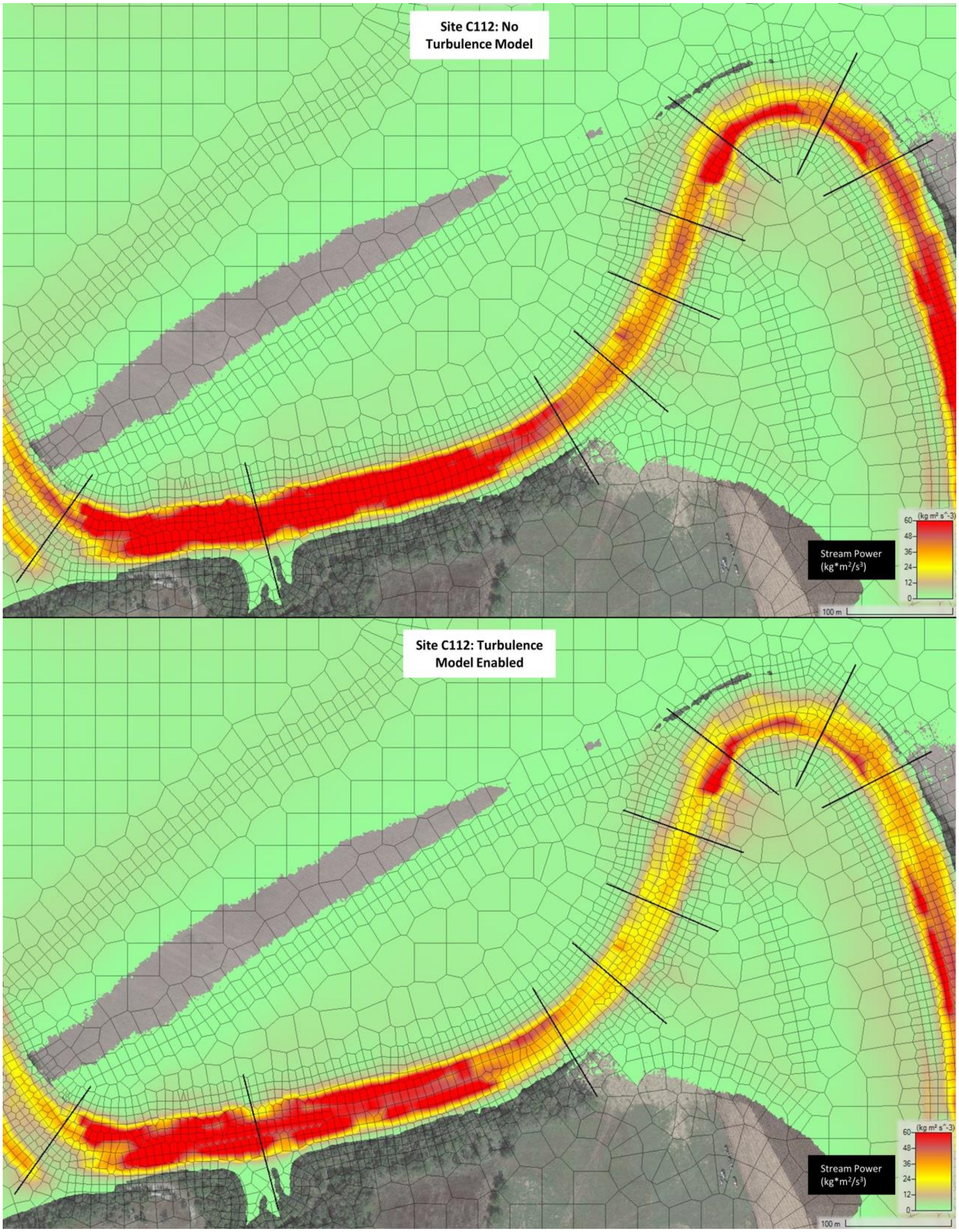

4.2.5 Modeling Scenarios for Sites C112 and C102

In the post-calibration phase shown in Figure 4.1, the calibrated HEC-RAS models for Site C112 and Site C102 were used to simulate various scenarios to assess the effectiveness of streambank stabilization techniques and their impact on flow dynamics. These scenarios aimed to explore different stages of channel stabilization and alternative stabilization strategies to inform future management decisions.

The first scenario involved simulating the pre-stabilization conditions using terrain data from 2018. This scenario served as a baseline to understand the natural flow dynamics of the river before any stabilization techniques were implemented. In addition, the models simulated the post-stabilization conditions using terrain data from 2022 and 2023 for Sites C112 and C102, respectively, which included the physical locations of the rock vanes, toe rock, and the actual bank shaping. This post-stabilization scenario allowed for an assessment of the effectiveness of the stabilization techniques implemented at each site in mitigating erosion. By comparing the pre- and post-stabilization scenarios to the observed field data, insights were gained into the models' ability to simulate different flow conditions, how flow patterns change with stabilization efforts, and the overall effectiveness of the stabilization projects.

In the next scenario, a mock floodplain bench was introduced as part of the streambank stabilization techniques. Positioned midway up the right bank, this bench was 15 meters wide or approximately one-third to a half of the channel width. The bench was integrated into the 3:1 bank shaping and aimed to replicate a small floodplain within the channel (Figure 4.7). The purpose was to establish a connection between high frequency flow events and the mock floodplain, thereby mitigating the impacts of gravitational and hydraulic forces (Bigham, 2020). Unlike the actual post-stabilization scenario, this approach excluded the use of rock vanes and toe rock for simplicity, focusing solely on evaluating the effectiveness of the bench. By comparing the results of this scenario with those of the pre-stabilization scenario, valuable insights could be gained regarding the potential advantages and disadvantages of a mock floodplain bench.

Figure 4.7 Diagram depicting the mock floodplain bench as modeled in HEC-RAS

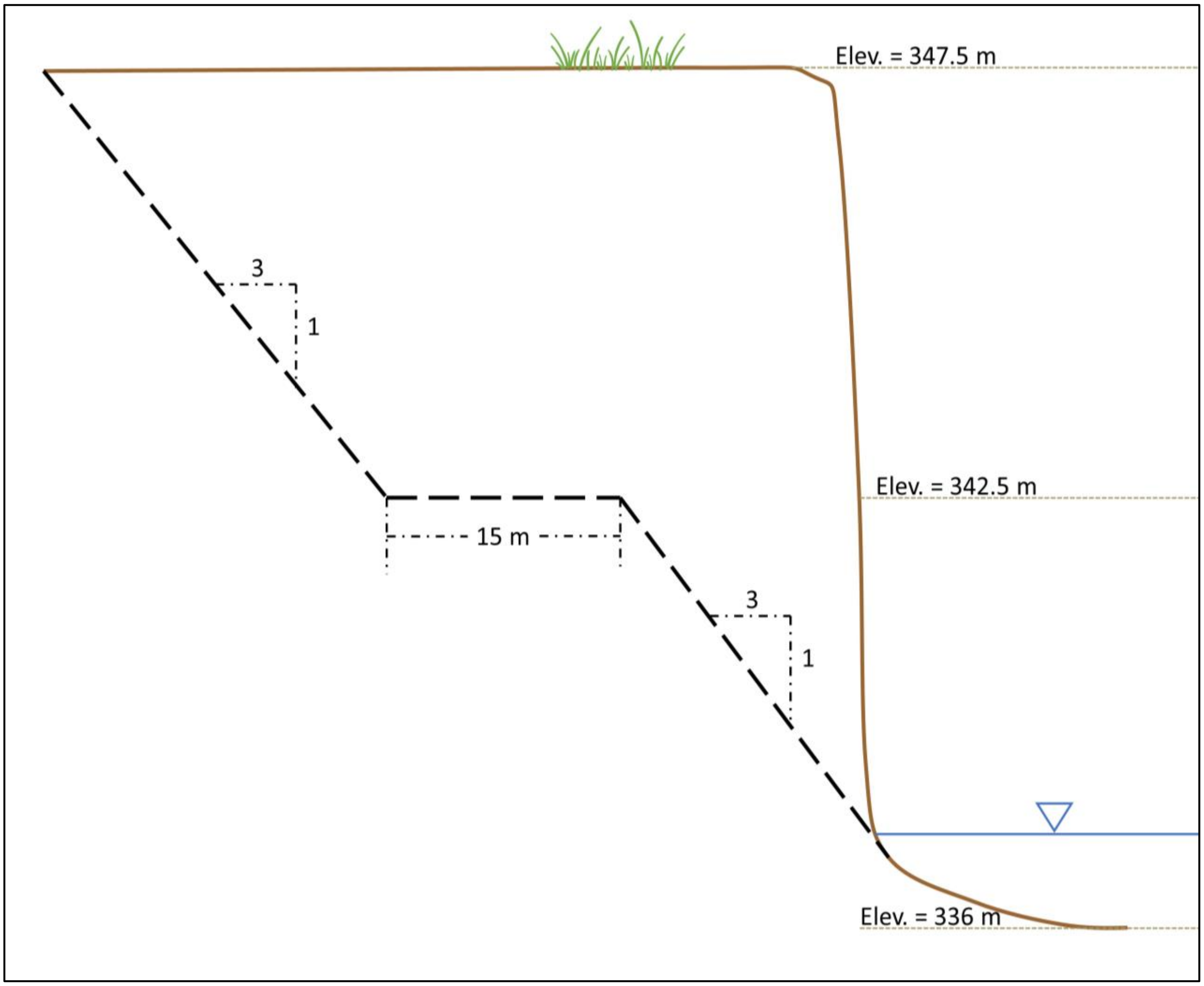

The final scenario focused on assessing the effectiveness of bank shaping without the use of rock vanes, toe rock, or a bench. This approach aimed to evaluate the effect of the rock vanes and toe rock within the post-stabilization model. By comparing this scenario with the pre-stabilization scenario, the results could quantify the impact of the rock vanes and toe rock on flow dynamics, and thereby evaluate their significance in streambank stability.

For this study, all of the previously described scenarios were simulated using hourly stream flow data spanning from April 15th, 2019 to May 15th, 2019. This timeframe encompassed the low flow leading up to the rising limb, the peak flow, and the receding limb of the May 9th, 2019 10-year return interval flow event. The objective was to analyze the scenarios under the most intense stream flow conditions recorded during the monitoring period. By focusing on this timeframe, the models could provide insights into the effectiveness of different stabilization techniques and their resilience to extreme hydrological events.

4.2.6 HEC-RAS Output

The next phase of Figure 4.1 is outputting the results from the calibrated simulations. HEC-RAS offers a wide range of result map layers including water depth, flow velocity, and water surface elevation, among others. In this specific case study, a stream power map layer was generated for each HEC-RAS simulation to aid further analysis and comparisons between different scenarios. A stream power analysis, as mentioned by Bizzi and Lerner (2013), offers a targeted approach to evaluating channel sensitivity to erosion and deposition process. By utilizing stream power as an indicator of fluvial dynamics, critical zones susceptible to erosion or deposition were identified, aiding in decision making and future stream restoration efforts (Bizzi & Lerner, 2013). The following equations show the relationship between stream power and shear stress, a commonly used indicator of erosion and deposition processes (e.g., Clark & Wynn, 2007; Frothingham, 2008; Layzell, Peterson et al., 2022).

Equation 4.7 Shear Stress Equation (Rosgen, 1996)

$$\tau = \gamma * d * S_f$$

This shear stress equation is similar to the equation used by HEC-RAS (Equation 4.5) except the hydraulic radius was substituted for the average depth of water. The channel width is assumed to be wide, as described by Rosgen (2009), allowing the hydraulic radius, R, to be simplified to the depth, d. This simplification allows depth to be used as a tool for identifying potential deviations in shear stress. Erosion can occur when the shear stress acting on the streambank exceeds the critical shear stress of the soil particles. The direct relationship between shear stress and erosion rate is depicted in the following equation.

Equation 4.8 Excess Shear Stress Equation (Clark & Wynn, 2007)

$$\varepsilon_r = k_d * (\tau_a - \tau_c)^a$$

Here, ε_r symbolizes the erosion rate (cm/s), k_d represents the erodibility coefficient (cm^3/Ns), τ_a represents the average applied shear stress on the soil boundary (Pa), τ_c represents the critical shear stress of the soil (Pa), and a represents the empirical exponent usually assumed to be 1.

Shear stress and stream power, equations 4.7 and 4.6, respectively, have a direct relationship. The velocity term in stream power helps emphasize areas with higher flow velocities, potentially indicating areas with more potential for dislodging soil particles. New RAS results layers were generated to analyze the differences in stream power between scenarios on a reach scale. These new layers produced color coded plan view maps for the max flow depth, highlighting areas where the scenarios diverged.

4.3 Results and Discussion

4.3.1 Stream Power Analysis of SBS

4.3.1.1 Site C112

In Figure 4.8, red indicates areas where the stream power for the post-stabilization scenario was greater than the pre-stabilization scenario, green identifies areas where the post-stabilization scenario resulted in smaller stream power values, and blue depicts areas where the two models had similar stream power results. With this symbology, green highlights favorable areas that had a decrease in stream power (Bizzi & Lerner, 2013).

Figure 4.8 Difference in stream power (SP, kg*m^2/s^3) between Pre- and Post-simulations at Max Flow Depth 892 m^3/s. Map output is Pre-Stabilization SP minus Post-Stabilization SP. A negative value means the stream power increased.

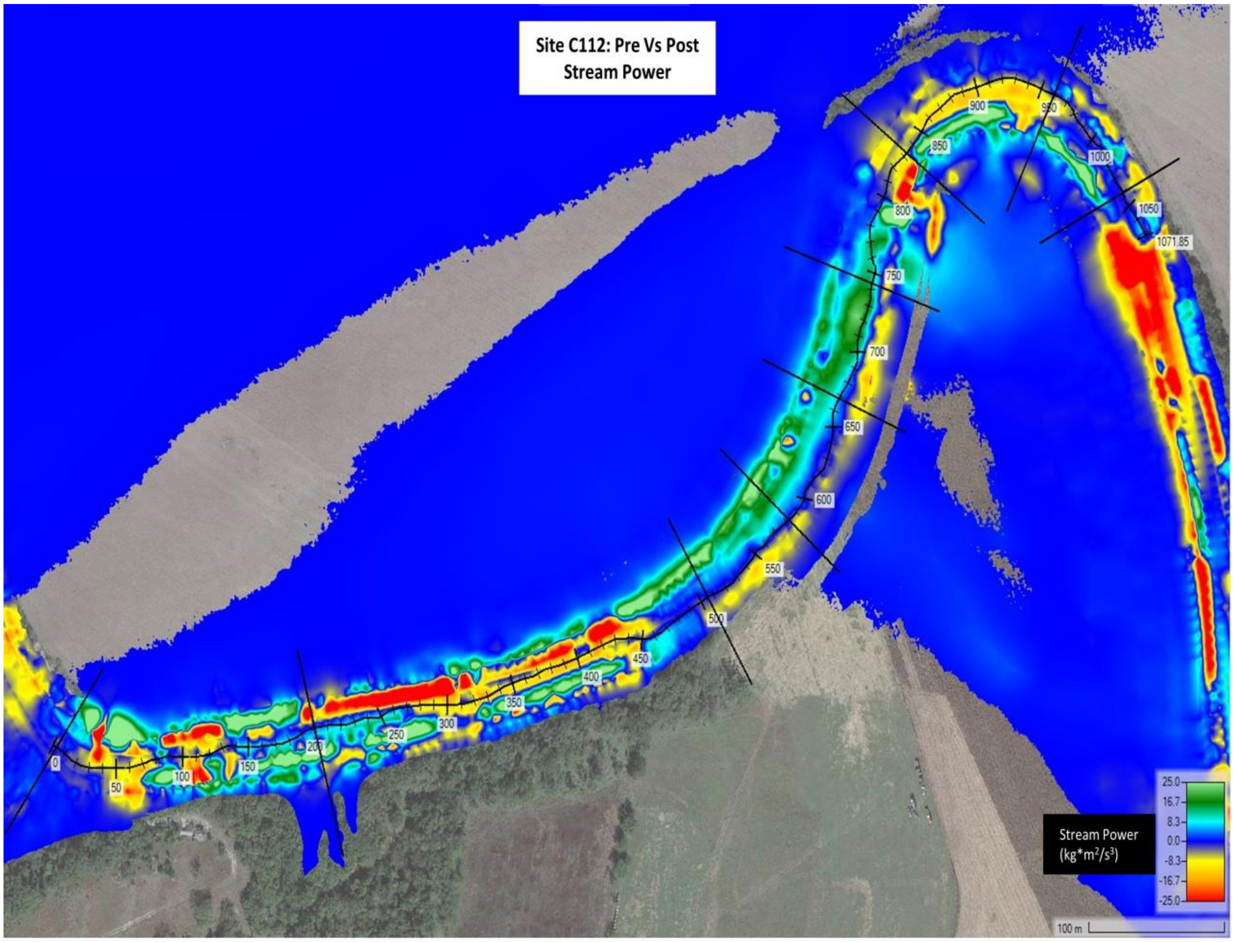

Notably, the toe on the right bank between stations 525 to 800 is a cyan color indicating a decrease in stream power of approximately 5 to 10 kg*m^2/s^3 from the pre- to post-scenario. However, in the region directly above the identified toe, in the low to mid bank region, the stream power increased by 5 to 16 kg*m^2/s^3 along the right bank as shown by the yellow spots within the SBS meander (similar trends were observed for the 1.5-year return interval and floodplain flow depths). This increase in stream power directly above the toe rock aligns with observed scouring reported by Layzell, Peterson, et al. (2022).

To understand these findings, the components of stream power (Equation 4.6), including velocity, depth, and stream slope, were isolated and compared in HEC-RAS. Analysis revealed that velocity and depth had the greatest impact on the stream power results for the pre- and post-stabilization scenarios, while changes in stream slope were negligible between the two. In particular, notable changes were observed in velocity and flow depths within the stabilized portion of the reach due to the bank shaping activities.

The greatest increase in flow velocity was approximately 1 m/s near station 680, while the flow depth increased by up to 6 meters across much of the bank shaped area, as illustrated in Figure 4.9, which depicts the differences in flow velocity and depth between the pre- and post-stabilization scenarios for Site C112. Furthermore, Figure 4.10 provides a detailed look at the pre- and post-stabilization flow velocity and corresponding channel profiles for Cross Section 3, which underwent bank shaping.

Figure 4.9 HEC-RAS layers showing the velocity (top) and flow depth difference (bottom) by taking the pre-stabilization value minus the post-stabilization value. A negative value means the velocity or depth increased.

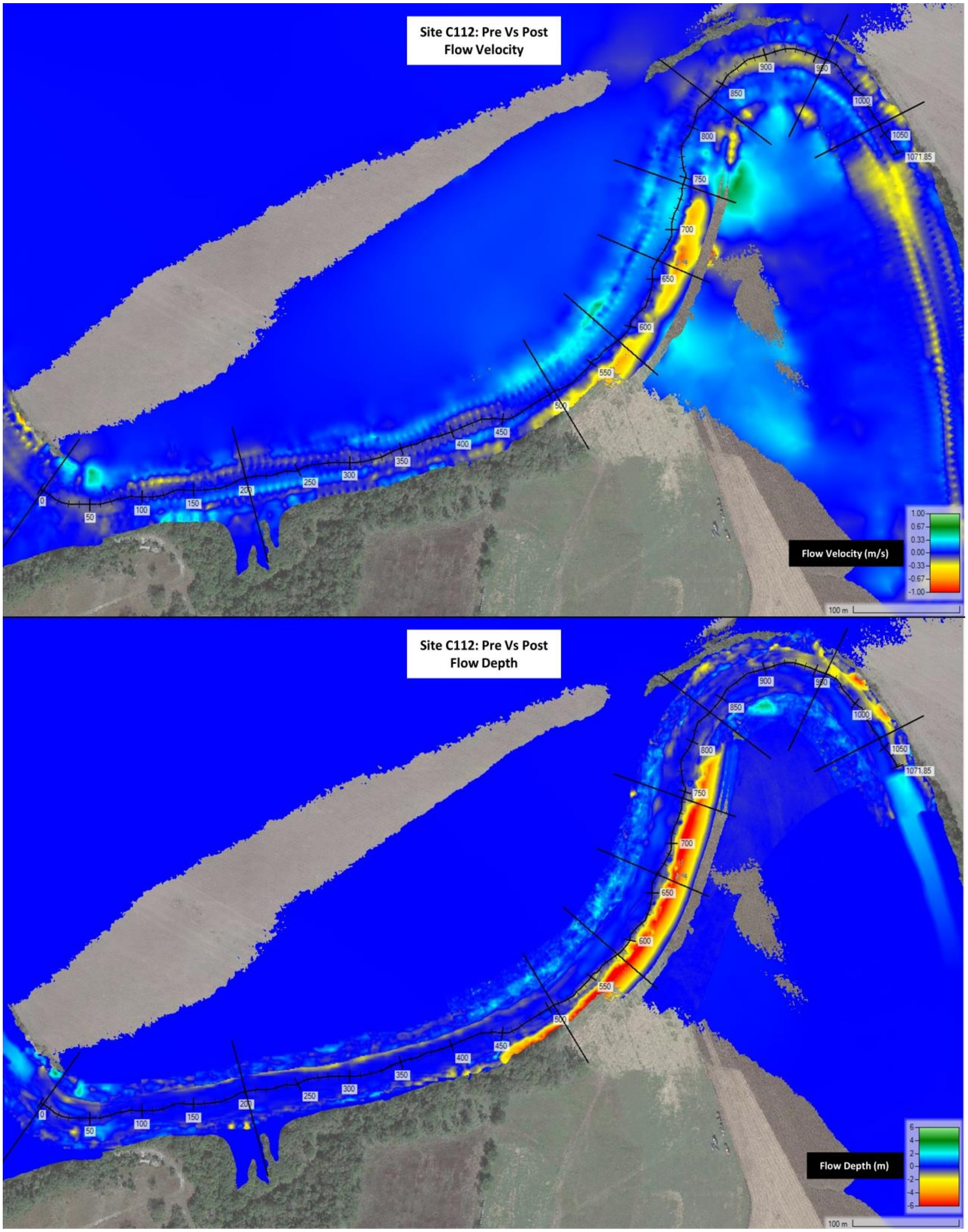

Figure 4.10 HEC-RAS velocity during the max flow depth for the pre- and post-scenarios.

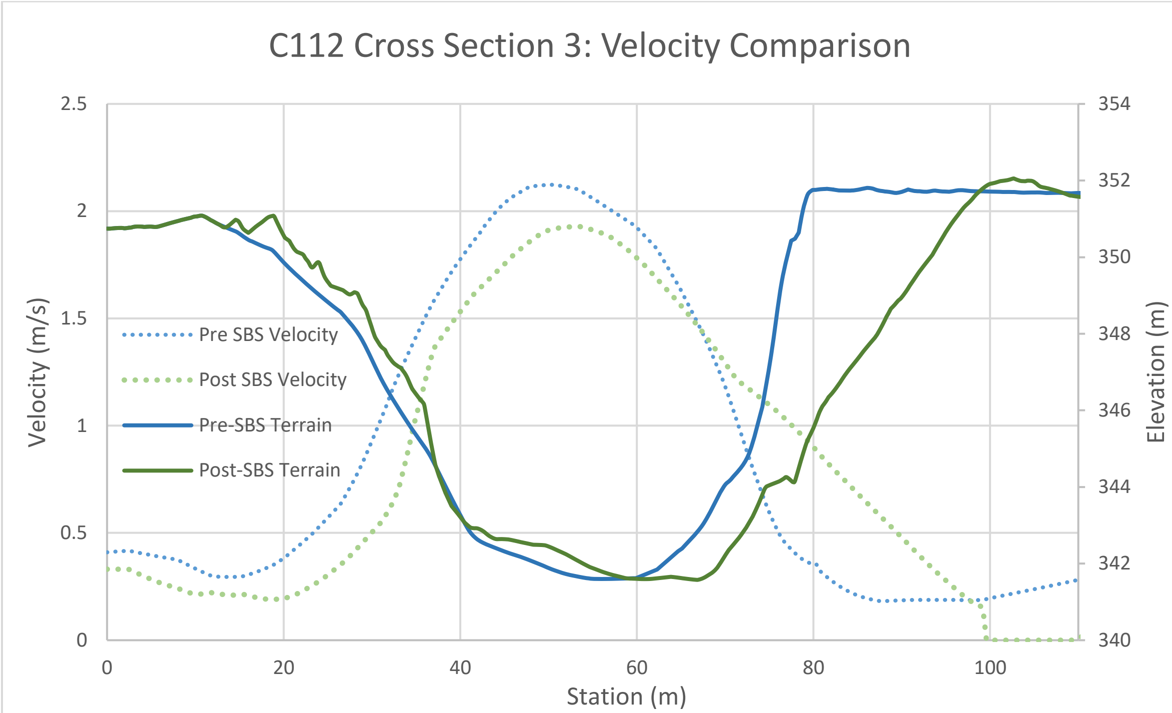

Figure 4.10, located in the stabilized meander, demonstrates how bank shaping activities increased the flow velocity on the right bank above the toe. This heightened flow velocity in the low to mid-bank region could potentially be responsible for the observed scouring above the toe rock, which was evident in all of the stabilized cross sections. In contrast, Figure 4.10 also shows that the flow velocity was reduced on the left bank, middle of the channel, and up to the toe on the right bank for Cross Section 3. This aligns with the decrease in stream power shown within the stabilized meander in Figure 4.8. The Manning's n within the stabilized portion of the reach was updated from barren land with a roughness coefficient of 0.030 during the pre-stabilization scenario to a roughness coefficient of 0.045 for the post-stabilization scenarios to be more representative of the vegetation established on the bank after construction. While an increase in the roughness coefficient should have resulted in reduced flow velocities within the stabilized

meander post-construction (refer to Equation 4.1), the bank shaping activities increased the flow depth and area enough to overcome this relationship.

The results in the upstream meander, specifically at Cross Section 1, are likely significantly influenced by the exposed bedrock spanning from station 50 to 450 in Figure 4.8. This bedrock layer serves as grade control, as indicated in the streambed analysis and surveys of Riffle Cross Section 1 (Section 3.3.2, Appendix D), and could potentially isolate the upstream meander of Site C112 from downstream activities. It is unknown whether the differences in stream power between the pre- and post-stabilization models are directly caused by the SBS activities downstream or if upstream factors, such as other SBS projects or bank erosion events, are impacting the post-stabilization terrain model and consequently the stream power calculations. Despite the uncertainty regarding the upstream meander's differences between the pre- and post-scenarios, the corresponding differences in flow velocities and depths shown in Figure 4.9 align reasonably well with the changes in stream power. At Cross Section 1 and Riffle Cross Section 1, the depth in the middle of the channel increased approximately 0.20 and 0.15 meters, respectively, during the post-stabilization simulation. This increase in flow depth caused higher stream power values. Additionally, the dark red spot on the left bank of Riffle Cross Section 1 at station 200 indicates an increase in stream power between the pre- and post-scenarios. This was supported by a 1-meter drop in the left top of the bank in the field measurements between 2018 and 2023 (see Appendix D, Figure D.2).

After examining the downstream meander, notable differences in stream power between the two scenarios were apparent. The dark red and yellow area between stations 800 and 830 in Figure 4.8 corresponds to the section where the SBS bank shaping technique merges with the existing streambank. This creates a contraction area where the channel width narrows back to the existing streambank, and consequently increasing the flow velocity, as depicted in Figure 4.9 (top picture). The peak difference in this transition zone is approximately -54.27 kg*m^2/s^3 This heightened zone of stream power extends downstream along the outside bend of the unstabilized meander, aligning with the increased lateral retreat rates calculated during the post-stabilization timeframe for the downstream meander (see Table 3.1).

4.3.1.2 Site C102

The entire reach of Site C102 was compared using the RAS mapper calculator to compute the differences in stream power between the different scenarios. Figure 4.11 shows the difference between the pre- and post-simulation stream power values on a reach scale using the same color coded symbology described in the previous section.

Figure 4.11 Difference in stream power (SP, kg*m^2/s^3) between Pre- and Post-simulations at Max Flow Depth 892 m^3/s. Map output is Pre-Stabilization SP minus Post-Stabilization SP. A negative value means the stream power increased.

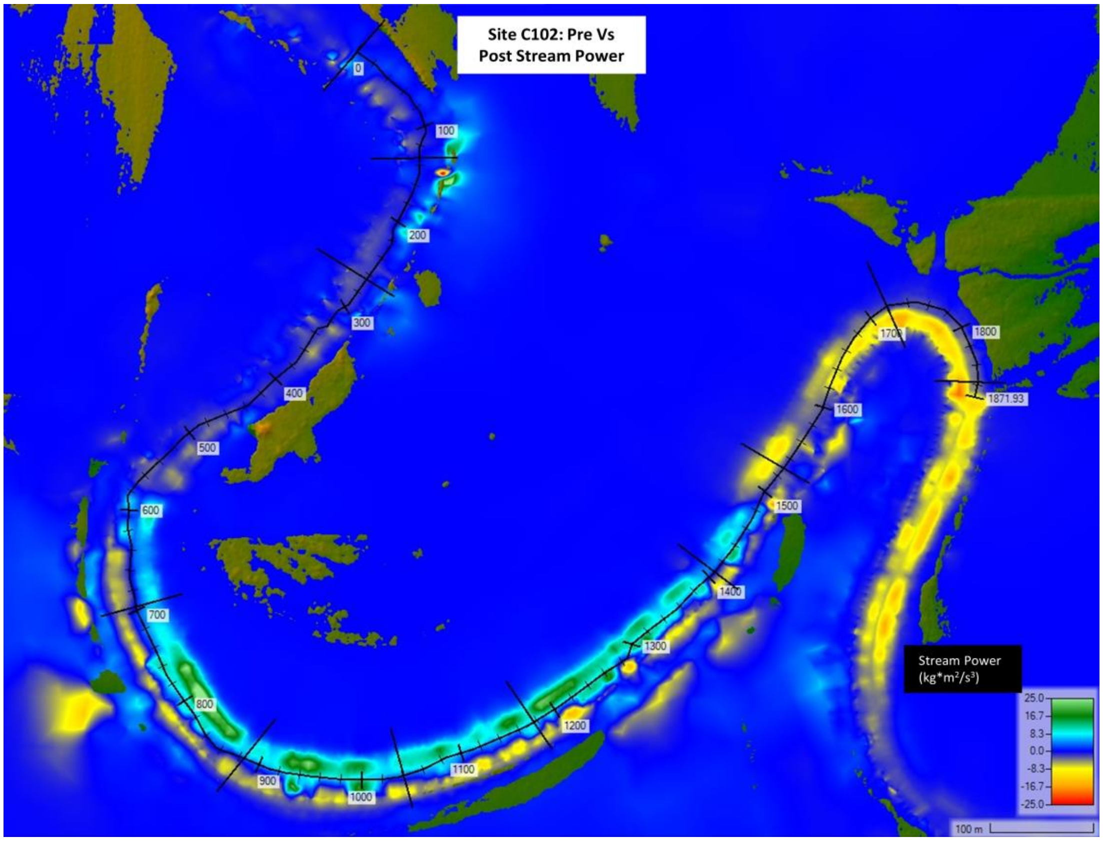

The cyan color between stations 580 and 1480 aligns with the extent of the SBS. This color indicates a decrease in stream power of approximately 5 to 10 kg*m^2/s^3 from the pre- to post-scenario. However, in the low to mid bank region above the toe, the stream power increased by 5 to 16 kg*m^2/s^3 along the right bank as shown by the yellow areas within the SBS meander, once again aligning with the results of Layzell, Peterson, et al. (2022).

The components of stream power (i.e., velocity, depth, and stream slope) were isolated and compared in HEC-RAS to help understand these results. This approach revealed notable changes in velocity and flow depths within the stabilized portion of the reach due to the bank shaping activities. The greatest increase in flow velocity was approximately 0.7 m/s near station 820, while the flow depth increased by up to 5 meters across much of the bank shaped area. Figure 4.12 shows the flow velocity and corresponding channel profiles for Cross Section 6 before and after stabilization. Additionally, Figure 4.13 depicts the differences in flow velocity and depth between the pre- and post-stabilization scenarios for Site C102.

Figure 4.12 HEC-RAS velocity during the max flow depth for the pre- and post-scenarios.

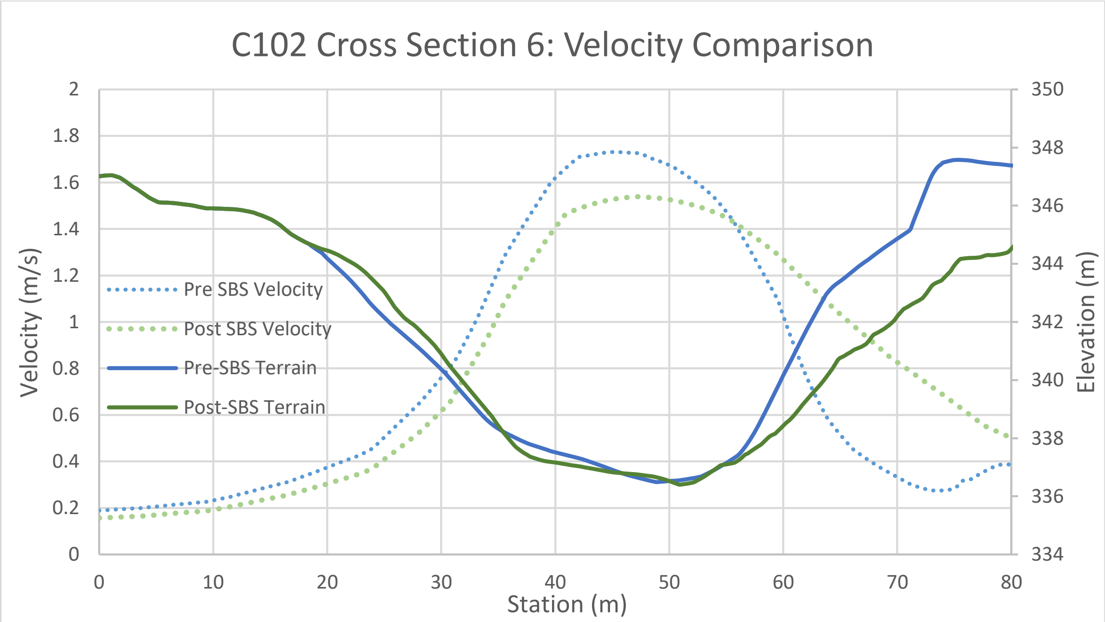

Figure 4.13 HEC-RAS layers showing the velocity (top) and flow depth difference (bottom) by taking the pre-stabilization value minus the post-stabilization value for Site C102. A negative value means the velocity or depth increased.

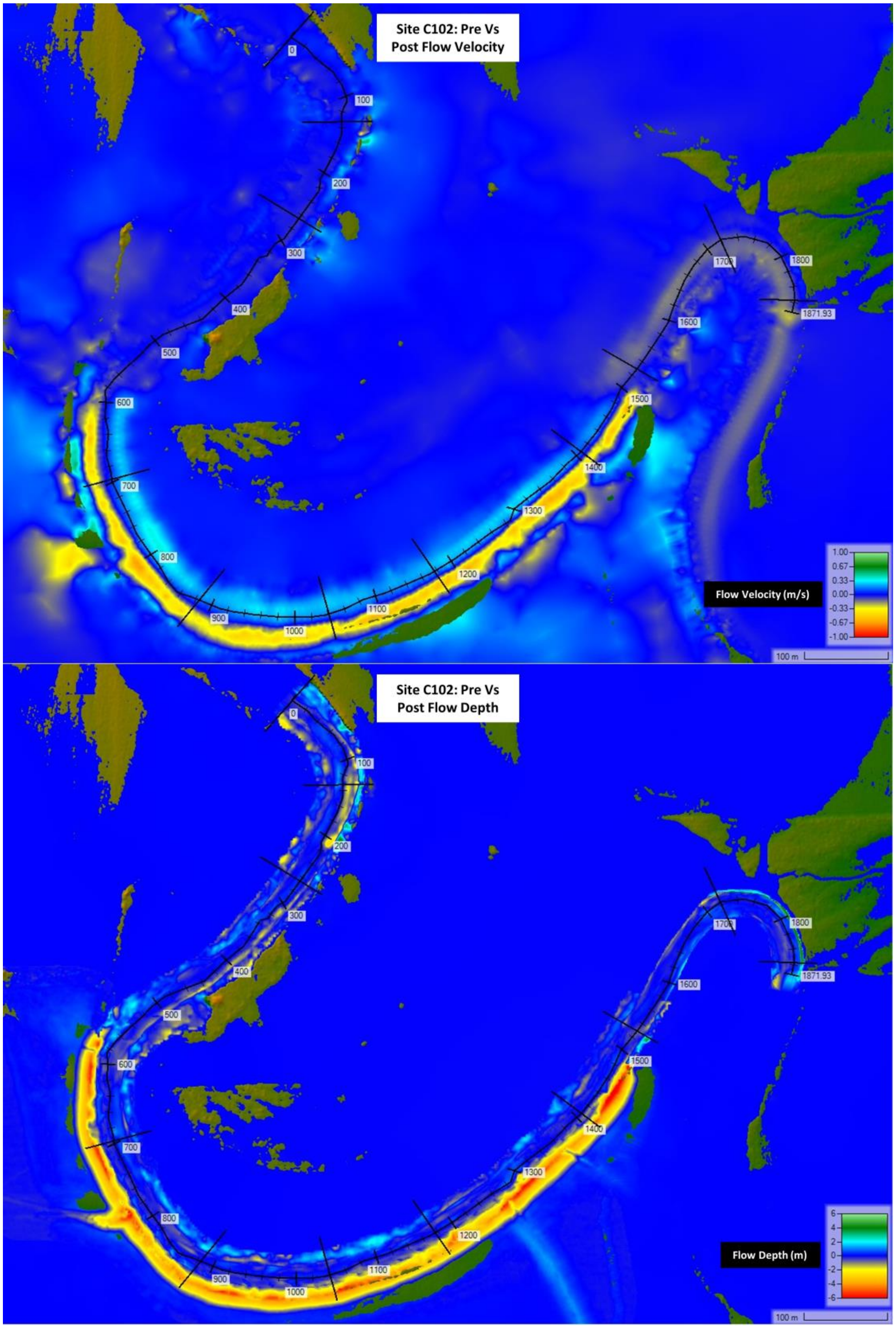

Figure 4.12 of Cross Section 6 in the stabilized meander demonstrates how bank shaping activities increased the flow velocity and depth on the right bank above the toe. In contrast, the figure also shows that the flow velocity was reduced on the left bank, middle of the channel, and up to the toe on the right bank for Cross Section 6. These observations align with the results shown within the stabilized meander in Figure 4.11.

The stream power results in the upstream meander seem to correspond closely with differences in flow depths shown in Figure 4.13. While changes in flow velocity were detected in the upstream meander of Site C112 (Figure 4.9, top picture), very little change in flow velocity was observed in the upstream meander of Site C102. Furthermore, the increase in flow depth in the upstream portion of Site C102 (Figure 4.13, bottom picture) seems to align with the observed increases in stream power. Additionally, the small green spot on the top left bank of Cross Section 1 at station 132 indicates a decrease in stream power between the pre- and post-scenarios. This matches the calculated depositional lateral retreat derived from field measurements taken in 2022 (pre-stabilization) and 2023 (post-stabilization, see Table 3.2).

Notable differences in stream power between the two scenarios were apparent in the downstream unstabilized meander. The yellow and orange areas between stations 1480 and 1870 in Figure 4.11 correspond to a stream power increase between 4 to 12 $kg*m^2/s^3$. This increase in stream power appears to be the direct result of the widespread increase in flow velocity in the downstream meander (e.g., 0.2 m/s increase downstream of SBS). These results suggest that the SBS activities in the middle stabilized meander affected the flow dynamics and stream power in the downstream meander during the post-construction simulation.

The models of sites C112 and C102 reported similar findings within both the stabilized and unstabilized meanders. In general, the stabilized portion of both reaches had a decrease in stream power in the post-stabilization scenario, which is consistent with the findings of Layzell, Peterson, et al. (2022), who also observed lower local scale erosion rates following stabilization. Conversely, the unstabilized meanders generally showed an increase in stream power post-stabilization, enhancing the understanding of how SBS affects the adjacent unstabilized meanders.

Furthermore, when comparing the findings of the HEC-RAS modeling with those of the streambed analysis, it becomes evident that the outer bends of the upstream and downstream meanders at both sites experienced localized bed erosion and exhibited heightened stream power (see Appendix B, Figures B.4 and B.9; Figures 4.8 and 4.11). This suggests that the increased stream power caused by the SBS contributes to localized bed erosion.

After analyzing the pre- and post-construction scenarios and comparing the findings to the field data and lateral retreat rates, it becomes clear that the models are capable of generating relatively accurate results. Hence, the HEC-RAS model of sites C112 and C102 can serve as an effective tool for analyzing other SBS design scenarios, including alternatives such as bank shaping without rock vanes or toe rock, and a mock floodplain bench, as presented in the following section.

4.3.2 2D Analysis of Alternative SBS Designs

4.3.2.1 Site C112 SBS Alternatives

This section evaluates two hypothetical post-stabilization scenarios that have slightly different SBS techniques than the ones implemented in the field to see how changing the stabilization methods affects stream power on the reach scale. It is worth noting that all post-stabilization scenarios have the same Manning’s n values. Figure 4.14 depicts the difference in stream power between pre-stabilization and bank shaping only scenarios.

Figure 4.14 Difference in stream power (SP, kg*m^2/s^3) between Pre and Bank Shaping Only simulations at Max Flow Depth 892 m^3/s. Map output is Pre-Stabilization SP minus Bank Shaping Only SP. A negative value means the stream power increased.

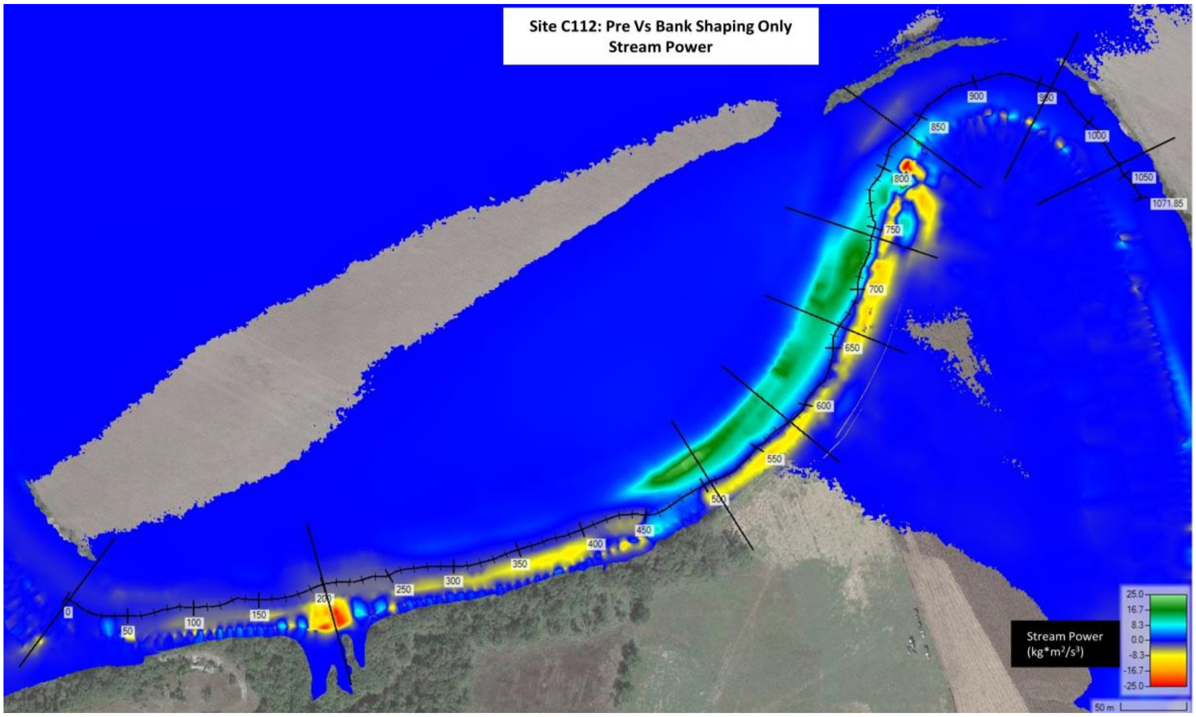

In Figure 4.14, the green area spanning the majority of the stabilized meander demonstrates how bank shaping only at a 3H:1V slope, is capable of reducing stream power. However, when comparing these results to the pre- versus post-stabilization scenarios shown in Figure 4.8, it is apparent that the stream power in the low to mid bank region of the stabilized meander between station 500 and 800 appears to increase as shown by the expansion of the yellow region. This may be attributed to the absence of rock vanes in the bank shaping only scenario, which would otherwise slow the flow and perhaps redirect the streamflow toward the middle of the channel. In contrast, Figure 4.14 shows a decrease in stream power in the unstabilized area upstream of the construction zone when compared to Figure 4.8. This may be attributed to the 0.10 to 0.30 meter decrease in flow depth from the post-stabilization scenario to the bank shaping only scenario.

Additionally, in Figure 4.14, there is a dark red region near station 810 where the bank shaping transitions back into the existing stream bank. The peak difference in this transition zone is approximately -36.35 $kg*m^2/s^3$. This area of increased stream power may warrant additional consideration when designing future SBS projects, as it is observed consistently across all stabilization scenarios (i.e., Figure 4.8, Figure 4.14, Figure 4.15).

Another notable observation from Figure 4.14 is the absence of significant yellow and red areas in the downstream meander when compared with the pre- versus post-stabilization scenarios depicted in Figure 4.8. This observation can be attributed to the consistently higher velocity values for the post-stabilization simulation, suggesting that the rock vanes in the post-stabilization scenario effectively redirect the stream flow towards the middle of the channel, leading to increased stream power values in the downstream unstabilized meander. Bhuiyan et al. (2009) also noted the capability of rock vanes to redirect flow towards the center of the channel.

Figure 4.15 compares stream power between pre-stabilization and the bench scenario. In Figure 4.15, the mock floodplain bench appears to reduce stream power even more than the bank shaping only scenario. The vast majority of the stabilized meander is a darker green than in Figure 4.14. In the low to mid bank region between stations 475 and 750, the extent of the yellow stream power area increased slightly when compared to the other SBS scenarios. However, this can be explained by the increase in flow depth and velocity caused by cutting a bench into the streambank. Although the bench itself may experience higher fluvial stress, due to increased flow depths locally, the mock floodplain was able to reduce the stream power elsewhere by spreading out the streamflow.

Figure 4.15 Difference in stream power (SP, kg*m^2/s^3) between Pre and Bench simulations at Max Flow Depth 892 m^3/s. Map output is Pre-Stabilization SP minus Bench Stabilization SP. A negative value means the stream power increased.

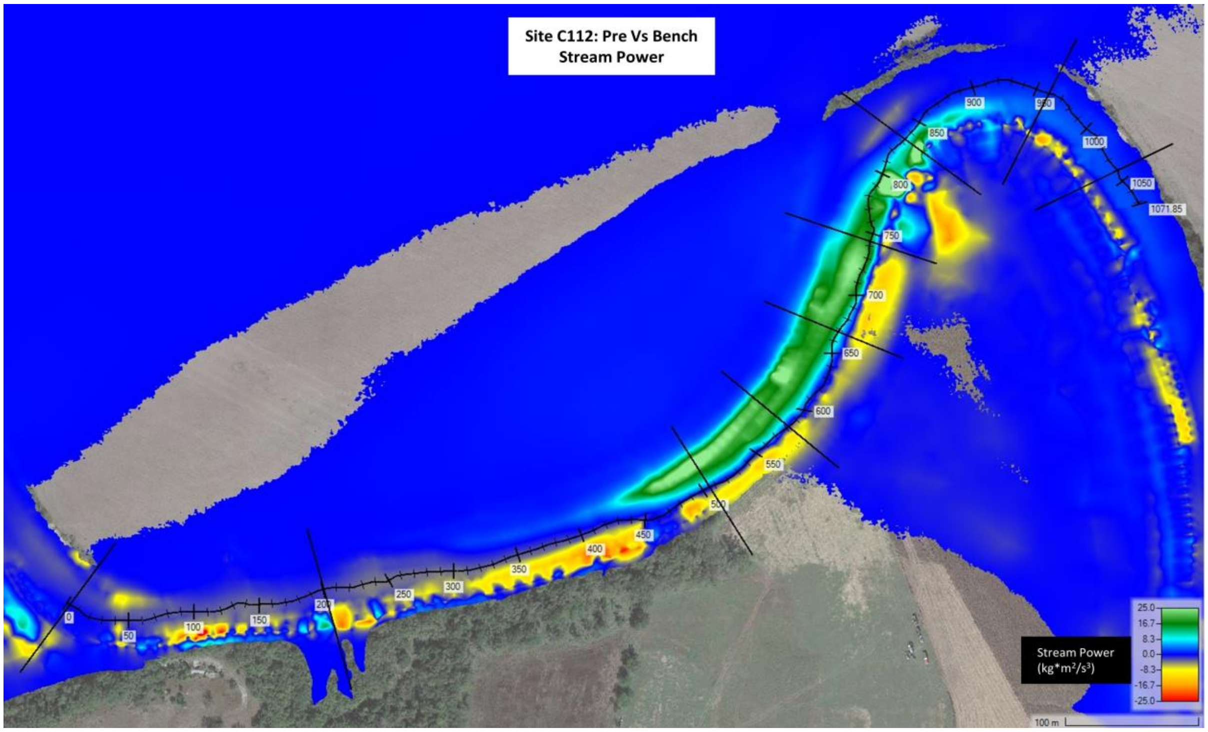

Furthermore, the transition zone between the SBS and the unstabilized downstream meander also appears to benefit from the bench, with the peak difference being the smallest among all the SBS scenarios at -16.16 kg*m^2/s^3. This reduction in stream power extends downstream along the outside bend of the meander, as evidenced by the presence of cyan and light blue areas.

When comparing Figure 4.14 to Figure 4.15, subtle variations in the location and intensity of stream power values were observed in the upstream meander. In general, the bench scenario had slightly higher velocity values in the upstream meander when compared to the bank shaping only scenario, which contributed to the subtle differences between the two hypothetical alternatives.

Overall, the pre- and post-stabilization scenarios helped validate the accuracy of the models by comparing the simulated results to what was recorded in the field. Also, the two alternative SBS scenarios were necessary for understanding how changes in the SBS techniques directly affect the stabilized meander and the adjacent meanders at Site C112.

4.3.2.2 Site C102 SBS Alternatives

This section evaluates two hypothetical post-stabilization scenarios for Site C102 that have slightly different SBS techniques than the one that was implemented in the field. This will help identify how changing the stabilization methods affect stream power on a reach scale. Figure 4.16 shows the stream power difference between the pre-stabilization and bank shaping only scenarios for Site C102.

Figure 4.16 Difference in stream power (SP, kg*m^2/s^3) between Pre and Bank Shaping Only simulations at Max Flow Depth 892 m^3/s for Site C102. Map output is equal to Pre-Stabilization SP minus Bank Shaping Only SP. A negative value means the stream power increased.

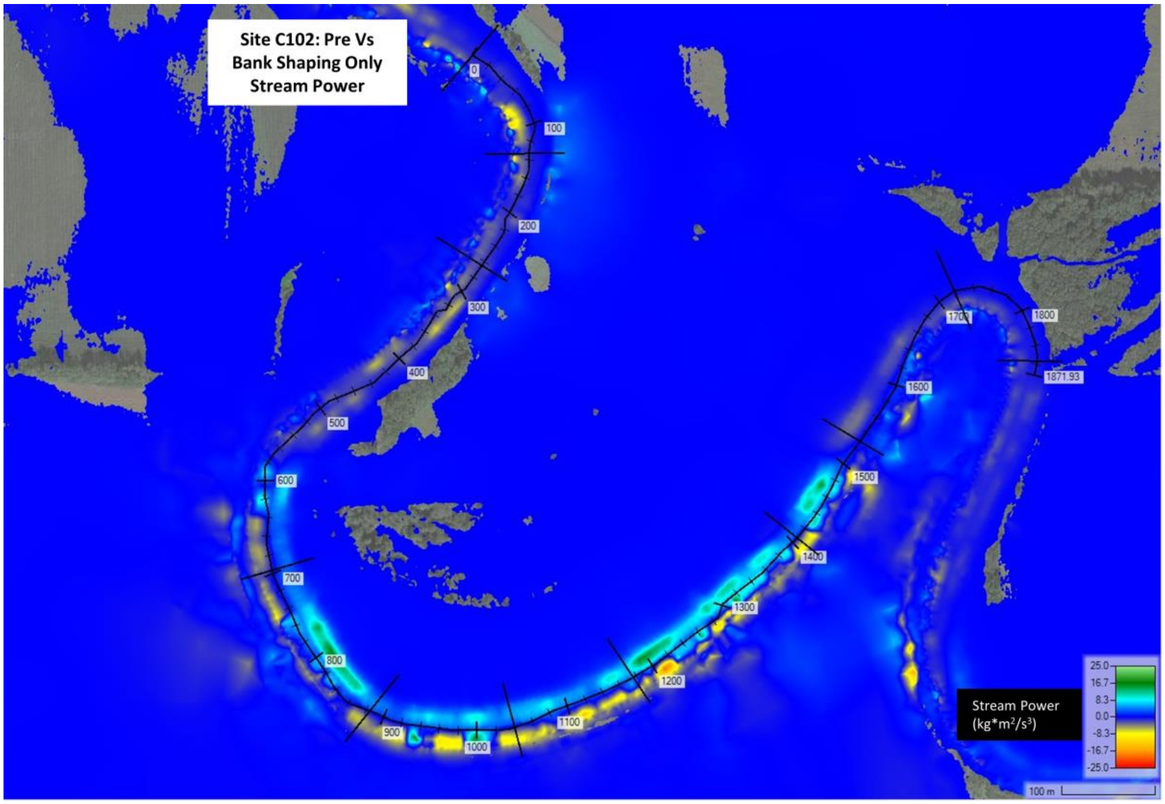

In Figure 4.16, the green areas between stations 580 to 1480 in the stabilized meander depict a notable reduction in stream power even with only bank shaping at a 3H:1V slope as the sole SBS technique. However, when comparing these results to the pre- versus post-stabilization scenarios shown in Figure 4.11, it is evident that bank shaping alone is not as effective at reducing stream power within the stabilized meander. This is illustrated by the reduction of green in the toe, middle, and left bank regions.

Additionally, Figure 4.16 indicates a decrease in yellow in the low to mid bank region when compared to Figure 4.11. These results may be attributed to the absence of rock vanes in the bank shaping only scenario. Interestingly, this contradicts what was observed in the model of Site C112. One potential factor contributing to the differing results between the two sites is the presence of a small bench constructed during the bank shaping activities in the post-stabilization scenario of Site C102 (Figure 4.17). This bench, located two-thirds up the right bank within the entire stabilized meander, is approximately three meters wide and was only modeled in the post-stabilization simulation (i.e., not incorporated into the bank shaping only scenario). Therefore, the flow depth and velocity on the right bank in the location of the bench are higher in the post-stabilization scenario, resulting in greater stream power values in these areas. Moreover, the bench may function as a small floodplain, helping reduce the velocity in the middle of the channel and left bank. This could explain the greater extent of green in the pre- versus post-stabilization comparison (Figure 4.11) compared to the pre- versus bank shaping only scenario (Figure 4.16).

Figure 4.17 Profile view of Cross Section 4 at Site C102 showing the small as-built bench

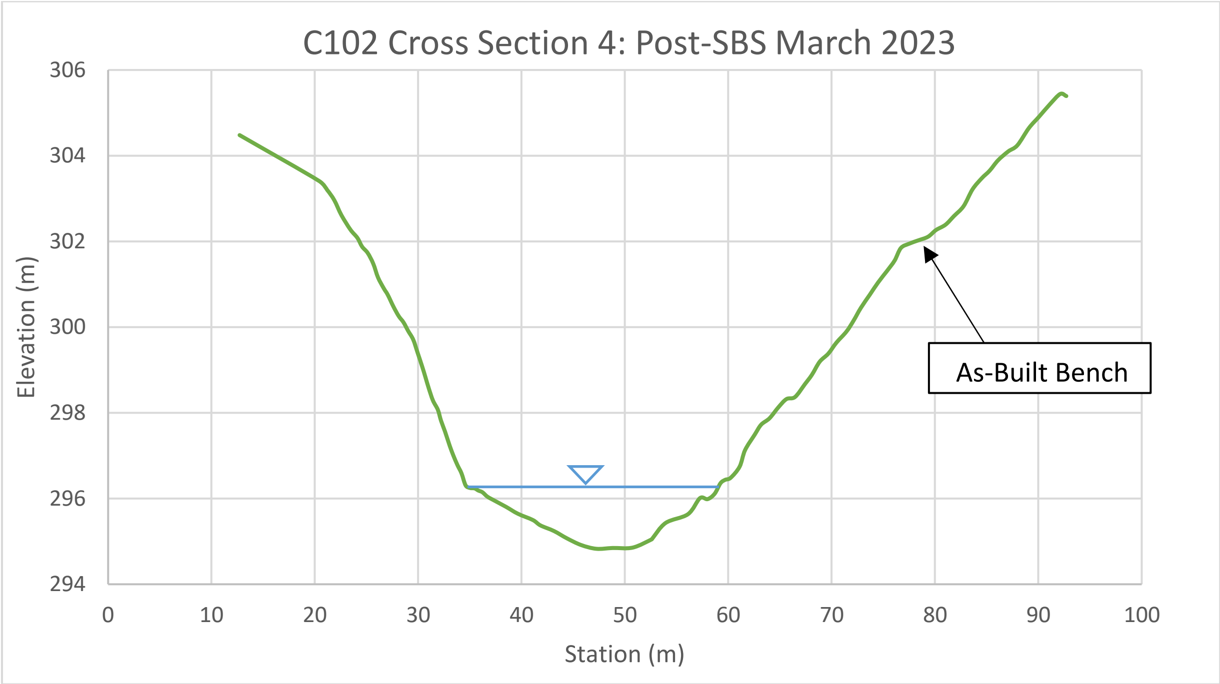

In the upstream meander, Figure 4.16 indicates an increase in stream power compared to Figure 4.11, likely due to the 0.03 to 0.12 m/s increase in flow velocity from the post-stabilization scenario to the bank shaping-only scenario. Since the Manning's n layer remained constant between the post-SBS and bank shaping-only scenarios, this increase in flow velocity, and consequently stream power, in the upstream meander is likely due to the change in SBS techniques. In the downstream meander of Site C102, Figure 4.16 illustrates a notable absence of yellow and red when compared with the pre- versus post-stabilization scenarios shown in Figure 4.11. This suggests that the rock vanes in the post-stabilization scenario redirected the stream flow towards the middle of the channel, resulting in the observed increase in flow velocity and stream power in the downstream unstabilized meander. In the bank shaping-only simulation, the downstream meander experienced flow velocities 0.1 to 0.2 m/s slower than the post-stabilization simulation, which likely explains the differences in stream power between the two figures. This is consistent with the results observed in the model of Site C112.

The bank shaping-only scenario seemed less effective at reducing stream power at the local scale when compared to the other two SBS alternatives. However, it also appeared to have the least detrimental effect on the upstream and downstream meanders, consistently yielding lower stream power values in these unstabilized meanders at both C112 and C102.

Figure 4.18 compares stream power between pre-stabilization and the bench scenario. The mock floodplain bench appears to reduce stream power even more than the post-stabilization and bank shaping only scenarios. The vast majority of the stabilized meander is a darker green than in Figures 4.11 and 4.16. In the low to mid bank region of the stabilized zone, the extent of the yellow stream power area increased slightly when compared to the other two SBS scenarios. However, similarly to Site C112, this can be explained by the increase in flow depth and velocity caused by cutting a bench into the streambank. While the bench itself experienced higher fluvial stress, due to its geometry, the mock floodplain reduced the stream power elsewhere by spreading out the streamflow.

Figure 4.18 Difference in stream power (SP, kg*m^2/s^3) between Pre and Bench simulations at Max Flow Depth 892 m^3/s. Map output is Pre-Stabilization SP minus Bench Stabilization SP. A negative value means the stream power increased.

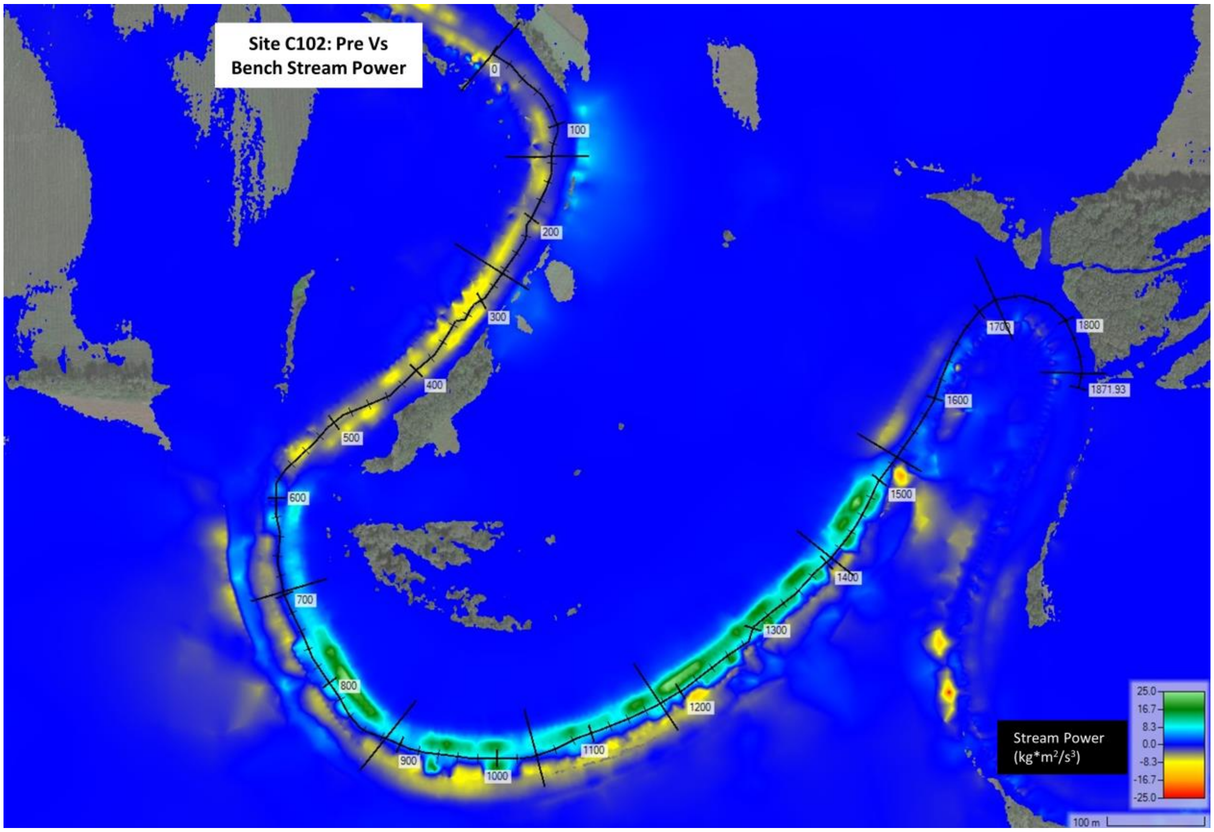

When comparing the upstream meander of Figures 4.11, 4.16, and 4.18, it is evident that the bench scenario recorded the highest stream power values. This could be attributed to the bench scenario spreading out the stream flow within the stabilized meander, resulting in reduced stage levels and a steeper energy slope in the upstream meander. Consequently, this led to consistently higher stream flow velocities upstream compared to any other alternative. In contrast, the downstream meander of the bench scenario had the lowest stream power values, which could be attributed to the reduced stream flow velocities.

For sites C112 and C102, the theoretical scenario featuring a 15-meter-wide bench halfway up the outside bank of the stabilized meander seemed to have the greatest impact on reducing stream power locally within the channel and along the toe of the stabilized meander.

However, this design also appeared to increase flow velocity and the corresponding stream power values in the upstream meander.

The HEC-RAS models, created using actual pre- and post-stabilization terrain and streamflow data from sites C112 and C102, offered an additional avenue for understanding the effects of SBS. While the stream power analysis in Chapter 4 indicates that SBS activities may increase stream power and influence scouring above the toe rock, a substantial portion of the stabilized reach below the toe rock, in the middle of the channel, and on the left bank exhibited lower stream power values in the post-stabilization scenario (see Figures 4.8 and 4.11). This suggests that the SBS is effective at reducing erosion within the stabilized zone.

However, the modeling also revealed that the current SBS techniques, as well as two alternative SBS designs tested in HEC-RAS, affect stream power in the adjacent unstabilized meanders. The SBS techniques themselves seemed to have an impact on how much and where stream power was affected. For example, the scenario of the mock floodplain bench reduced stream power within the toe region of the stabilized meander more than any other scenario, while also limiting stream power in the downstream meander (see Figures 4.15 and 4.18). However, this scenario had the greatest increase in stream power in the upstream meander, while the bank shaping only scenario had the least effect on stream power upstream. This may suggest that there is a smaller bench size somewhere in the middle of the current design (15 meters wide) and the bank shaping only design with no bench that maximizes the reduction in stream power within the stabilized zone while minimizing the upstream and downstream effects.

Furthermore, the rock vanes appeared to reduce stream power in the low to mid bank region (see Figures 4.8, 4.11, 4.14, and 4.16). If included on a smaller mock floodplain bench design, they could offset some of the inherent stream power increases resulting from increasing the flow depth and velocity on the flat bench. Additionally, special attention is needed when designing the transition between SBS and the existing channel to minimize the effects of channel contractions.

The analyses of the streambank, streambed, and HEC-RAS modeling were closely intertwined and supported each other. For example, the HEC-RAS simulations revealed a distinct pattern in stream power across the three meanders, which was consistent with the retreat rates derived from the field data. The correlation between increased stream power and heightened streambank retreat rates upstream and downstream of the SBS demonstrates the predictive capability of the HEC-RAS models. Furthermore, the decrease in stream power observed within the stabilized meander, attributed to SBS, corresponds with the post-construction analyses of the streambed and streambank that indicated a net deposition of streambed material and a reduction in lateral retreat rates. The connection of these three analyses contributes to a more comprehensive understanding of the fluvial dynamics occurring on the Cottonwood River.

Various papers have indicated the success of SBS at reducing streambank erosion locally (Layzell, Peterson, et al., 2022; Naisargi & Mittelstet, 2017; Russell et al., 2021b), which is consistent with the findings of this paper. The aerial imagery analysis used by Russell et al. (2021b) found no significant impact of SBS on adjacent unstabilized reaches. However, they recommended more advanced monitoring techniques to accurately assess the influence of SBS projects on the entire fluvial system. The monitoring and modeling methods employed in this study indicate that SBS does indeed have a measurable effect on streambank erosion in adjacent unstabilized meanders. This contradiction to Russel et al. (2021b) suggests that it is necessary for additional monitoring and research to fully comprehend the reach scale impacts of SBS.

Several limitations were identified within this analysis. The availability of survey data from the post-stabilization period was limited, hindering the ability to discern between long-term trends or a "break-in" period. Additionally, the absence of stream velocity profiles from an ADCP impeded the calibration of turbulence model coefficients. Furthermore, the simulations were based solely on a 10-year return interval flow event. This restricts the understanding of how stream power is affected within the models to that specific flow event, rather than considering variations in stream flow magnitudes, intensities, and durations.

4.4 Summary

The models of sites C112 and C102 revealed consistent findings across both stabilized and unstabilized meanders. Generally, the stabilized portions of both reaches exhibited a decrease in stream power from pre- to post-stabilization scenarios, while the unstabilized meanders typically showed an increase in stream power post-stabilization. The effects of SBS on stream power at the reach scale align with the lateral retreat rates derived from field data in Chapter 3, which indicated that SBS is effective locally at reducing erosion but can exacerbate it in adjacent meanders.

The accuracy of the models was validated by comparing pre- and post-stabilization results to field observations. Additional simulations were conducted to assess how altering SBS techniques would affect stream power at the reach scale. For sites C112 and C102, a theoretical scenario featuring a 15-meter-wide bench had the greatest impact on reducing stream power locally but increased flow velocity and stream power upstream. The actual post-stabilization terrain scenario also reduced stream power within the stabilized zone but exhibited higher stream power values downstream. Conversely, the bank shaping-only scenario was less effective locally but had the least impact on upstream and downstream meanders.

The SBS alternative scenarios showed varying success in reducing stream power and erosion rates within the stabilized zone compared to the pre-stabilization baseline. Each scenario—whether involving bench construction, bank shaping alone, or modeling the actual post-stabilization terrain—had its advantages and limitations. These findings underscore the need for careful consideration of SBS techniques in future designs to achieve desired outcomes while minimizing unintended consequences on the broader river system.

Chapter 5 - Conclusion and Future Work

The need for SBS arises from centuries of human alterations to fluvial systems and the surrounding environment, leading to increased channel instability and erosion rates. These modifications, which were intended to satisfy economic and social needs, have disrupted the natural geomorphic processes and worsened erosion and sedimentation issues in river systems worldwide. In regions such as Kansas, where erosion threatens valuable land and infrastructure, and sedimentation undermines the functionality of reservoirs, the adoption of SBS has become a prominent strategy in combating streambank erosion. However, despite the optimism surrounding SBS, its long-term effectiveness at the reach scale remained uncertain, necessitating further research to fully understand its impact on fluvial systems. The literature review in Chapter 1 identified several research questions for this case study on SBS. The research questions included:

1. Does SBS decrease streambank erosion at the stabilized site?
2. Does SBS increase streambank erosion upstream or downstream of the SBS site?
3. Does SBS induce aggradation or degradation at the reach scale?
4. Does SBS affect stream power at the reach scale?

To answer these questions, a reach scale case study was conducted on two sites located upstream of the John Redmond Reservoir on the Cottonwood River in east-central Kansas. The following research objectives were completed:

- Evaluate lateral erosion rates pre- and post-stabilization by comparing channel cross sections from topographic surveys (Chapter 3).

- Assess reach scale bed erosion and/or deposition rates pre- and post-stabilization by comparing surface models created in Civil3D using bathymetric data (Chapter 3).
- Assess stream power at a reach scale pre- and post-stabilization by modeling SBS site configurations and reach conditions in HEC-RAS (Chapter 4).

After the literature review and site description in chapters 1 and 2, the subsequent chapters focused on the objectives and answering the research questions. In Chapter 3, the lateral erosion rates and bed erosion and/or deposition rates were calculated before and after SBS at the reach scale. The streambank results showed that SBS reduced lateral erosion at the stabilized sites during the initial post-stabilization timeframes. The results also indicated an increase in streambank erosion upstream and downstream during the same timeframes. The streambed results indicated that SBS and a lack of flow events induced aggradation at the reach scale after stabilization. However, these results are based on the limited post-stabilization terrain data, and more monitoring is necessary to determine the long-term effects of SBS on the streambank and streambed of these two sites.

The hypothesis posed in Chapter 1 stated that degradation would be the dominant fluvial adjustment directly upstream of the stabilized site, and aggradation would take place downstream. However, this hypothesis was incorrect as the sites did not act as “sediment transfer zones” during the initial post-construction period. This was evident by the majority of both reaches experiencing deposition.

Chapter 4 focused on modeling stream power using HEC-RAS. The two-dimensional models predicted that all of the combinations of SBS studied in this paper would affect stream power at the reach scale. The simulations indicated stream power would increase in the upstream and downstream meander while decreasing locally in the stabilized zone. These results were influenced by changes in flow velocity and depth caused by channel alteration from SBS.

This research has many potential avenues for future work. One such avenue is simulating various flow events with different durations and magnitudes, which could provide valuable insights and enhanced understanding of the impacts of streambank stabilization across the entire reach. While this study focused on a 10-year return interval flow event, smaller and more frequent flow events, such as the bankfull discharge occurring within a 1-year to 2-year return interval, play a significant role in sediment transport within the stream (Leopold et al., 1964). These modest events, despite their lower magnitude, contribute substantially to geomorphic processes due to their frequency (Leopold et al., 1964). Therefore, future research should consider incorporating simulations corresponding to a 1.5-year flow event to capture the effects of these more frequent events on sediment transport dynamics. Moreover, it may be necessary to simulate larger stream flow events, such as the 25-year, 50-year, and 100-year return interval flow events, which are responsible for sediment movement on a less frequent, but more extreme basis (Whiting et al., 1999). This paper is limited to the simulation of a single flow event, and a broader range of simulated flow events is necessary to fully understand the impacts of streambank stabilization across different flow conditions.

Sediment transport modeling is another aspect of this research that should be evaluated in great detail. A viable option is to use one-dimensional sediment transport modeling in HEC-RAS to analyze how these SBS projects are impacting the transportation of streambank sediment directly. In addition, HEC-RAS offers a two-dimensional option as well that may be able to run more detailed sediment analyses. Valuable insights could be gained by quantifying how the reach scale sediment load changes in response to site specific SBS construction. Along with the sediment transport modeling, HEC-RAS is also capable of performing one-dimensional bank erosion modeling which could be utilized as another method of analyzing SBS.

Furthermore, it may be worth considering an alternative approach to estimating the input flow hydrograph at Site C112. Instead of assuming that the input hydrograph mirrors the flow recorded at the downstream USGS stream gage, a potential option would be to use a HEC-HMS model to simulate the watershed upstream of Site C112. This approach involves using inflow hydrographs from multiple USGS stream gages located on tributaries upstream of Site C112, alongside the original downstream USGS stream gage on the Cottonwood River for calibration and validation against observed data. By using a HEC-HMS model, future analyses could derive a more accurate inflow hydrograph at the boundary of the RAS model for Site C112, mitigating the errors associated with assuming identical input hydrographs for both sites. A preliminary HEC-HMS model was briefly developed for this study. However, more data collection, model refinement, and testing were needed before integrating it into the methodology.

Finally, alternative methods for surveying the river’s bathymetry emerge as possible avenues for future work. While the current use of a robotic total station offers precision, cost-effectiveness, and minimal risk, it's inherently time consuming and tedious. Alternative techniques such as GNSS and sonar surveying present promising avenues for overcoming these limitations. GNSS-based methods offer rapid data acquisition capabilities, enabling more efficient coverage of larger areas within the reach. Similarly, sonar surveying methods provide a non-invasive and time-efficient means of collecting detailed bathymetric data, especially in deeper sections where traditional methods may prove challenging. Exploring these alternative surveying methods not only enhances the efficiency of data collection but also provides an opportunity to extend the reach boundaries. By enabling data collection further upstream and downstream of the SBS projects, these surveying methods allow for a more comprehensive understanding of the hydraulic conditions, morphological changes, and impacts of SBS projects across even broader spatial scales.

Through comprehensive analyses of lateral erosion rates, changes in streambed morphology, and simulations of stream power, this study provided insights into the overall impact of SBS techniques on streambank erosion at a reach scale. While more research is needed to determine if the net amount of sediment that is carried by the river was reduced by these projects, it is clear that localized SBS has reach scale impacts that can increase streambank erosion. Therefore, when designing projects, it is important to consider the entire reach instead of just the site. Additionally, HEC-RAS can help designers make decisions and reduce impacts. Ultimately, these findings contribute to a deeper understanding of the effectiveness and broader implications of SBS projects on river systems, guiding future monitoring and decision-making for sustainable river management practices.

References

Anstead, L., & Boar, R. R. (2010). Willow Spiling: Review of Streambank Stabilisation Projects in the UK. *Freshwater Reviews*, *3*(1), 33–47. https://doi.org/10.1608/FRJ-3.1.2

Anstead, L., Boar, R. R., & Tovey, N. K. (2012). The effectiveness of a soil bioengineering solution for river bank stabilisation during flood and drought conditions: Two case studies from East Anglia: Soil bioengineering solution for river bank stabilisation. *Area*, *44*(4), 479–488. https://doi.org/10.1111/j.1475-4762.2012.01132.x

Arthington, A. H. (2012). *Environmental flows: Saving rivers in the third millennium*. University of California Press.

Beeton, J. M., & Mandel, R. D. (2011). Soils and late-Quaternary landscape evolution in the Cottonwood River basin, east-central Kansas: Implications for archaeological research. *Geoarchaeology*, *26*(5), 693–723. https://doi.org/10.1002/gea.20367

Bhuiyan, F., Hey, R. D., & Wormleaton, P. R. (2009). Effects of Vanes and W-Weir on Sediment Transport in Meandering Channels. *Journal of Hydraulic Engineering*, *135*(5), 339–349. https://doi.org/10.1061/(ASCE)0733-9429(2009)135:5(339)

Bhuiyan, F., Hey, R. D., & Wormleaton, P. R. (2010). Bank-Attached Vanes for Bank Erosion Control and Restoration of River Meanders. *Journal of Hydraulic Engineering*, *136*(9), 583–596. https://doi.org/10.1061/(ASCE)HY.1943-7900.0000217

Bigham, K. A. (2020). Streambank Stabilization Design, Research, and Monitoring: The Current State and Future Needs. *Transactions of the ASABE*, *63*(2), 351–387. https://doi.org/10.13031/trans.13647

Bizzi, S., & Lerner, D. N. (2013). The Use of Stream Power as an Indicator of Channel Sensitivity to Erosion and Deposition Processes. *River Research and Applications*, *31*(1), 16–27. https://doi.org/10.1002/rra.2717

Bressan, F., Wilson, C. G., & Papanicolaou, A. N. T. (2014). Improved streambank countermeasures: The Des Moines River (USA) case study. *International Journal of River Basin Management*, *12*(1), 69–86. https://doi.org/10.1080/15715124.2014.882844

Buchanan, B. P., Nagle, G. N., & Walter, M. T. (2014). LONG-TERM MONITORING AND ASSESSMENT OF A STREAM RESTORATION PROJECT IN CENTRAL NEW YORK: LONG-TERM MONITORING OF A STREAM RESTORATION PROJECT IN NEW YORK. *River Research and Applications*, *30*(2), 245–258. https://doi.org/10.1002/rra.2639

Cavaillé, P., Dommanget, F., Daumergue, N., Loucougaray, G., Spiegelberger, T., Tabacchi, E., & Evette, A. (2013). Biodiversity assessment following a naturality gradient of riverbank protection structures in French prealps rivers. *Ecological Engineering*, *53*, 23–30. https://doi.org/10.1016/j.ecoleng.2012.12.105

Cavaillé, P., Ducasse, L., Breton, V., Dommanget, F., Tabacchi, E., & Evette, A. (2015). Functional and taxonomic plant diversity for riverbank protection works: Bioengineering techniques close to natural banks and beyond hard engineering. *Journal of Environmental Management*, *151*, 65–75. https://doi.org/10.1016/j.jenvman.2014.09.028

Cavaillé, P., Dumont, B., Van Looy, K., Floury, M., Tabacchi, E., & Evette, A. (2018). Influence of riverbank stabilization techniques on taxonomic and functional macrobenthic communities. *Hydrobiologia*, *807*(1), 19–35. https://doi.org/10.1007/s10750-017-3380-3

Chow, V. T. (1959). *Open Channel Hydraulics*.

Clark, L., & Wynn, T. (2007). Methods for Determining Streambank Critical Shear Stress and Soil Erodibility: Implications for Erosion Rate Predictions. *Transactions of the ASABE*, *50*(1), 95–106. https://doi.org/10.13031/2013.22415

Cluer, B., & Thorne, C. (2014). A Stream Evolution Model Integrating Habitat and Ecosystem Benefits: SEM Incorporating Habitat and Ecosystem Benefits. *River Research and Applications*, *30*(2), 135–154. https://doi.org/10.1002/rra.2631

Coduto, D. P., Yeung, M.-C., & Kitch, W. A. (2011). *Geotechnical engineering: Principles and practices* (2nd ed). Pearson.

Correll, D. L. (2005). Principles of planning and establishment of buffer zones. *Ecological Engineering*, *24*(5), 433–439. https://doi.org/10.1016/j.ecoleng.2005.01.007

D. N. Moriasi, J. G. Arnold, M. W. Van Liew, R. L. Bingner, R. D. Harmel, & T. L. Veith. (2007). Model Evaluation Guidelines for Systematic Quantification of Accuracy in Watershed Simulations. *Transactions of the ASABE*, *50*(3), 885–900. https://doi.org/10.13031/2013.23153

Ding, C., Li, C., Song, L., & Chen, S. (2023). Numerical Investigation on Flow Characteristics in a Mildly Meandering Channel with a Series of Groynes. *Sustainability*, *15*(5), 4124. https://doi.org/10.3390/su15054124

Doll, B. A., Grabow, G. L., Hall, K. R., Halley, J., Harman, W. A., Jennings, G. D., & Wise, D. E. (2003). *Stream restoration: A natural channel design handbook*.

Dudgeon, D., Arthington, A. H., Gessner, M. O., Kawabata, Z.-I., Knowler, D. J., Lévêque, C., Naiman, R. J., Prieur-Richard, A.-H., Soto, D., Stiassny, M. L. J., & Sullivan, C. A. (2006). Freshwater biodiversity: Importance, threats, status and conservation challenges. *Biological Reviews*, *81*(02), 163. https://doi.org/10.1017/S1464793105006950

Elhakeem, M., Papanicolaou, A. N. (Thanos), & Wilson, C. G. (2017). Implementing streambank erosion control measures in meandering streams: Design procedure enhanced with numerical modelling. *International Journal of River Basin Management*, *15*(3), 317–327. https://doi.org/10.1080/15715124.2017.1315816

Enlow, H. K., Fox, G. A., Boyer, T. A., Stoecker, A., Storm, D. E., Starks, P., & Guertault, L. (2018). A modeling framework for evaluating streambank stabilization practices for reach-scale sediment reduction. *Environmental Modelling & Software*, *100*, 201–212. https://doi.org/10.1016/j.envsoft.2017.11.010

Fischenich, J. C. (1989). Channel erosion analysis and control. *Proceedings of the Symposium on Headwaters Hydrology. American Water Resources Association, Bethesda Maryland. 1989. p 101-109, 1 Fig, 1 Tab, 6 Ref, 1989*.

Florsheim, J. L., Mount, J. F., & Chin, A. (2008). Bank Erosion as a Desirable Attribute of Rivers. *BioScience*, *58*(6), 519–529. https://doi.org/10.1641/B580608

Fox, G. A., Sheshukov, A., Cruse, R., Kolar, R. L., Guertault, L., Gesch, K. R., & Dutnell, R. C. (2016). Reservoir Sedimentation and Upstream Sediment Sources: Perspectives and Future Research Needs on Streambank and Gully Erosion. *Environmental Management*, *57*(5), 945–955. https://doi.org/10.1007/s00267-016-0671-9

Frothingham, K. M. (2008). Evaluation of stability threshold analysis as a cursory method of screening potential streambank stabilization techniques. *Applied Geography*, *28*(2), 124–133. https://doi.org/10.1016/j.apgeog.2007.07.006

Frye, J. C., & Leonard, A. B. (1959). In: Flint Hills Physiography. *Kansas Geological Survey Guidebook, 24th Field Conference South-Central Kansas*, 79–85.

Gray, D. H., & Sotir, R. B. (1996). *Biotechnical and soil bioengineering slope stabilization: A practical guide for erosion control*. John Wiley & Sons.

Hemmati, M., & Daraby, P. (2019). Erosion and sedimentation patterns associated with restoration structures of bendway weirs. *Journal of Hydro-Environment Research*, *22*, 19–28. https://doi.org/10.1016/j.jher.2018.11.001

Hemmati, M., Ghomeshi, M., Ahmadi, H., & Lanzoni, S. (2016). Scour depth around flat and sloped crest bendway weirs: A laboratory study. *International Journal of River Basin Management*, *14*(1), 83–93. https://doi.org/10.1080/15715124.2015.1085870

IDNR. (2018). *River Restoration Toolbox Practice Guide 2*. Vegetative Restoration. Iowa Department of Natural Resources. https://www.iowadnr.gov/Portals/idnr/uploads/RiverRestoration/toolbox/vegetative-restoration/Practice%202_Vegetative_Restoration_Full_Chapter.pdf

Jamieson, E. C., Rennie, C. D., & Townsend, R. D. (2013a). 3D Flow and Sediment Dynamics in a Laboratory Channel Bend with and without Stream Barbs. *Journal of Hydraulic Engineering*, *139*(2), 154–166. https://doi.org/10.1061/(ASCE)HY.1943-7900.0000655

Jamieson, E. C., Rennie, C. D., & Townsend, R. D. (2013b). Turbulence and Vorticity in a Laboratory Channel Bend at Equilibrium Clear-Water Scour with and without Stream Barbs. *Journal of Hydraulic Engineering*, *139*(3), 259–268. https://doi.org/10.1061/(ASCE)HY.1943-7900.0000673

Johnson, P. A., Hey, R. D., Brown, E. R., & Rosgen, D. L. (2002). STREAM RESTORATION IN THE VICINITY OF BRIDGES. *Journal of the American Water Resources Association*, *38*(1), 55–67. https://doi.org/10.1111/j.1752-1688.2002.tb01534.x

Johnson, P. A., Hey, R. D., Tessier, M., & Rosgen, D. L. (2001). Use of Vanes for Control of Scour at Vertical Wall Abutments. *Journal of Hydraulic Engineering*, *127*(9), 772–778. https://doi.org/10.1061/(ASCE)0733-9429(2001)127:9(772)

Juracek, K. E., & Ziegler, A. C. (2007). *Estimation of Sediment Sources Using Selected Chemical Tracers in the Perry Lake and Lake Wabaunsee Basins, Northeast Kansas* (Scientific Investigations Report) [Scientific Investigations Report].

Karki, S., Nakagawa, H., Kawaike, K., & Hashimoto, M. (2018). *Experimental Study on the Performance of Slope-crested Groynes in Erodible Meandering Channels of Different Sinuosity* (S05). Japan Society for Natural Disaster Science. https://doi.org/10.24762/jndsj.37.S05_93

Khosronejad, A., Hill, C., Kang, S., & Sotiropoulos, F. (2013). Computational and experimental investigation of scour past laboratory models of stream restoration rock structures. *Advances in Water Resources*, *54*, 191–207. https://doi.org/10.1016/j.advwatres.2013.01.008

Khosronejad, A., Kozarek, J. L., Palmsten, M. L., & Sotiropoulos, F. (2015). Numerical simulation of large dunes in meandering streams and rivers with in-stream rock structures. *Advances in Water Resources*, *81*, 45–61. https://doi.org/10.1016/j.advwatres.2014.09.007

Koehn, W. (2023). *Civil Engineering 752—Advanced Hydrology* [Lecture Presentation].

Kondolf, G. M., & Micheli, E. R. (1995). Evaluating stream restoration projects. *Environmental Management*, *19*(1), 1–15. https://doi.org/10.1007/BF02471999

KWO. (2015). *John Redmond Reservoir Watershed Streambank Projects*. Kansas Water Office. https://kwo.ks.gov/projects/john-redmond-streambank

Lagasse, P. F., Clopper, P. E., Pagan-Ortiz, J. E., Zevenbergen, L. W., Arneson, L. A., Schall, J. D., & Girard, L. G. (2009). *Bridge Scour and Stream Instability Countermeasures: Experience, Selection and Design Guidance* (Technical Report FHWA-HI-97-030). Hydraulic Engineering Circular No. 23. Arlington, VA: U.S. Department of Transportation.

Layzell, A., Bigham, K. A., & Moore, T. L. (2019). *Streambank Evaluation of the Cottonwood and Neosho Rivers above John Redmond Reservoir: FINAL REPORT* (Technical Report 1). Kansas Water Office.

Layzell, A., Bigham, K. A., & Moore, T. L. (2020). *Streambank Evaluation of the Cottonwood and Neosho Rivers above John Redmond Reservoir: FINAL REPORT* (Technical Report 2). Kansas Water Office.

Layzell, A., Bigham, K. A., & Moore, T. L. (2021). *Streambank Evaluation of the Cottonwood and Neosho Rivers above John Redmond Reservoir: FINAL REPORT* (Technical Report 3). Kansas Water Office.

Layzell, A., Bigham, K. A., & Moore, T. L. (2022). *Streambank Evaluation of the Cottonwood and Neosho Rivers above John Redmond Reservoir: FINAL REPORT* (Technical Report 4). Kansas Water Office.

Layzell, A., & Mandel, R. (2014). An assessment of the erodibility of Holocene lithounits comprising streambanks in northeastern Kansas, USA. *Geomorphology*, *213*, 116–127. https://doi.org/10.1016/j.geomorph.2014.01.003

Layzell, A., Peterson, A., Moore, T. L., & Bigham, K. A. (2022). UAS-based assessment of streambank stabilization effectiveness in an incised river system. *Geomorphology*, *408*, 108240. https://doi.org/10.1016/j.geomorph.2022.108240

Leopold, L. B., Wolman, M. G., & Miller, J. P. (1964). *Fluvial processes in geomorphology*. Dover publ.

Logar, R., & Scianna, J. (2005). Improving the Establishment of Willow Cuttings in Riparian Areas. *Forestry Technical Note. No. MJ-25. United States Department of Agriculture. NRCS*.

Matsuura, T., & Townsend, R. (2004). Stream-barb installations for narrow channel bends—A laboratory study. *Canadian Journal of Civil Engineering*, *31*(3), 478–486. https://doi.org/10.1139/l04-017

Miller, E. S. (2022). *Analysis of river restoration and stabilization practitioners, their design tools and limits* [Kansas State University]. https://krex.k-state.edu/dspace/bitstream/handle/2097/42833/EliMiller2022.pdf?sequence=3&isAllowed=y

Miller, J., & Kochel, C. (2010). Assessment of channel dynamics, in-stream structures and post-project channel adjustments in North Carolina and its implications to effective stream restoration. *Environmental Earth Sciences*, *59*(8), 1681–1692. https://doi.org/10.1007/s12665-009-0150-1

Miller, J. R., & Kochel, C. (2013). Use and performance of in-stream structures for river restoration: A case study from North Carolina. *Environmental Earth Sciences*, *68*(6), 1563–1574. https://doi.org/10.1007/s12665-012-1850-5

Moerke, A., & Lamberti, G. (2004). Restoring Stream Ecosystems: Lessons from a Midwestern State. *Restoration Ecology*, *12*(3), 327–334. https://doi.org/10.1111/j.1061-2971.2004.0340.x

Naisargi, D., & Mittelstet, A. (2017). Quantifying Effectiveness of Streambank Stabilization Practices on Cedar River, Nebraska. *Water*, *9*(12), 930. https://doi.org/10.3390/w9120930

Nassar, D. M. B. (2019). *Monitoring the Effectiveness of Streambank Stabilization Projects in Northeast Kansas.* [Masters Thesis]. Kansas State University.

Niedzinski, V. (2021). *Studying the soil-strength effects of vegetation for slope stabilization and erosion control along streambanks and roadside slopes* [Auburn University]. http://oatd.org/oatd/record?record=oai\:etd.auburn.edu\:10415\%2F7743&q=Studying%20the%20Soil-Strength%20Effects%20of%20Vegetation%20for%20Slope%20Stabilization%20AND%20Erosion%20Control%20Along%20Streambanks%20AND%20Roadside%20Slopes

Niezgoda, S. L., & Johnson, P. A. (2006). Modeling the Long Term Impacts of using Rigid Structures in Stream Channel Restoration [1]. *Journal of the American Water Resources Association*, *42*(6), 1597–1613. https://doi.org/10.1111/j.1752-1688.2006.tb06023.x

NRCS. (2013). *Design of Stream Barbs* [Kansas Engineering Technical Note No. KS-1 (Revision 1)]. Salina, Kansas: USDA Natural Resources Conservation Service.

Nunnally, N. R., & Keller, E. (1979). *Use of Fluvial Process to Minimize Adverse Effects of Stream Channelization* (144). Water Resources Research lnstitute. https://repository.lib.ncsu.edu/bitstream/handle/1840.4/1686/NC-WRRI-144.pdf?sequence=1

Pagliara, S., Kurdistani, S. M., & Santucci, I. (2013). Scour downstream of J-Hook vanes in straight horizontal channels. *Acta Geophysica*, *61*(5), 1211–1228. https://doi.org/10.2478/s11600-013-0143-z

Pagliara, S., & Mahmoudi Kurdistani, S. (2015). Clear water scour at J-Hook Vanes in channel bends for stream restorations. *Ecological Engineering*, *83*, 386–393. https://doi.org/10.1016/j.ecoleng.2015.07.003

Papanicolaou, A. N. (Thanos), Elhakeem, M., & Wardman, B. (2011). Calibration and Verification of a 2D Hydrodynamic Model for Simulating Flow around Emergent Bendway Weir Structures. *Journal of Hydraulic Engineering*, *137*(1), 75–89. https://doi.org/10.1061/(ASCE)HY.1943-7900.0000280

Patel, H. K., Arora, S., Lade, A. D., Kumar, B., & Azamathulla, H. Md. (2023). Flow behaviour concerning bank stability in the presence of spur dike – A review. *Water Supply*, *23*(1), 237–258. https://doi.org/10.2166/ws.2022.418

Peel, M. C., Finlayson, B. L., & McMahon, T. A. (2007). Updated world map of the Köppen-Geiger climate classification. *Hydrology and Earth System Sciences*, *11*(5), 1633–1644. https://doi.org/10.5194/hess-11-1633-2007

PRISM Climate Group, Oregon State U. (2011). *Average monthly and average annual precipitation, 1981–2010 by State*. Northwest Alliance for Computational Science & Engineering. https://prism.oregonstate.edu/

Radspinner, R. R., Diplas, P., Lightbody, A. F., & Sotiropoulos, F. (2010). River Training and Ecological Enhancement Potential Using In-Stream Structures. *Journal of Hydraulic Engineering*, *136*(12), 967–980. https://doi.org/10.1061/(ASCE)HY.1943-7900.0000260

Recking, A., Piton, G., Montabonnet, L., Posi, S., & Evette, A. (2019). Design of fascines for riverbank protection in alpine rivers: Insight from flume experiments. *Ecological Engineering*, *138*, 323–333. https://doi.org/10.1016/j.ecoleng.2019.07.019

Rosgen, D. (1996). *Applied river morphology* (Second). Wildland Hydrology.

Rosgen, D. (2009). *Watershed Assessment of River Stability and Sediment Supply (WARSS)* (Second). Wildland Hydrology.

Russell, M., Mittelstet, A. R., Messer, T. L., Korus, J. T., & Joeckel, R. M. (2021a). Evolution of three streambanks before and after stabilization and record flooding. *Ecological Engineering*, *170*, 106357. https://doi.org/10.1016/j.ecoleng.2021.106357

Russell, M. V., Mittelstet, A. R., Joeckel, R. M., Korus, J. T., & Castro-Bolinaga, C. F. (2021b). Impact of Bank Stabilization Structures on Upstream and Downstream Bank Mobilization at Cedar River, Nebraska. *Transactions of the ASABE*, *64*(5), 1555–1567. https://doi.org/10.13031/trans.14551

Schiff, R., Benoit, G., & MacBroom, J. (2011). Evaluating stream restoration: A case study from two partially developed 4th order Connecticut, U.S.A. streams and evaluation monitoring strategies: EVALUATING STREAM RESTORATION. *River Research and Applications*, *27*(4), 431–460. https://doi.org/10.1002/rra.1365

Schumm, S. A., Harvey, M. D., & Watson, C. C. (1984). *Incised channels: Morphology, dynamics, and control*. Water Resources Publications.

Shields, F. D., Copeland, R. R., Klingeman, P. C., Doyle, M. W., & Simon, A. (2003). Design for Stream Restoration. *Journal of Hydraulic Engineering*, *129*(8), 575–584. https://doi.org/10.1061/(ASCE)0733-9429(2003)129:8(575)

Shields, F. D., Knight, S. S., & Cooper, C. M. (2000). Warmwater Stream Bank Protection and Fish Habitat: A Comparative Study. *Environmental Management*, *26*(3), 317–328. https://doi.org/10.1007/s002670010089

Shields, F. D., Knight, S. S., & Cooper, C. M. (1998b). Rehabilitation of aquatic habitats in warmwater streams damaged by channel incision in Mississippi. *Hydrobiologia*, *382*(1/3), 63–86. https://doi.org/10.1023/A:1003485021076

Simon, A., & Collison, A. J. C. (2002). Quantifying the mechanical and hydrologic effects of riparian vegetation on streambank stability. *Earth Surface Processes and Landforms*, *27*(5), 527–546. https://doi.org/10.1002/esp.325

Simon, A., Curini, A., Darby, S. E., & Langendoen, E. J. (2000). Bank and near-bank processes in an incised channel. *Geomorphology*, *35*(3–4), 193–217. https://doi.org/10.1016/S0169-555X(00)00036-2

Simon, A., & Hupp, C. R. (1986). Channel Evolution in Modified Tennessee Channels. *Proceedings of the 4th Federal Interagency Sedimentation Conference*, *2*, 5.71-5.82.

Simon, A., Pollen-Bankhead, N., Mahacek, V., & Langendoen, E. (2009). Quantifying Reductions of Mass-Failure Frequency and Sediment Loadings From Streambanks Using Toe Protection and Other Means: Lake Tahoe, United States. *JAWRA Journal of the American Water Resources Association*, *45*(1), 170–186. https://doi.org/10.1111/j.1752-1688.2008.00268.x

Simon, A., & Rinaldi, M. (2000). CHANNEL INSTABILITY IN THE LOESS AREA OF THE MIDWESTERN UNITED STATES. *Journal of the American Water Resources Association*, *36*(1), 133–150. https://doi.org/10.1111/j.1752-1688.2000.tb04255.x

Simon, K., & Steinemann, A. (2000). Soil Bioengineering: Challenges for Planning and Engineering. *Journal of Urban Planning and Development*, *126*(2), 89–102. https://doi.org/10.1061/(ASCE)0733-9488(2000)126:2(89)

Uijttewaal, W. S. (2005). Effects of Groyne Layout on the Flow in Groyne Fields: Laboratory Experiments. *Journal of Hydraulic Engineering*, *131*(9), 782–791. https://doi.org/10.1061/(ASCE)0733-9429(2005)131:9(782)

U.S. Geological Survey. (2014). *National Land Cover Database (NLCD) 2011 Land Cover Conterminous United States*. https://doi.org/10.5066/P97S2IID

USACE. (2024a). *HEC-RAS 1D Sediment Transport: BSTEM - Technical Reference Manual*. United States Army Corps of Engineers. https://www.hec.usace.army.mil/confluence/rasdocs/rassed1d/1d-sediment-transport-technical-reference-manual/bstem-technical-reference-manual/overview

USACE. (2024b). *HEC-RAS Hydraulic Reference Manual*. United States Army Corps of Engineers. https://www.hec.usace.army.mil/confluence/rasdocs/ras1dtechref/latest

Vörösmarty, C. J., McIntyre, P. B., Gessner, M. O., Dudgeon, D., Prusevich, A., Green, P., Glidden, S., Bunn, S. E., Sullivan, C. A., Liermann, C. R., & Davies, P. M. (2010). Global threats to human water security and river biodiversity. *Nature*, *467*(7315), 555–561. https://doi.org/10.1038/nature09440

Watson, C. C., Abt, S. R., & Derrick, D. (1997). WILLOW POSTS BANK STABILIZATION [1]. *JAWRA Journal of the American Water Resources Association*, *33*(2), 293–300. https://doi.org/10.1111/j.1752-1688.1997.tb03510.x

Whiting, P. J., Stamm, J. F., Moog, D. B., & Orndorff, R. L. (1999). Sediment-transporting flows in headwater streams. *GSA Bulletin*, *111*(3), 450–466. https://doi.org/10.1130/0016-7606(1999)111<0450:STFIHS>2.3.CO;2

Wu, L., Xu, Y., Yuan, J., Xu, Y., Wang, Q., Xu, X., & Wen, H. (2018). Impacts of Land Use Change on River Systems for a River Network Plain. *Water*, *10*(5), 609. https://doi.org/10.3390/w10050609

Wynn, S. Mostaghimi, & Elizabeth F. Alphin. (2004). The Effects of Vegetation on Stream Bank Erosion. *2004, Ottawa, Canada August 1 - 4, 2004*. 2004, Ottawa, Canada August 1 - 4, 2004. https://doi.org/10.13031/2013.16423

Appendix A - Streambank Lateral Retreat Rate Analysis Tables

Appendix A Table A.1 Differences in cross-sectional area (A_d) between consecutive yearly surveys for streambank analysis at Site C112.

Site C112: Difference in Area (m^2)					
Cross Section ID	Bank of Interest	2018 to 2019	2019 to 2021	2021 to 2022	2022 to 2023
XS 1	Right	-2.87	-1.90	-1.83	0.16
XS 2	Right	10.45	5.62	Construction	0.32
XS 3	Right	22.23	7.58	Construction	-0.92
XS 4	Right	26.90	1.27	Construction	-0.88
RXS 2	Right	37.23	1.02	Construction	-0.44
XS 5	Left	-3.90	4.89	-0.37	0.99
XS 6	Left	11.48	8.71	8.52	0.02
XS 7	Left	5.42	2.85	3.38	4.73

Appendix A Table A.2 Differences in cross-sectional area (A_d) between consecutive yearly surveys for streambank analysis at Site C102.

Site C102: Difference in Area (m^2)						
Cross Section ID	Bank of Interest	2018 to 2019	2019 to 2021	2021 to 2022	2022 to 2023	2023 to 2024
XS 1	Left	9.94	6.26	10.95	-4.59	5.16
XS 2	Left	1.17	5.78	2.13		4.83
XS 3	Right	21.53	7.10	-3.04	Construction	-6.39
XS 4	Right	18.74	0.18	13.84	Construction	-4.08
XS 5	Right	15.96	9.67	4.92	Construction	-4.28
XS 6	Right	10.37	11.67	1.23	Construction	-2.63
XS 7	Right	22.46	6.22	2.68	Construction	-7.61
XS 8	Left	N/A	5.29	-0.03	0.18	15.48
XS 9	Left	N/A	5.86	2.15	-1.39	-12.84

Appendix A Table A.3 Illustrates the total streamflow volumes in cubic kilometers for the timeframes at both Site C112 and Site C112. The variations in flow volumes across the two site's timeframes are due to differences in the exact dates of the survey missions.

Site C112: Total Streamflow Volume (km^3)				Site C102: Total Streamflow Volume (km^3)				
2018 to 2019	**2019 to 2021**	**2021 to 2022**	**2022 to 2023**	**2018 to 2019**	**2019 to 2021**	**2021 to 2022**	**2022 to 2023**	**2023 to 2024**
2.26	1.01	0.76	0.09	2.25	1.11	0.67	0.07	0.25

Appendix A Table A.4 Summary of Average Bank Heights for each cross section at Site C112.

Site C112: Average Bank Height (m)					
Cross Section ID	Bank of Interest	2018 to 2019	2019 to 2021	2021 to 2022	2022 to 2023
XS 1	Right	6.40	6.34	6.17	6.01
XS 2	Right	9.85	10.03	Construction	4.88
XS 3	Right	9.98	10.51	Construction	4.05
XS 4	Right	9.49	9.80	Construction	4.92
RXS 2	Right	9.46	9.43	Construction	5.32
XS 5	Left	3.76	3.47	3.42	3.71
XS 6	Left	11.77	11.86	12.14	12.31
XS 7	Left	9.74	9.83	10.04	10.17

Appendix A Table A.5 Summary of Average Bank Heights for each cross section at Site C102.

Site C102: Average Bank Height (m)						
Cross Section ID	Bank of Interest	2018 to 2019	2019 to 2021	2021 to 2022	2022 to 2023	2023 to 2024
XS 1	Left	10.02	10.28	10.17	10.30	10.64
XS 2	Left	9.22	9.22	9.11		8.89
XS 3	Right	9.57	9.55	9.64	Construction	5.75
XS 4	Right	9.79	9.31	8.28	Construction	6.22
XS 5	Right	10.31	10.29	10.31	Construction	6.29
XS 6	Right	8.26	8.14	8.04	Construction	5.64
XS 7	Right	9.46	9.32	9.20	Construction	5.39
XS 8	Left	N/A	7.52	7.75	7.44	7.28
XS 9	Left	N/A	9.91	10.11	10.35	10.29

Appendix B - Streambed Analysis Maps

Appendix B Figure B.1 Site C112 Streambed Cut and Fill Map from 2018 to 2019

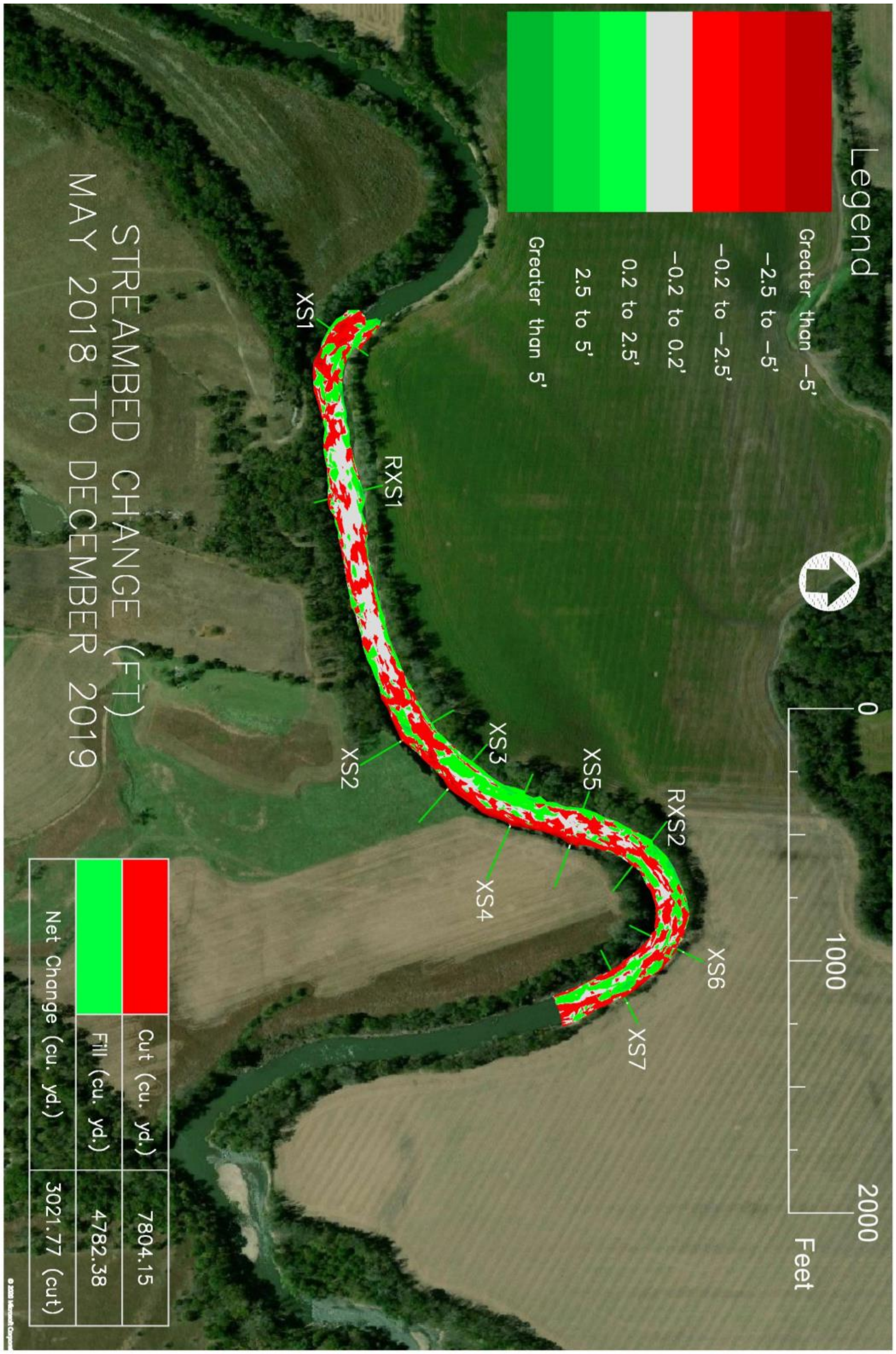

Appendix B Figure B.2 Site C112 Streambed Cut and Fill Map from 2019 to 2021

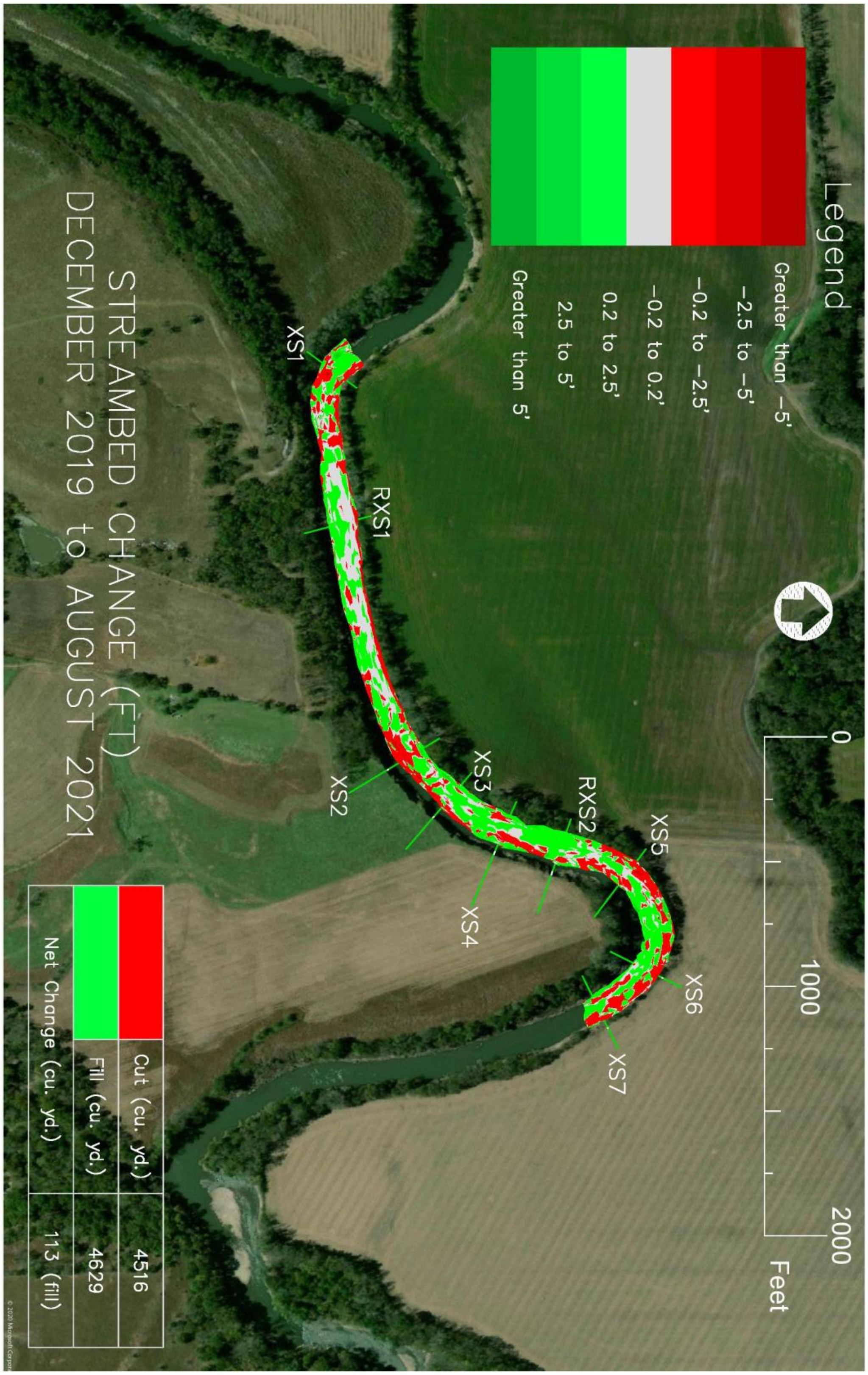

Appendix B Figure B.3 Site C112 Streambed Cut and Fill Map from 2021 to 2022

Appendix B Figure B.4 Site C112 Streambed Cut and Fill Map from 2022 to 2023

Appendix B Figure B.5 Site C102 Streambed Cut and Fill Map from 2018 to 2019

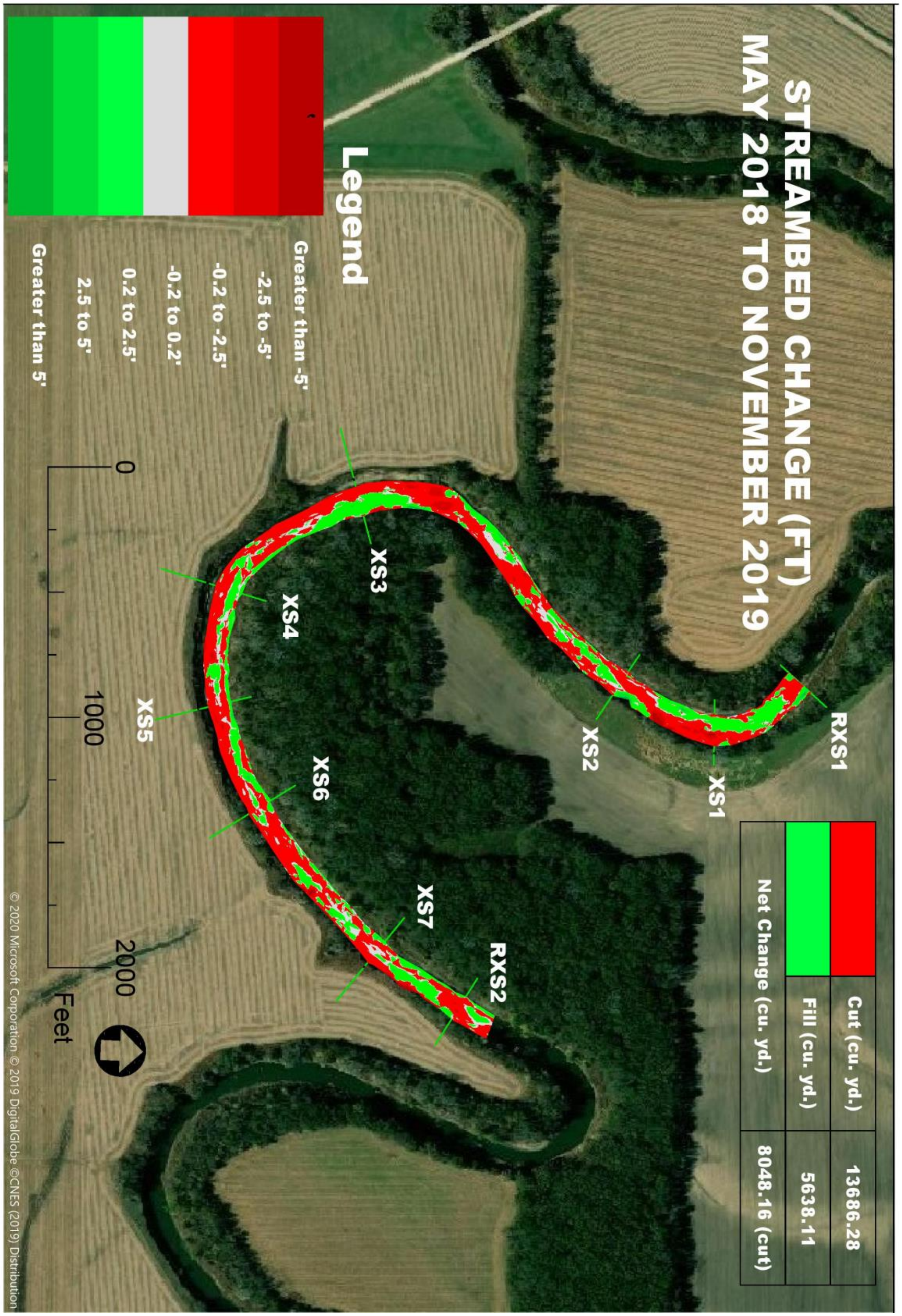

Appendix B Figure B.6 Site C102 Streambed Cut and Fill Map from 2019 to 2021

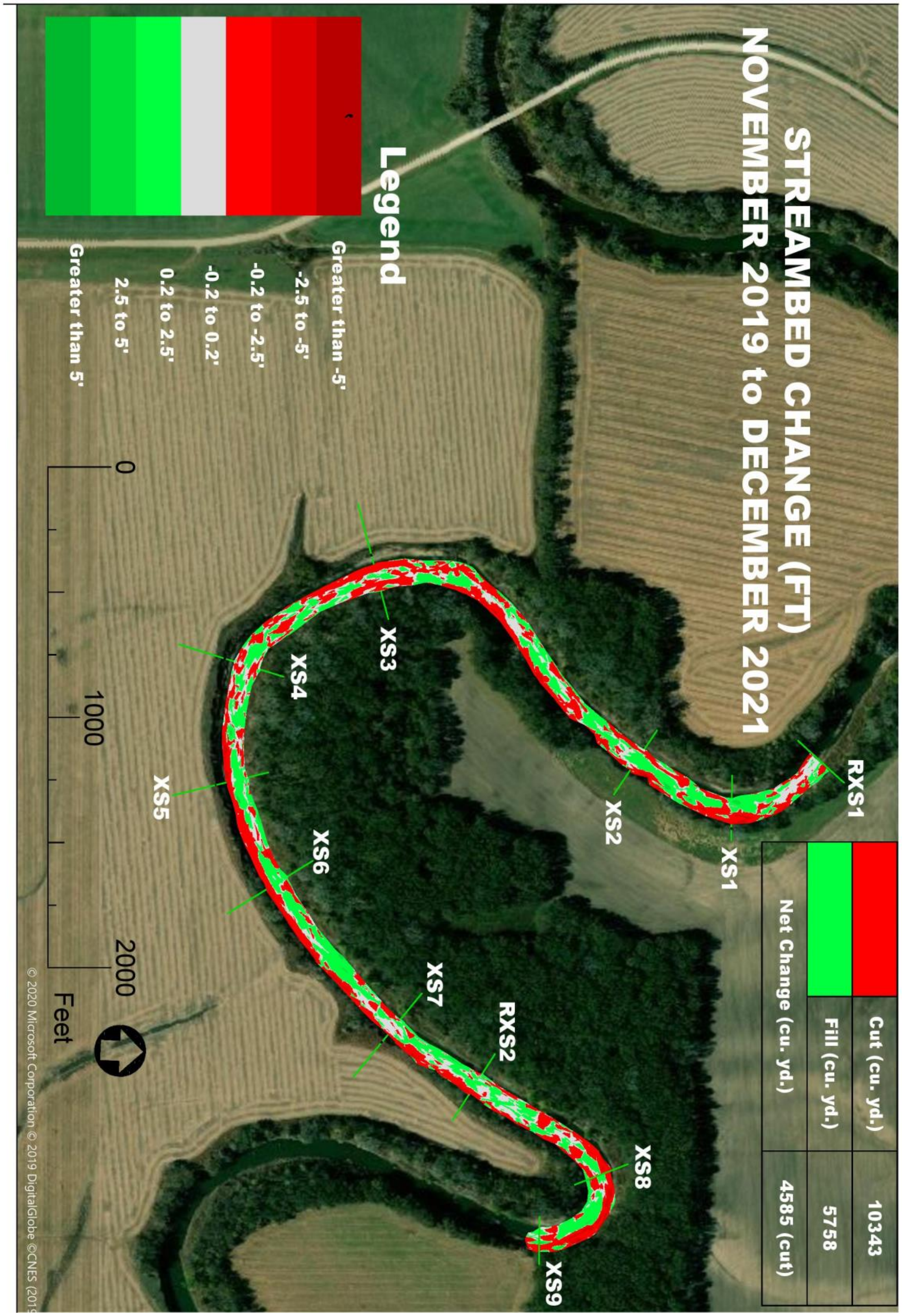

Appendix B Figure B.7 Site C102 Streambed Cut and Fill Map from 2021 to 2022

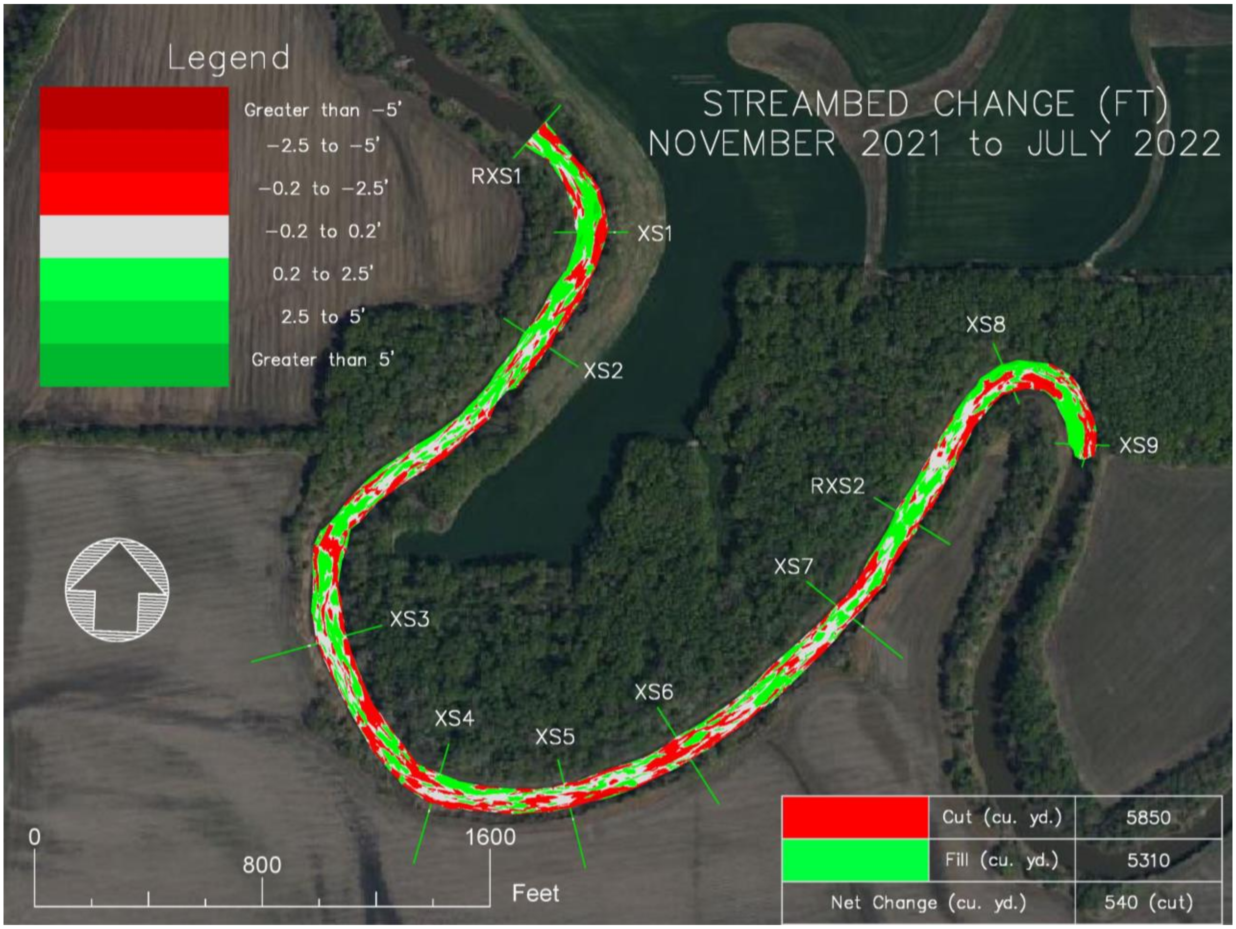

Appendix B Figure B.8 Site C102 Streambed Cut and Fill Map from 2022 to 2023

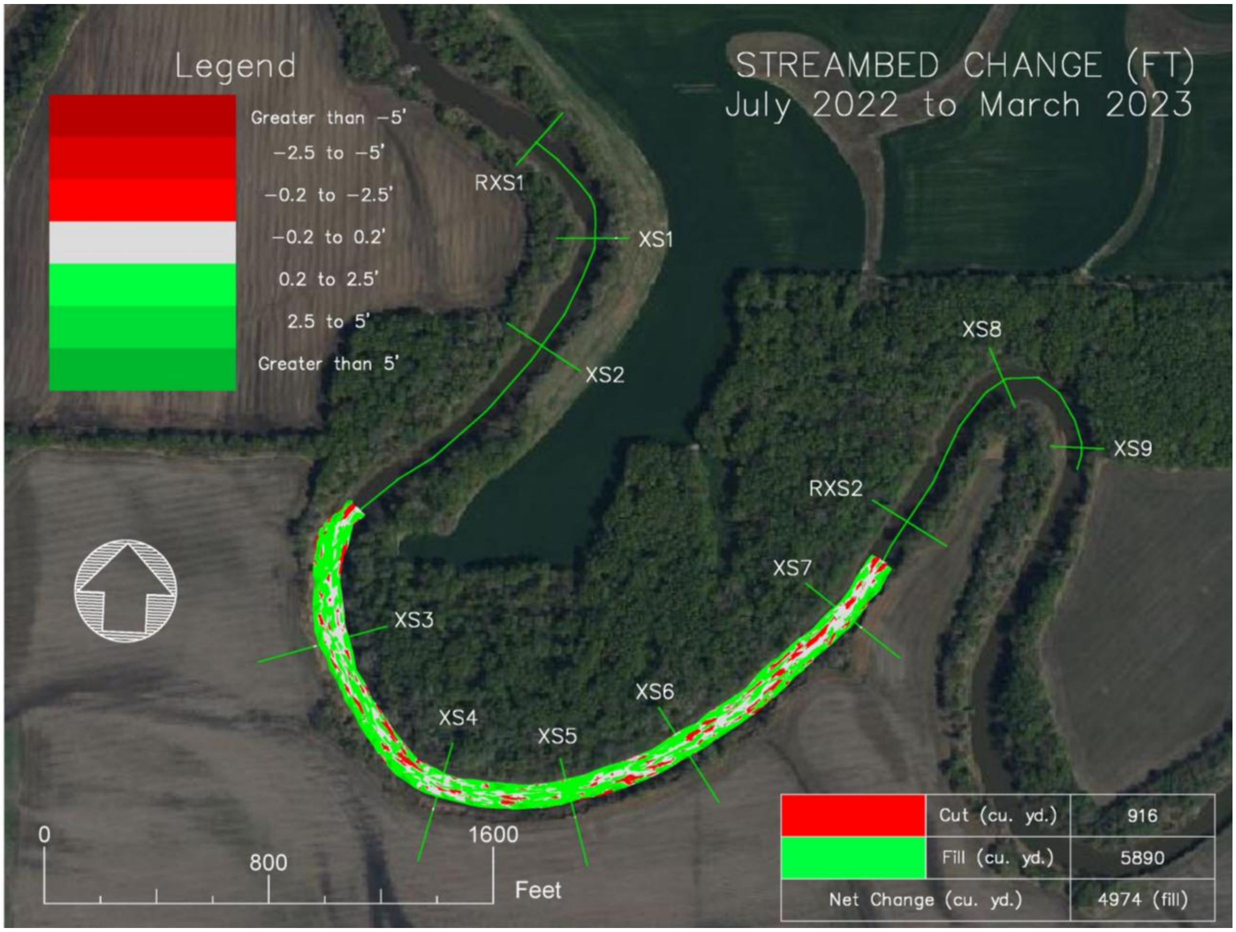

Appendix B Figure B.9 Site C102 Streambed Cut and Fill Map from 2022 to 2024

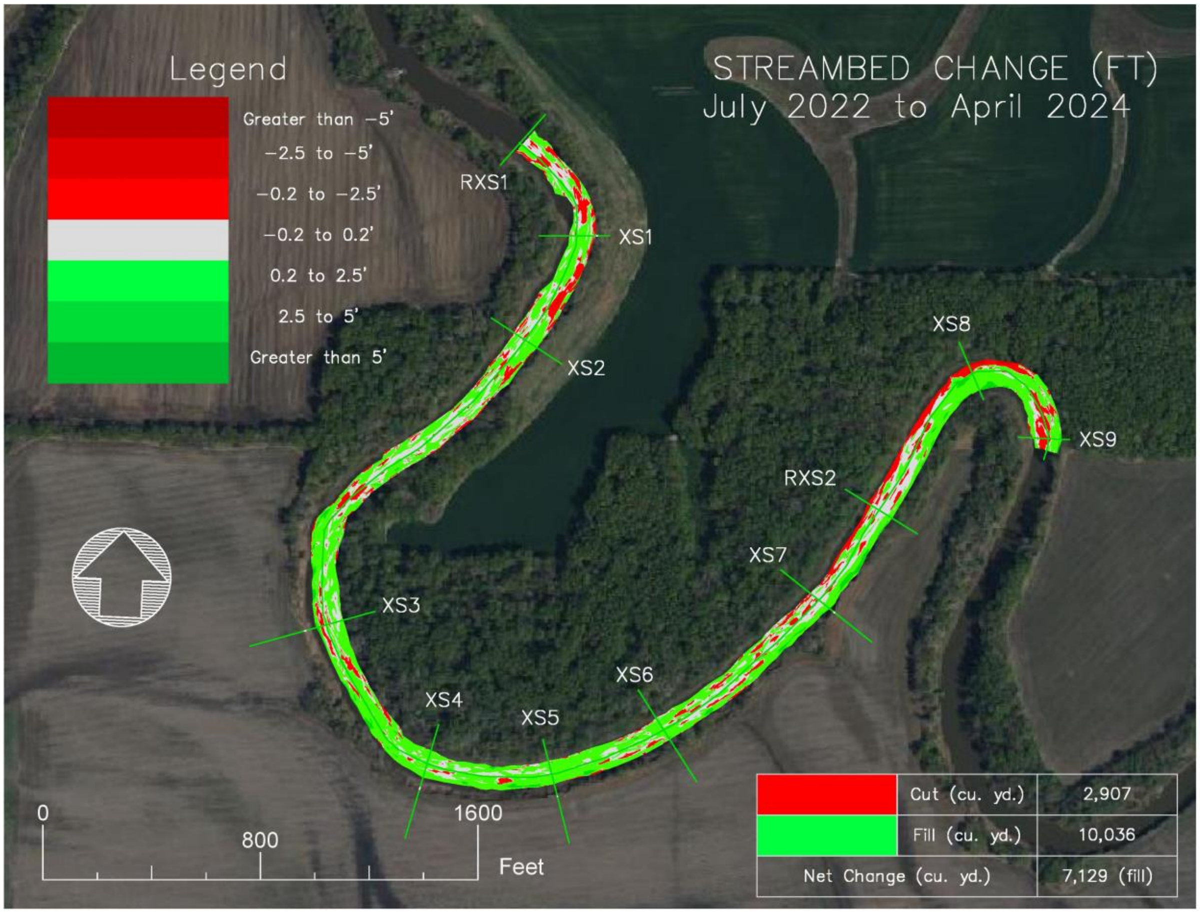

Appendix C - HEC-RAS Modeling Components

Appendix C Figure C.1 HEC-RAS perimeters for Site C112 (top) and Site C102 (bottom).

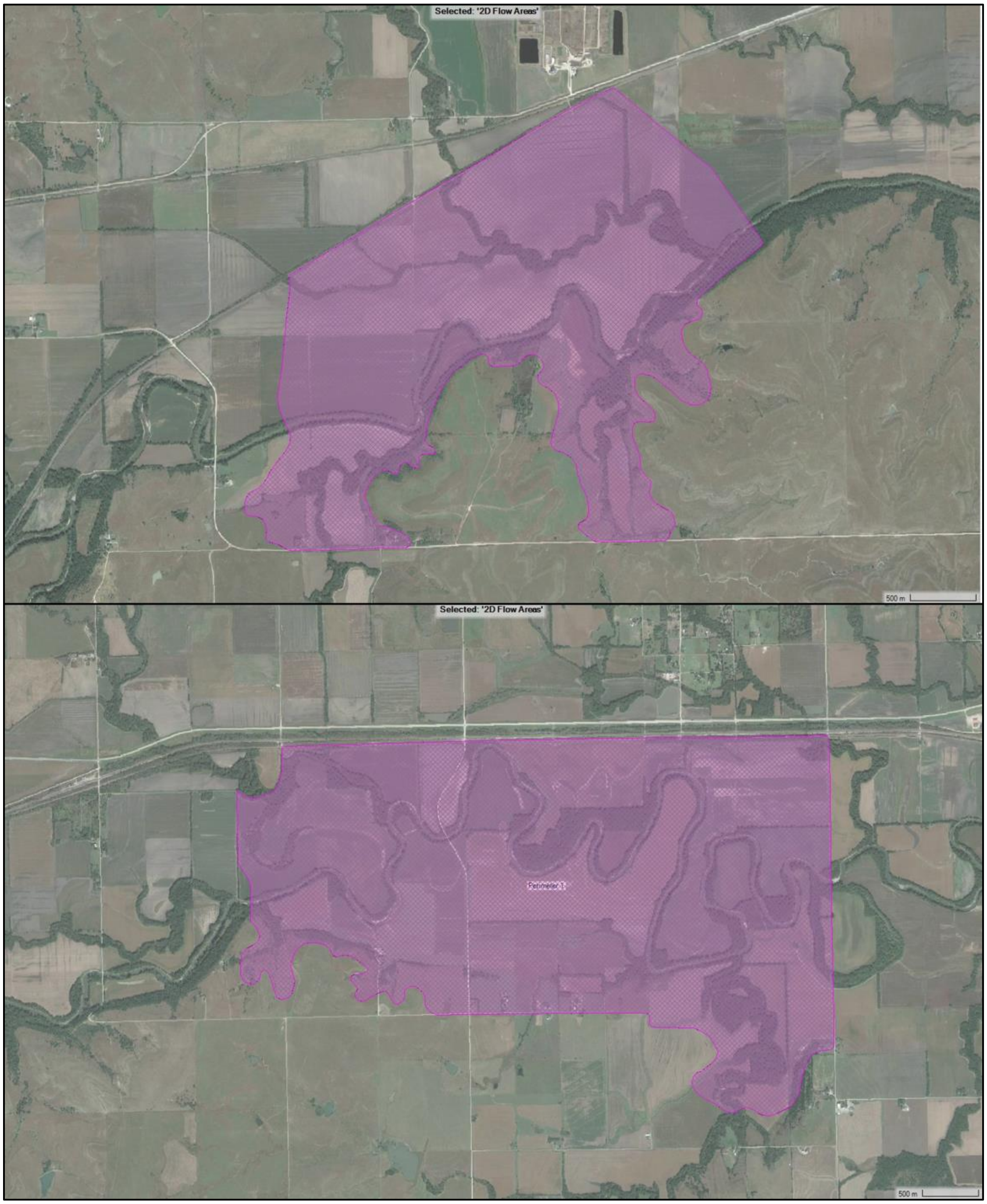

Appendix C Figure C.2 HEC-RAS pre-stabilization breaklines for Site C112 (top) and Site C102 (bottom).

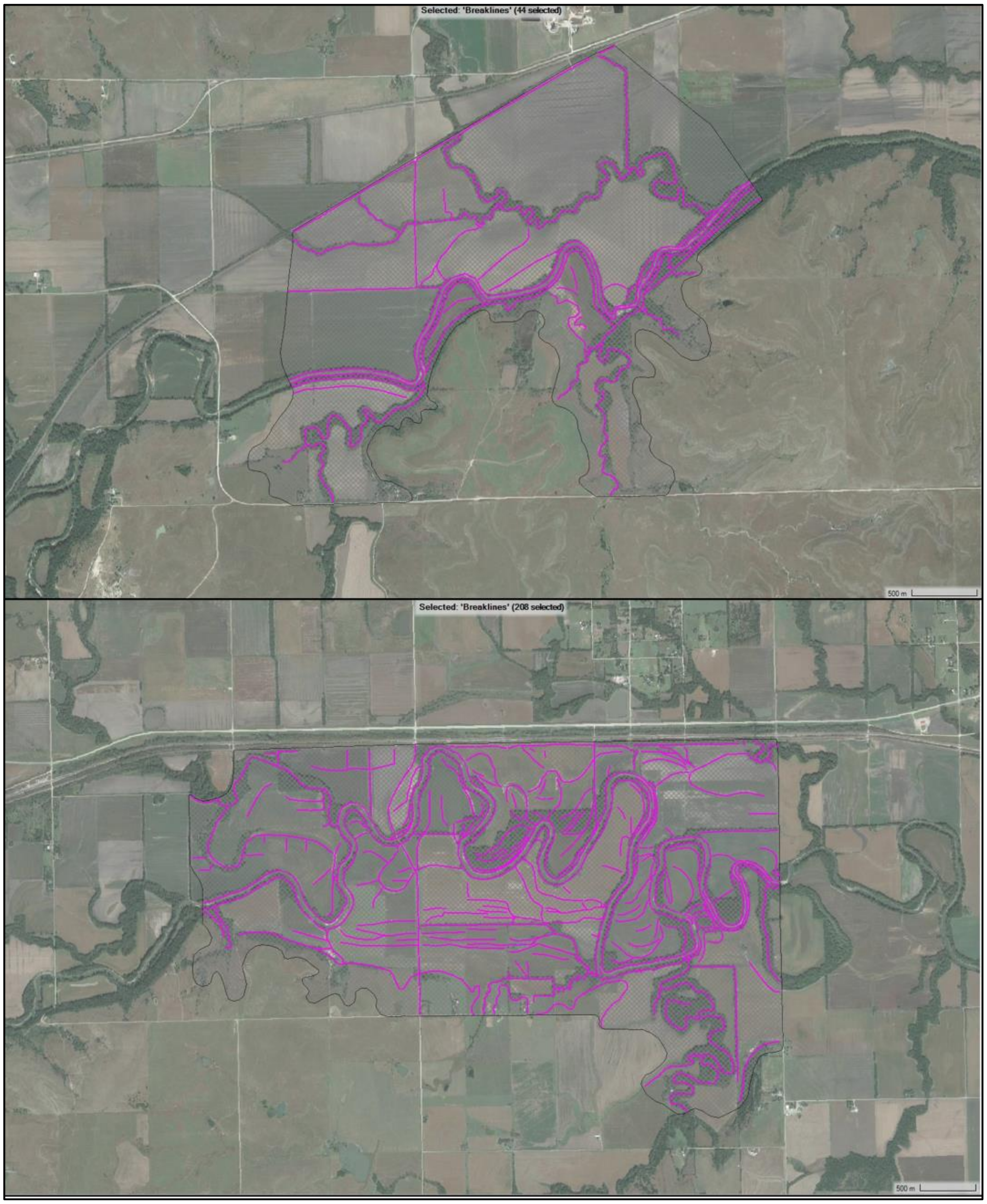

Appendix C Figure C.3 HEC-RAS refinement regions for Site C112 (top) and Site C102 (bottom).

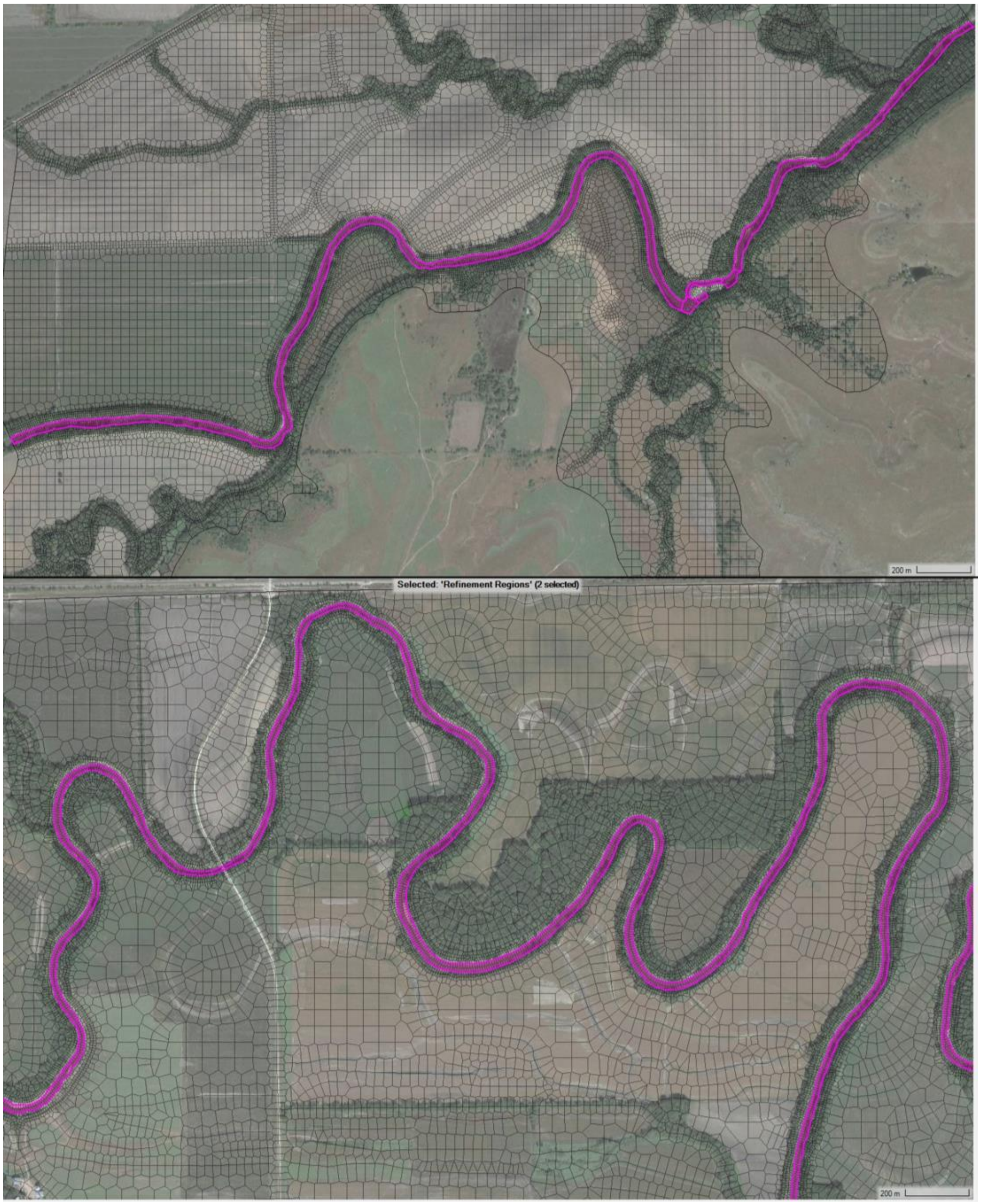

Appendix D - Cross Section Overlays

Appendix D Figure D.1 Site C112 Cross Section 1 Overlays

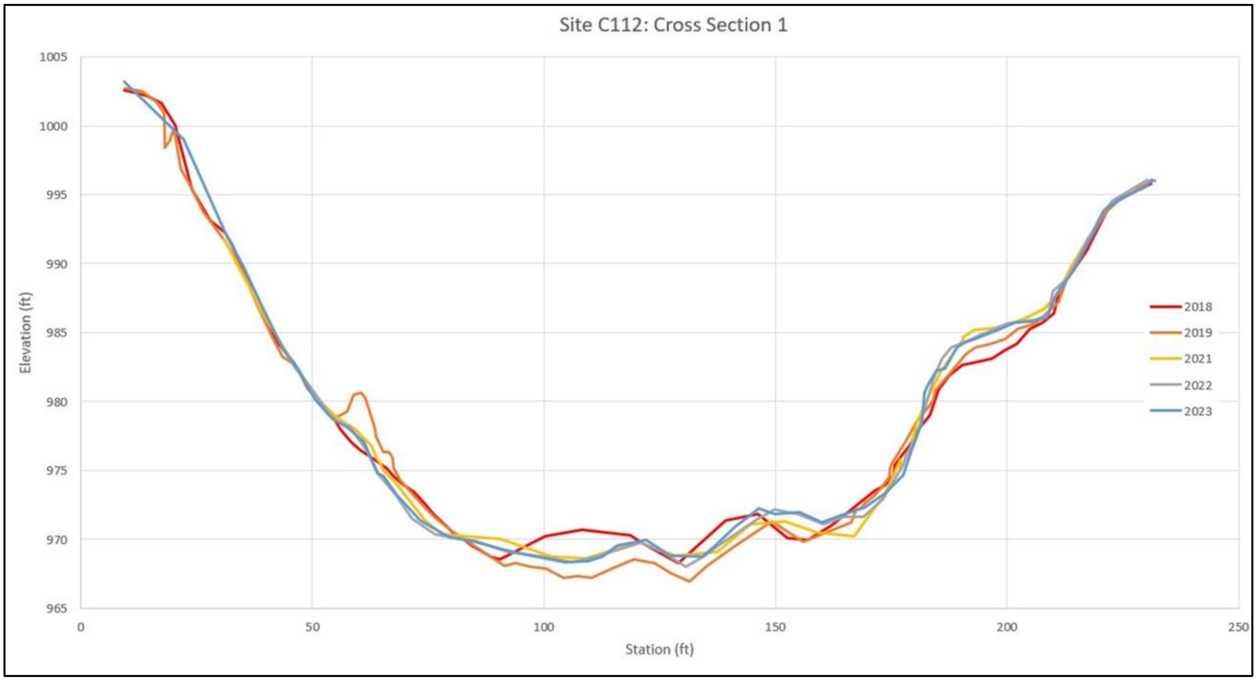

Appendix D Figure D.2 Site C112 Riffle Cross Section 1 Overlays

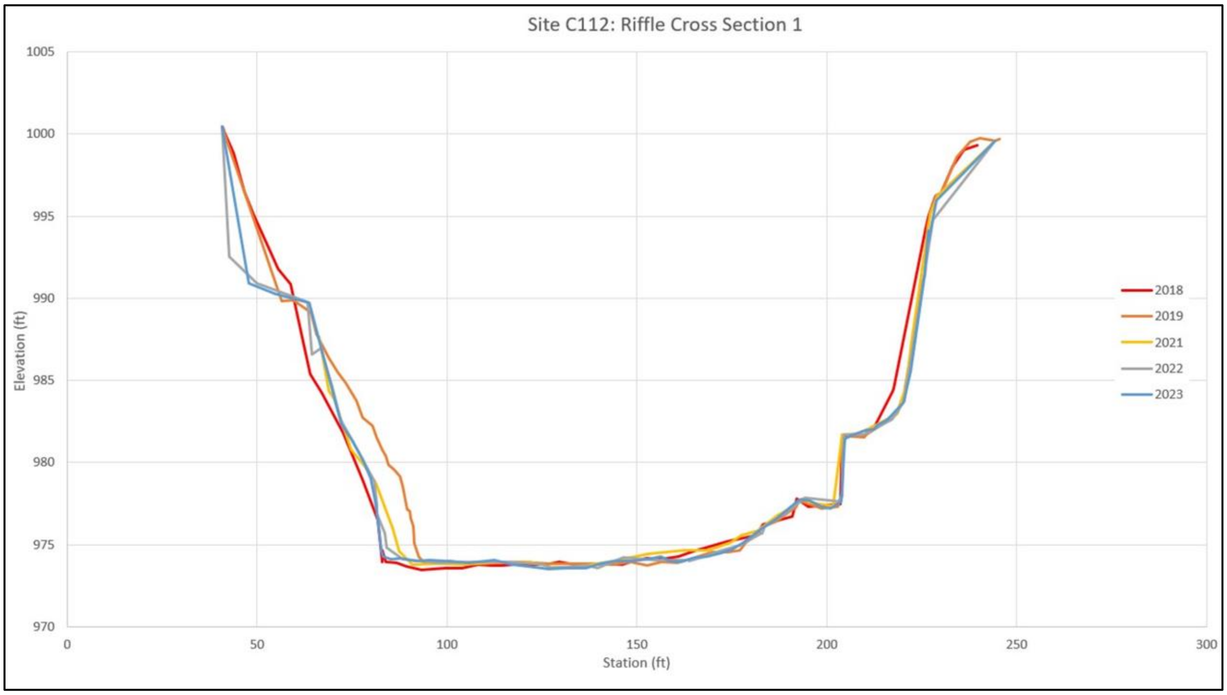

Appendix D Figure D.3 Site C112 Cross Section 2 Overlays

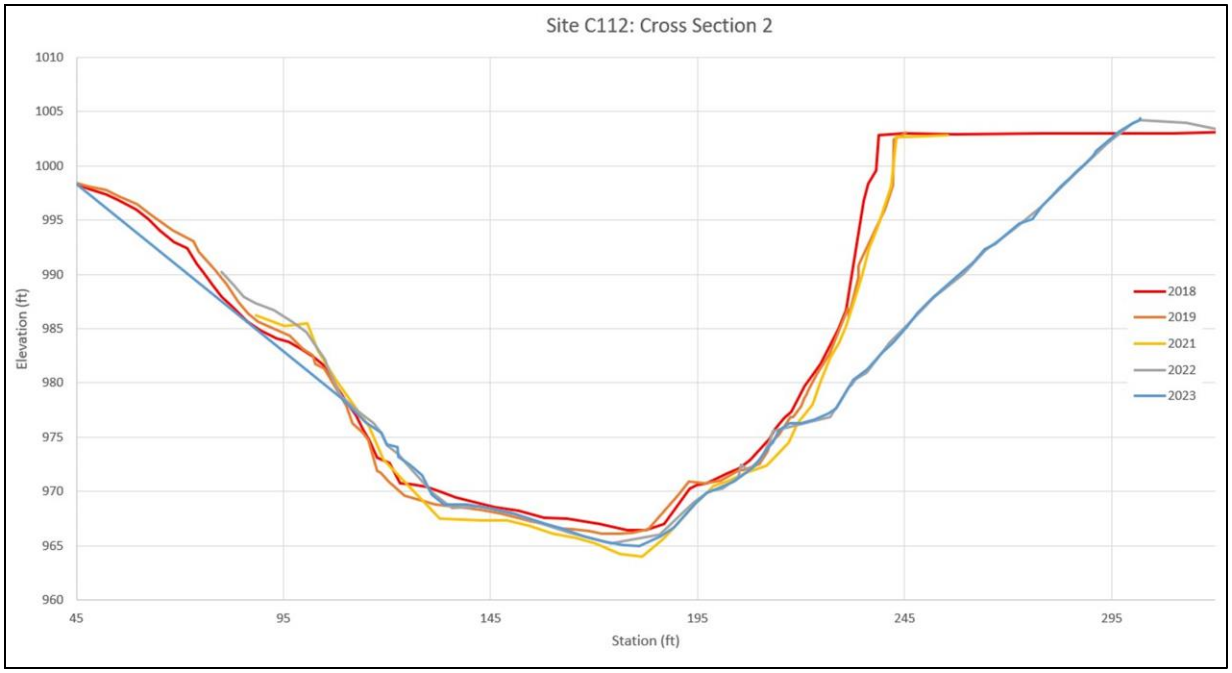

Appendix D Figure D.4 Site C112 Cross Section 3 (Stabilized) Overlays

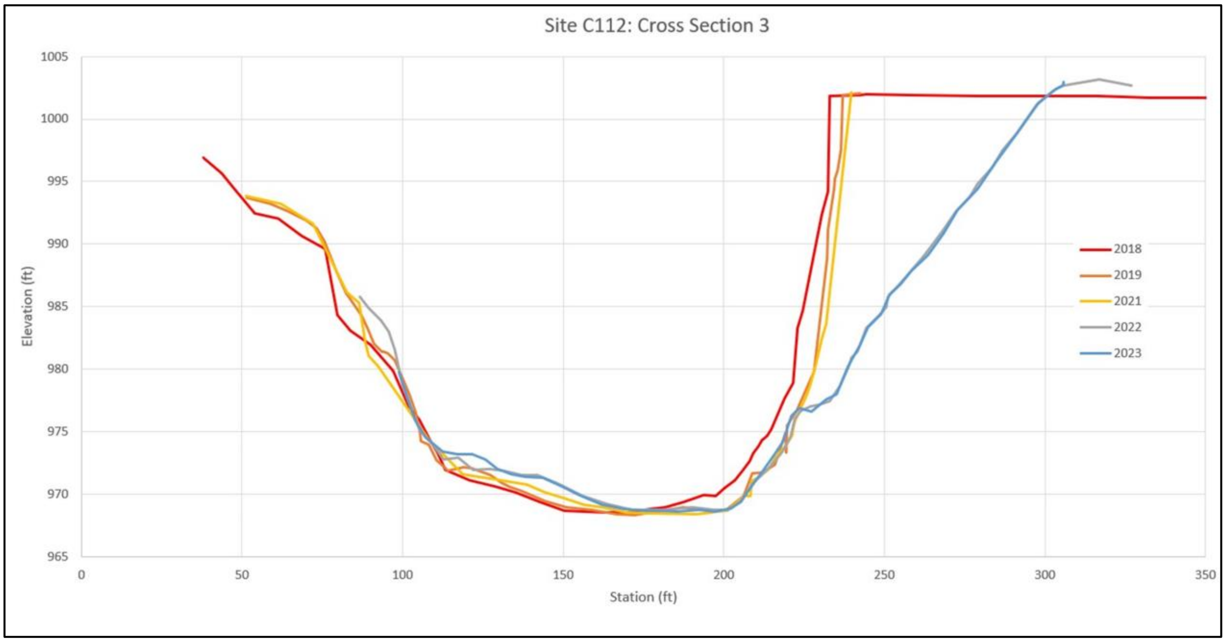

Appendix D Figure D.5 Site C112 Cross Section 4 (Stabilized) Overlays

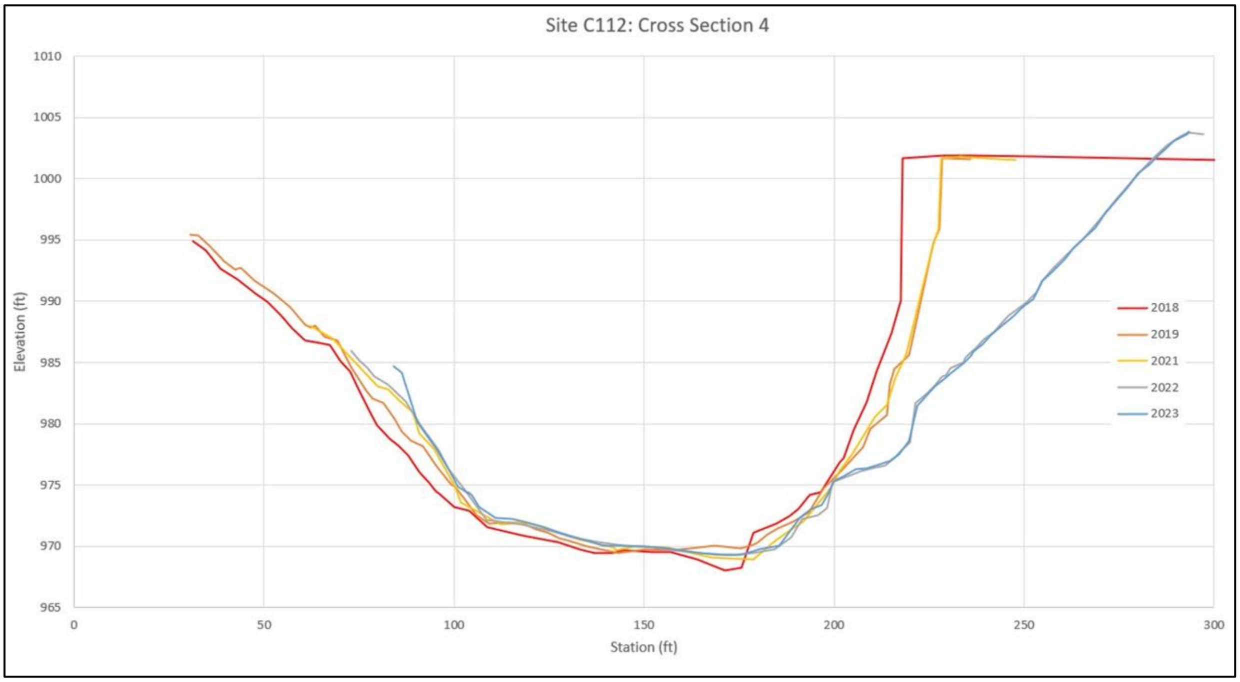

Appendix D Figure D.6 Site C112 Riffle Cross Section 2 (Stabilized) Overlays

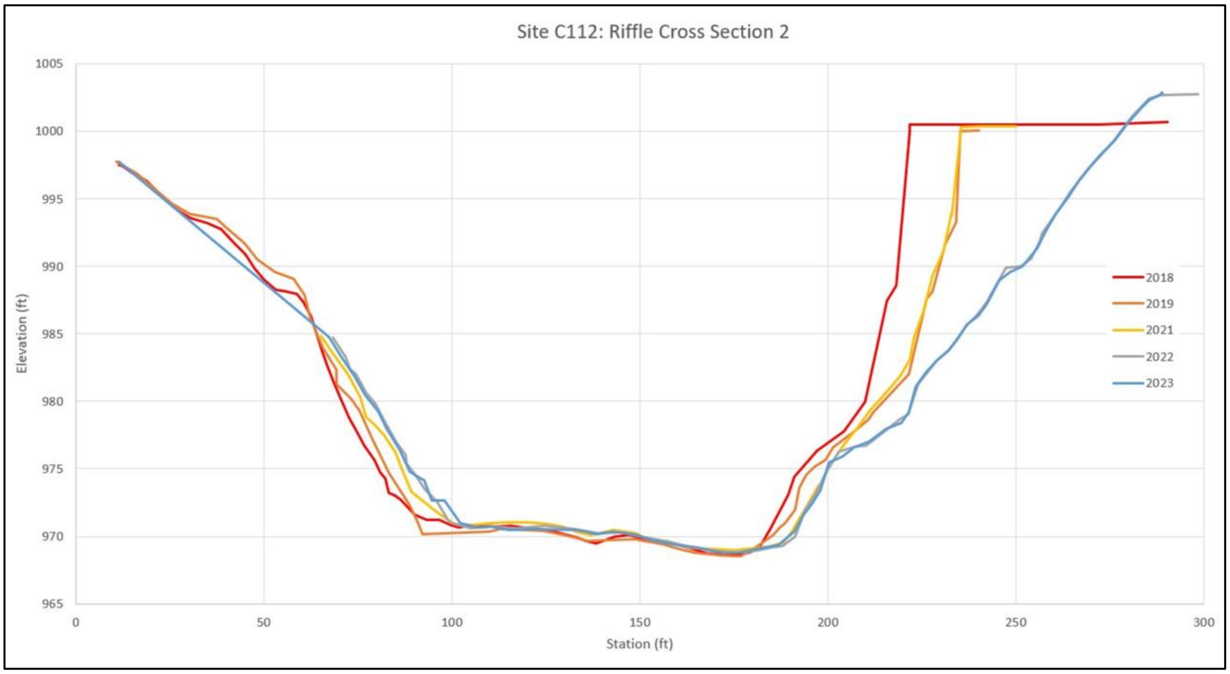

Appendix D Figure D.7 Site C112 Cross Section 5 Overlays

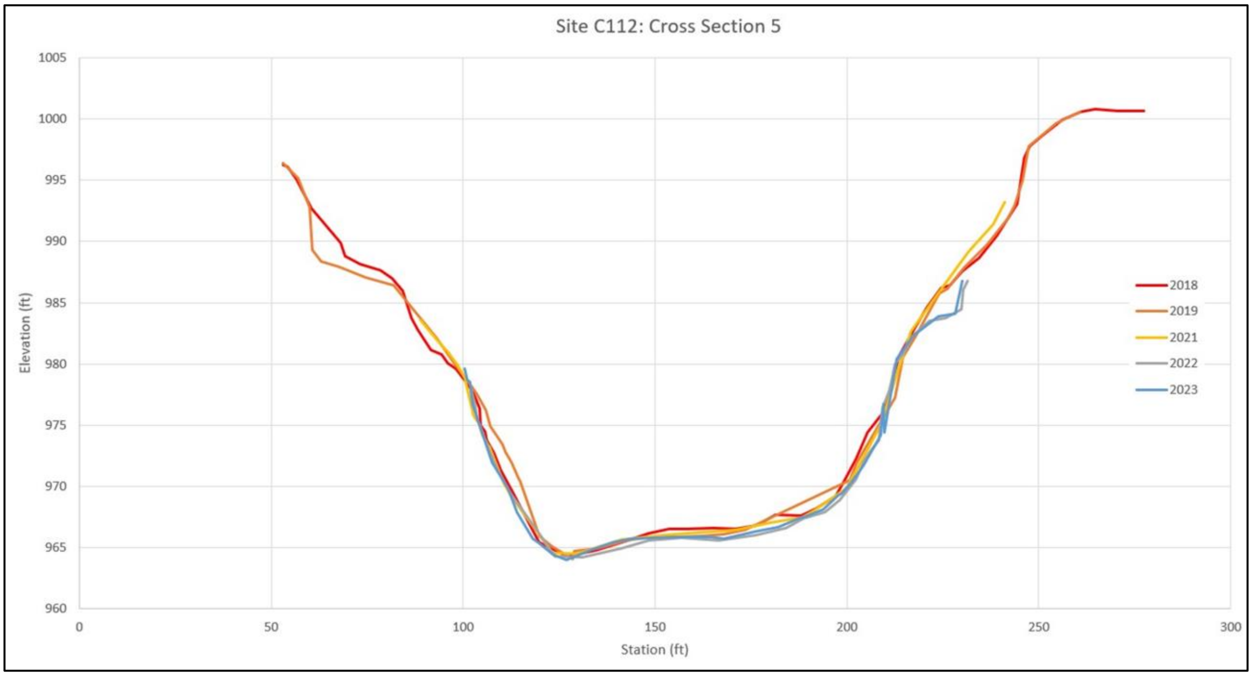

Appendix D Figure D.8 Site C112 Cross Section 6 Overlays

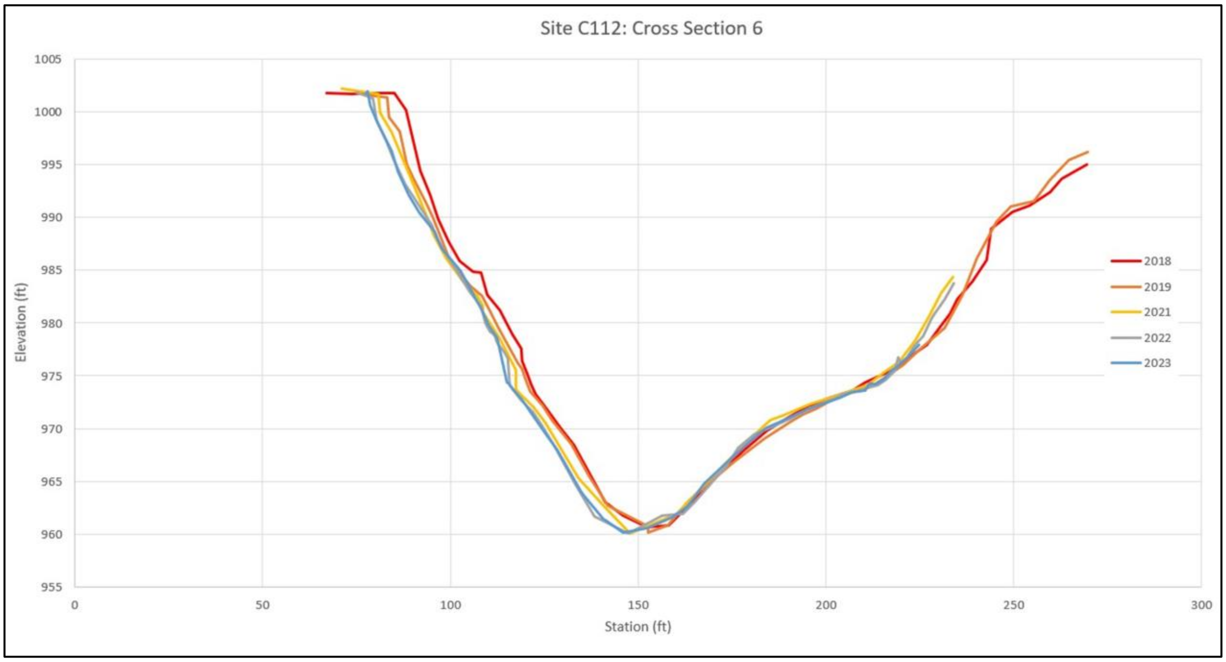

Appendix D Figure D.9 Site C112 Cross Section 7 Overlays

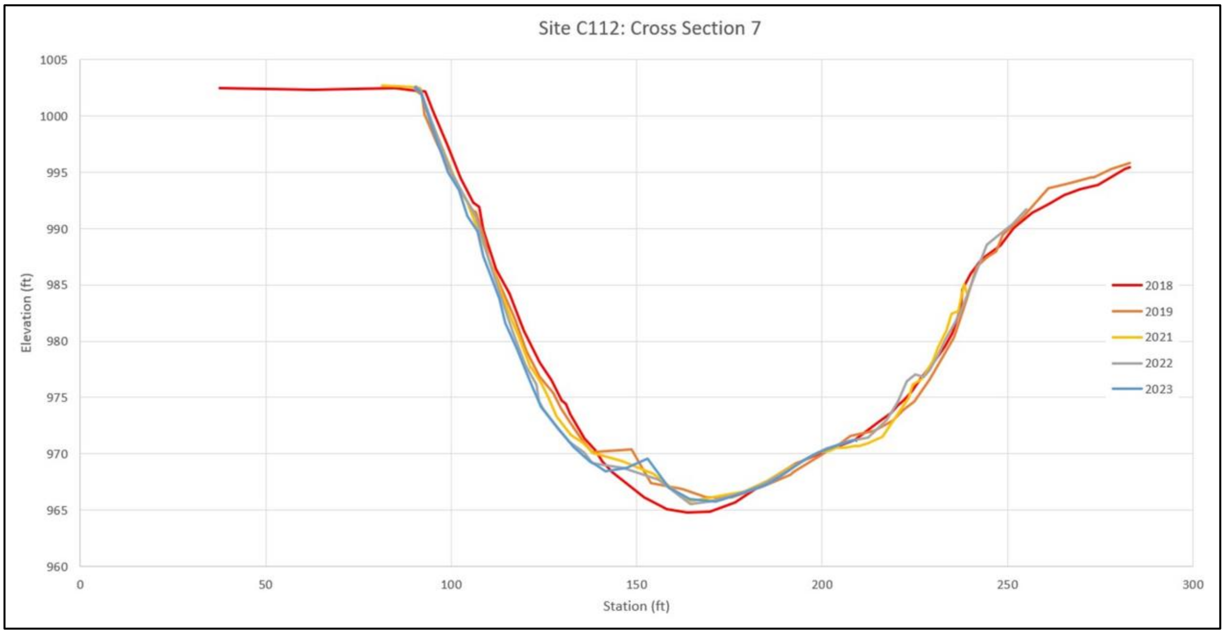

Appendix D Figure D.10 Site C102 Riffle Cross Section 1 Overlays

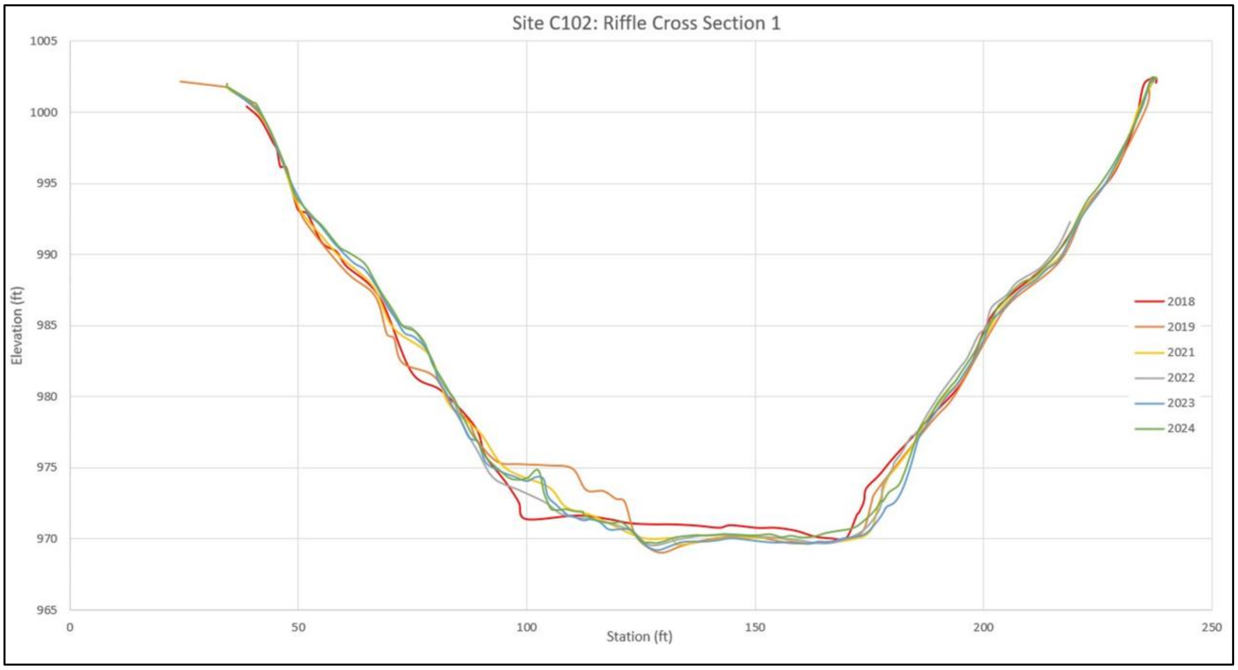

Appendix D Figure D.11 Site C102 Cross Section 1 Overlays

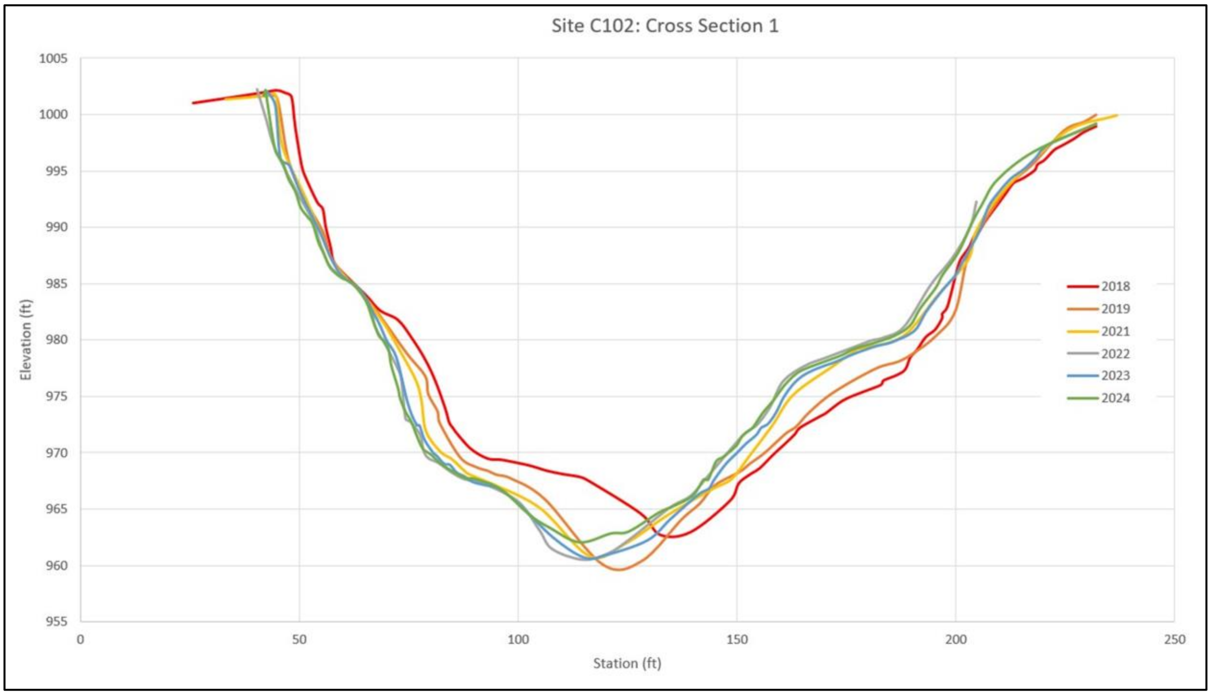

Appendix D Figure D.12 Site C102 Cross Section 2 Overlays

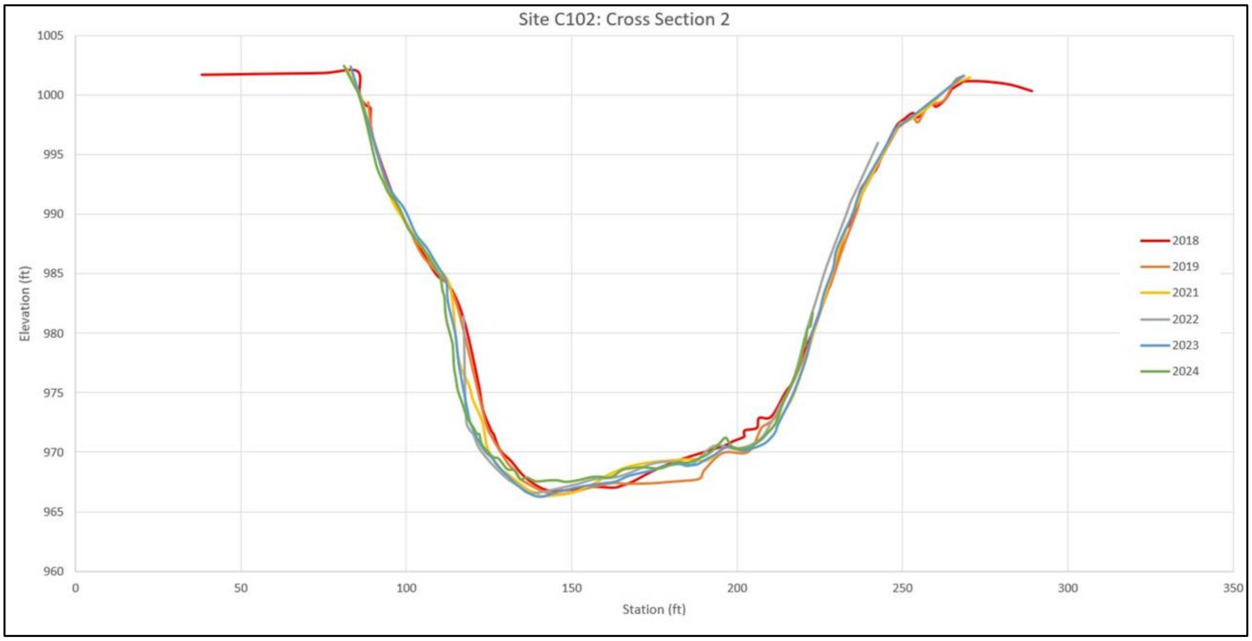

Appendix D Figure D.13 Site C102 Cross Section 3 (Stabilized) Overlays

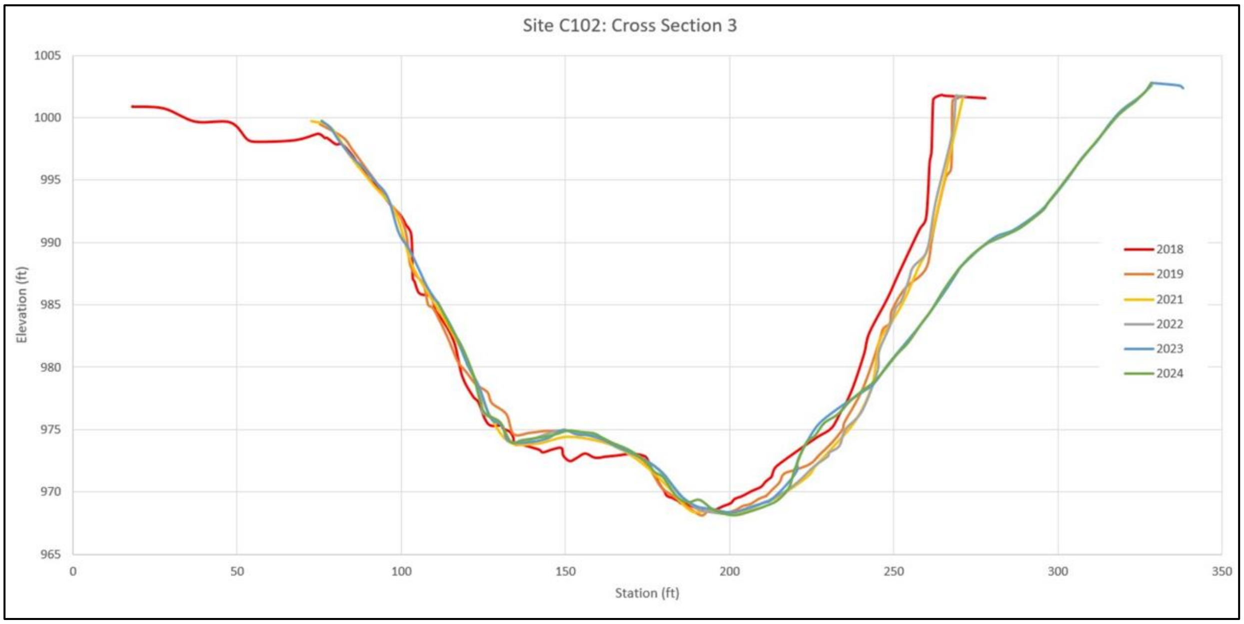

Appendix D Figure D.14 Site C102 Cross Section 4 (Stabilized) Overlays

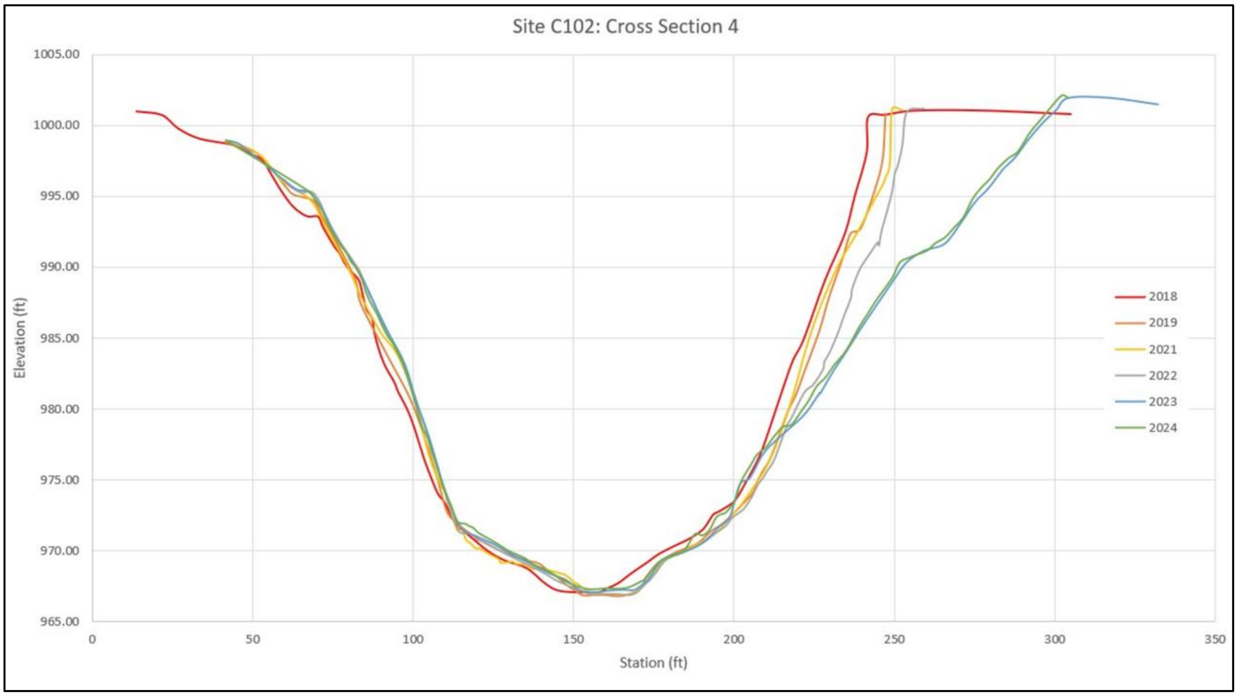

Appendix D Figure D.15 Site C102 Cross Section 5 (Stabilized) Overlays

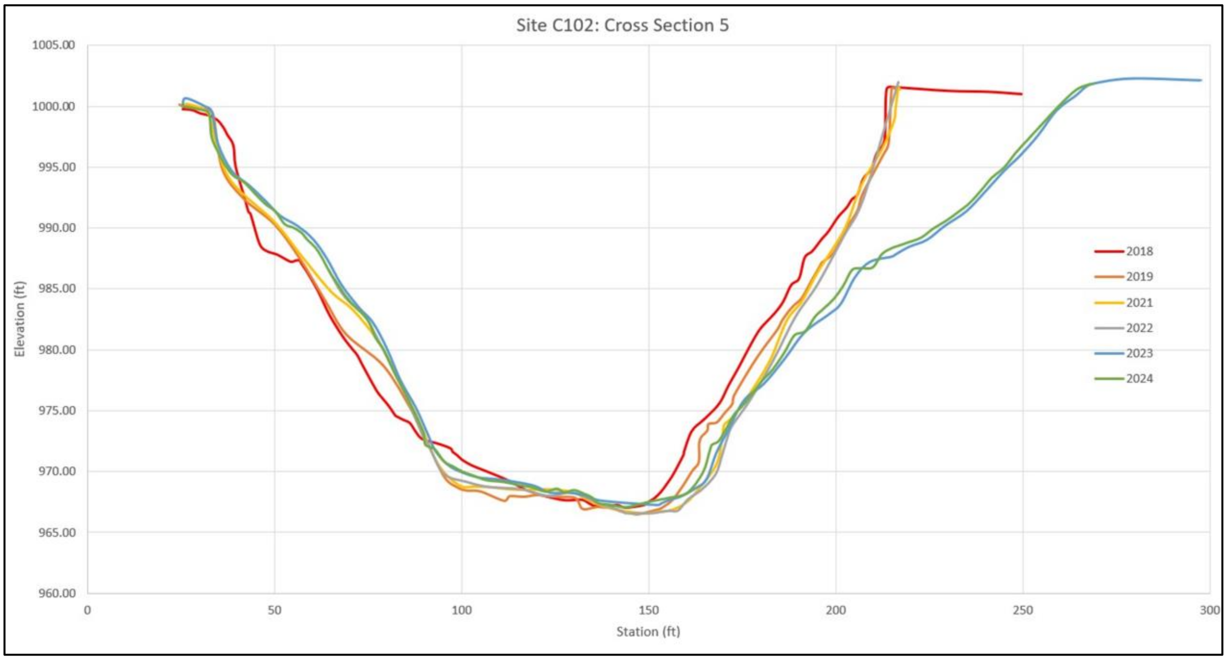

Appendix D Figure D.16 Site C102 Cross Section 6 (Stabilized) Overlays

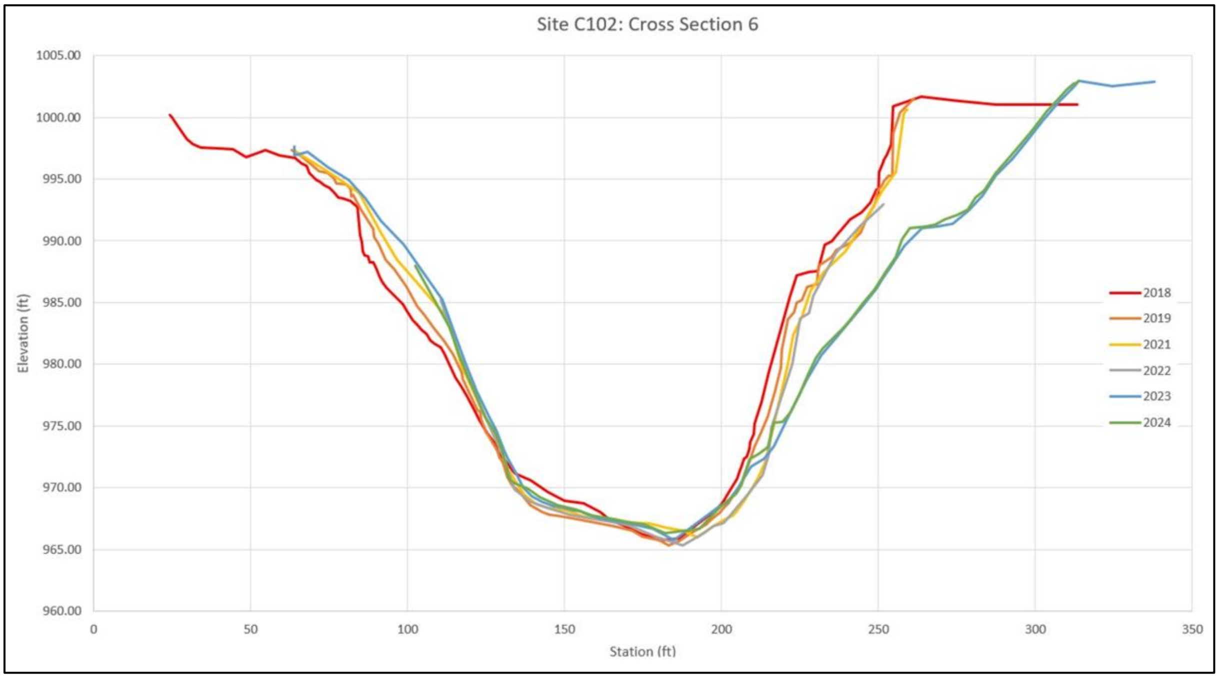

Appendix D Figure D.17 Site C102 Cross Section 7 (Stabilized) Overlays

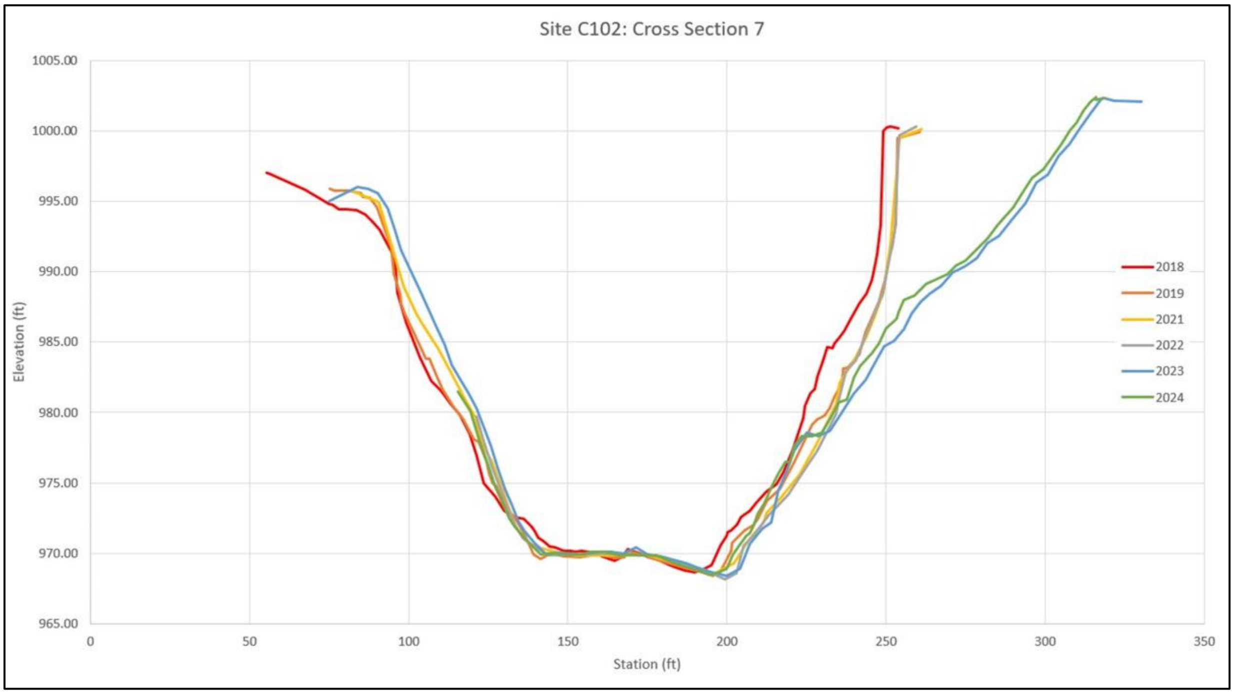

Appendix D Figure D.18 Site C102 Riffle Cross Section 2 Overlays

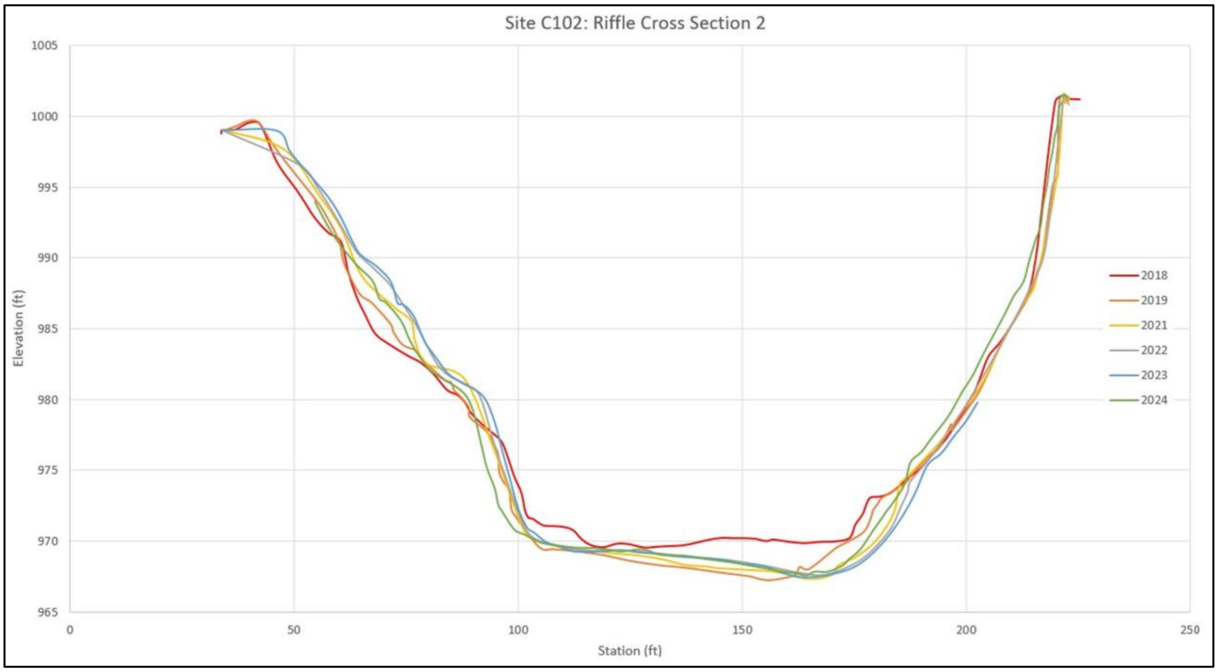

Appendix D Figure D.19 Site C102 Cross Section 8 Overlays

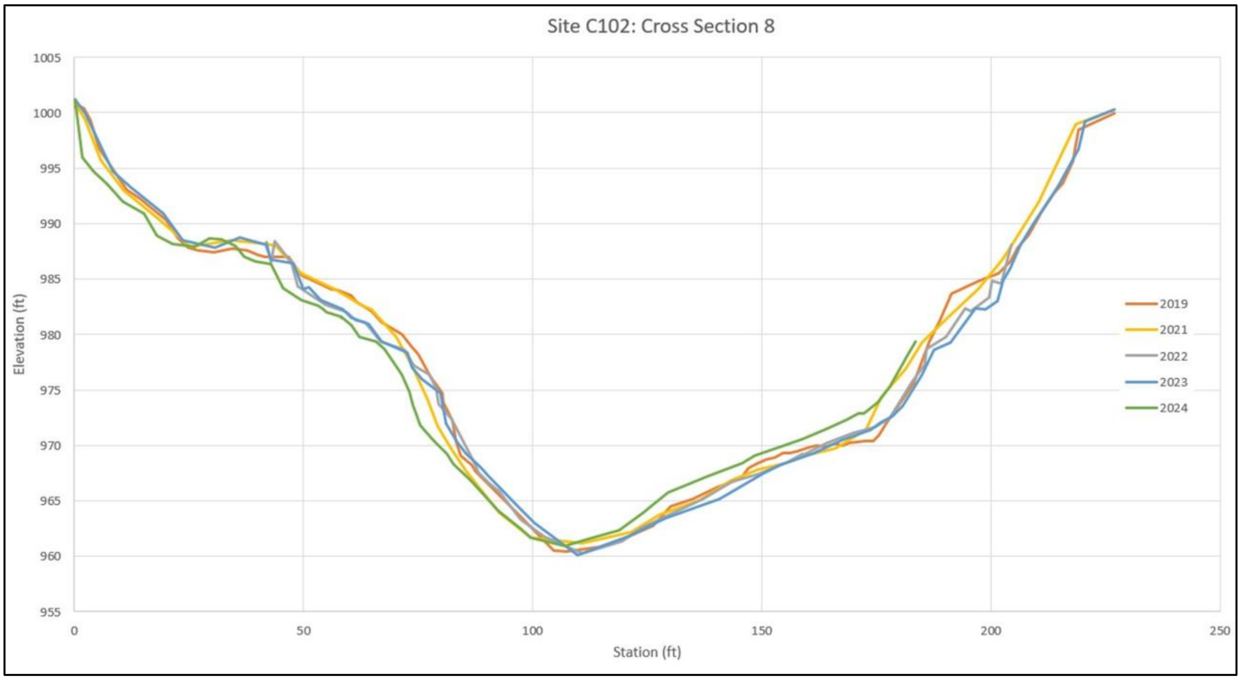

Appendix D Figure D.20 Site C102 Cross Section 9 Overlays